VIRGINIA COMMONWEALTH UNIVERSITY

Virginia Commonwealth University
VCU Scholars Compass

Theses and Dissertations | Graduate School

2012

DESIGN, FABRICATION, AND TESTING OF A PDMS MICROPUMP WITH MOVING MEMBRANES

Charles Cartin
Virginia Commonwealth University

Follow this and additional works at: http://scholarscompass.vcu.edu/etd

 Part of the Engineering Commons

© The Author

Downloaded from
http://scholarscompass.vcu.edu/etd/2742

This Dissertation is brought to you for free and open access by the Graduate School at VCU Scholars Compass. It has been accepted for inclusion in Theses and Dissertations by an authorized administrator of VCU Scholars Compass. For more information, please contact libcompass@vcu.edu.

© CHARLES P. CARTIN 2012
All Rights Reserved

DESIGN, FABRICATION, AND TESTING OF A PDMS MICROPUMP WITH MOVING MEMBRANES

A PhD Dissertation submitted in partial fulfillment of the requirements for the degree of Doctor of Philosophy in Engineering at Virginia Commonwealth University

By

CHARLES P. CARTIN

M.S.M.E., Virginia Commonwealth University School of Engineering, 2007
B.S.M.E., Virginia Commonwealth University School of Engineering, 2006

Advisor/Director: Ramana M. Pidaparti, Ph.D.
Professor, Department of Mechanical Engineering

Virginia Commonwealth University
Richmond, Virginia
May 2012

Acknowledgement

I would like to extend a heartfelt thank you to my advisor Dr. Ramana M. Pidaparti. Over the past four years Dr. Pidaparti gracefully provided me tremendous support, encouragement, mentorship, and guidance throughout my career as a graduate student. His knowledge and experience allowed me to complete my goals and make my dissertation a reality. Dr. Pidaparti has always encouraged me to attend conferences and student competitions where I was allowed to display my research progress. Throughout the time I have been a graduate student he has given me many opportunities to work on several research projects allowing my skills as a researcher to grow and expand drastically. I truly cannot thank Dr. Pidaparti enough for his never-ending support and guidance throughout the years.

I would also like to thank my committee members, Dr. P. Worth Longest, Dr. Gary M. Atkinson, Dr. Karla M. Mossi, and Dr. Everett Carpenter. Dr. Longest and Dr. Atkinson provided collaboration efforts on this project which in turn allowed the final realization of this interesting and challenging concept. Dr. Longest provided the conceptual fluid theories that assisted in the overall design of the micropump. His vast knowledge of computational fluid dynamics provided me with a valuable asset and resource. Dr. Atkinson provided his expertise and experience within the microfabrication laboratory at VCU to help develop and show the ways to successfully produce the device. Secondly, I would like to thank Dr. Mossi for her support, encouragement, and correspondence throughout my years at VCU. She has provided me great knowledge not only in my research, but in my career as an educator. Lastly, Dr. Carpenter provided interesting details concerning the characteristics of PDMS and possible actuation methods to successfully drive the micropump.

I also want to extend a special thank you to all of my colleagues within the Mechanical Engineering Department. These range from all of the graduate students to the faculty. I had the opportunity while at VCU to work on both sides of the spectrum, graduate student and faculty member. This was a valuable learning experience, because I have learned so much from everyone.

Lastly, I would like to thank my father and wife. My father has been there since the beginning, never losing faith or hope in me. He always has been there to support me in my endeavors and to push me when I had doubts. He gave me great guidance and encouragement to keep moving ahead and progressing in a positive direction. My wife has been supportive throughout my graduate career and has maintained patience, support, and strength. I must admit that without them, I probably would not have accomplished what I have done thus far in my life.

Table of Contents

List of Figures

List of Tables

Abstract

DESIGN, FABRICATION, AND TESTING OF A PDMS MICROPUMP WITH MOVING MEMBRANES

By: Charles P. Cartin, M.S.M.E.

A Dissertation submitted in partial fulfillment of the requirements for the degree of Doctor of Philosophy in Engineering at Virginia Commonwealth University.

Virginia Commonwealth University, 2012

Advisor/Director: Ramana M. Pidaparti, Ph.D.
Professor, Department of Mechanical Engineering

This dissertation will discuss the design, fabrication, and testing of a Poly(dimethylsiloxane) (PDMS) microfluidic pump. PDMS is commonly described as a soft polymer with very appealing chemical and physical properties such as optical transparency, low permeability to water, elasticity, low electrical conductivity, and flexible surface chemistry. PDMS microfluidic device fabrication is done easily with the use of soft lithography and rapid prototyping. PDMS microfluidic devices make it easier to integrate components and interface devices with particular users, than using typically harder materials such as glass and silicon. Fabrication and design of single and multilayer PDMS microfluidic devices is much easier and straightforward than traditional methods.

A novel design of a PDMS micropump with multiple vibrating membranes has been developed for application in drug delivery and molecule sorting. The PDMS micropump consists of three nozzle/diffuser elements with vibrating membranes, which are used to create

pressure difference in the pump chamber. Preliminary analysis of the fluidic characteristics of the micropump was analyzed with ANSYS to investigate the transient responses of fluid velocity, pressure distributions, and flow rate during the operating cycle of the micropump.

The design simulation results showed that the movement of the wall membranes combined with rectification behavior of three nozzle/diffuser elements can minimize back flow and improve net flow in one direction. To prove that the theoretical design is valid, the fabrication and testing process of the micropump has been carried out and completed. This paper will discuss in depth the design, fabrication, and testing of the PDMS micropump.

CHAPTER 1 Introduction

1.1: Motivation

Microfluidic systems have proved highly successful in biomedical applications by minimizing the size of electrophoresis chips, drug delivery systems, microfluidic mixers, pumps and valves, devices for cell or protein patterning, and microfluidic switches [1]. Specifically a PDMS pump is a device that is optimized for rapid prototyping and has proven to be a good material for microfluidic pump devices. First, one must know what PDMS means. PDMS stands for Polydimethylsiloxane and is most widely used as a silicon-based organic polymer. It is known for its unusual flow characteristics (rheological properties). The material is usually clear, inert, non-toxic, and non-flammable. The chemical formula for PDMS is: $(H_3C)[SiO(CH_3)_2]nSi(CH_3)_3$, where n is the number of repeating monomer $[SiO(CH_3)_2]$. Figure 1.1 and 1.2 below show the chemical structure for PDMS in 2-D and 3-D:

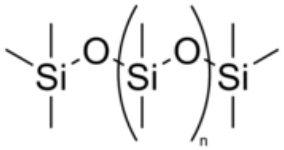

Figure 1.1: 2-D PDMS Chemical Structure

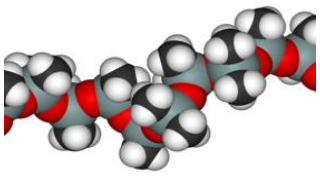

Figure 1.2: 3-D PDMS Chemical Structure

PDMS has mechanical properties that make it suitable for microelectromechanical systems (MEMS). These properties occur at high and low temperatures of the PDMS material. At high temperatures the PDMS material is viscoelastic (i.e., having long flow rates). An analogy for how this material reacts at high temperatures can be compared to honey being poured into a glass. On the other side of the spectrum, as PDMS experiences lower temperatures it becomes an elastic solid (i.e., having short flow rates). This can be compared to rubber material, such as a rubber ball.

PDMS material could be applied to several types of microfluidic devices such as mixers, filters, channels, reactors, extractors, valves, flow sensors, droplets, and pumps. These types of microfluidic devices can be applied to environmental scanning and monitoring, microreactors and mixers, filtering, inkjet printing, chemical analysis and sensing, molecular separation, biological sensing (in-vitro or in-vivo), and DNA analysis (amplification, sequencing, and synthesis). The benefits of such microfluidic devices are smaller sizes, better performance, reduction in power consumption, lowers costs, disposability, integration of control electronics, and the new functionality and reaction possibilities. These types of microfluidic devices have several characteristics and have flow that is generally laminar. They deal with smaller volumes of fluid, which results in higher precision of mixing and is safer to use with toxic and hazardous chemicals. Also these devices have high surface to volume ratio that results in efficient and effective heating and cooling, as well as fast and complete reaction with the surface.

1.2: Background of Micropumps

Silicon and glass-based microelectromechanical systems (MEMS) are slowly being replaced by polymer microfabrication methods. Presently limitations in the silicon and glass processing methods are becoming more relevant due to newer and more complex fabrication procedures, geometrical design restrictions, and escalating costs involved in reaching the goal of the finished product [1]. Polymers provide a wider range of material characteristics biochemical compatibility, ease of processing and prototyping, and lower cost [1]. Polymers are less expense and easier to fabricate than silicon based substrates [2]. Microfluidic systems have proved highly successful in biomedical applications by minimizing the size of electrophoresis chips, drug delivery systems, microfluidic mixers, pumps and valves, devices for cell or protein patterning, and microfluidic switches [1]. Advantages of microfluidics are enormous, while possessing very few disadvantages. The field of microfluidics has four parents: molecular analysis, biodefense, molecular biology and microelectronics [3]. Scientific investigations into the development of fluidic devices have increased due to the ability to create structures and patterns on micron and smaller length scales [2]. Development of new fluidic devices to transport, store, and manage very small quantity of fluids has found increased applications in the fields of chemistry, biology, and medicine [2].

Life science and materials communities are being rapidly drawn to microfluidic technology. Currently many of these communities do not have the proper access to these new revolutionary microfluidic chips and microfabrication facilities, which hinders their ability to explore new polydimethlysiloxane (PDMS) technology in microfluidic devices, thus limiting their contribution to the growth of the microfluidic field [4]. As a way to improve access to

PDMS microfluidic chips and facilities, studies are being conducted to eliminate the need for cleanrooms, while at the same time producing higher quality microfluidic systems [4].

Experimentation with polydimethylsiloxane (PDMS) has provided varying properties that are readily adaptable in microfluidic devices. Such devices far exceed those of known "benchtop" systems and provide a range of plausible advantages. Advantages associated with the PDMS include operating systems size reduction, faster analytical and probability data, savings in the form of power reductions, broader design flexibility, and decrease in harmful byproducts. Microfluidic device design and functionality hinge on the type of materials chosen for the design and the manner in which the device will be fabricated [5]. When considering a microfluidic device the material chosen should be compatible with sensitive methods of detection, enable easy interfacing with the user, and allow integration of functional components [5]. As the need for microfluidic devices increases and the necessity for fabrication for such devices become imperative to attract the interest of industry and scientific communities, the cost efficiency of such materials and the increasing ease of production will result in cost saving strategies [6].

1.3: Materials Utilized in Microfluidic Devices

Microfluidic systems fabricated in silicon and glass were the earliest microfluidic systems designed to take advantage of existing technology in microelectronics and mircoelectromechanical systems (MEMS). Although silicon and glass are outstanding materials for use in the fabrication of microfluidic devices, polymers are becoming advantageous and less expensive requiring simpler manufacturing processes [5]. The use of polymers to fabricate microfluidic devices has been expanded to include polydimethylsiloxane (PDMS) [2]. Because polymers have different physical and chemical property ranges than do silicon and glass they are more adaptable to specific applications and polymers are more mechanically stronger than silicon and glass [5].

PDMS, a soft polymer, is being developed for use in microfluidics. Soft polymers of this caliber have advantages in the fabrication of MEMS devices. Soft lithography using elastomeric polymer molding in PDMS devices allows for rapid prototyping of microfluidic devices [5]. Since polymer devices made of PDMS conforms to most materials and will conform uniformly to smooth plastic or glass substrates, reversible and irreversible sealing are possible [5]. Transparency of PDMS allows compatibility with many optical detection methods because it is unseen in the visible/UV region. PDMS channels are appropriate for cellular studies because PDMS is nontoxic to proteins and cells and is gas-permeable [7].

1.4: PDMS in Microfluidic Systems: Rapid Prototyping

Rapid prototyping of devices is made easy with the use of soft lithography. Soft lithography is the technique used as a non-photolithographic technique for pattern replication and enables rapid prototyping of devices [8]. A computerized design CAD program is used to create a design for a channel. Once the CAD file is obtained it is printed onto a transparency film with a high resolution setter (Fig. 1.3A).

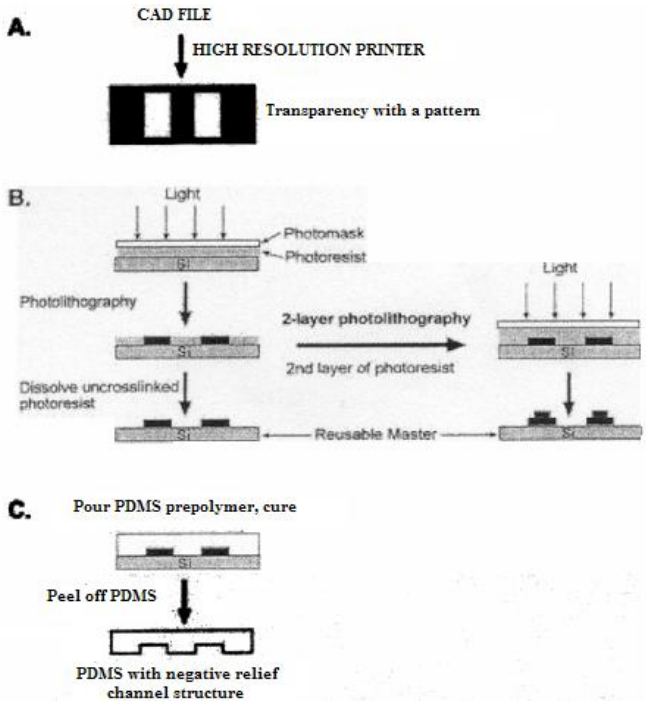

Fig.1.3. (A) Schemes for rapid prototyping, (B) fabrication of reusable masters, and (C) replica molding of PDMS microfluidic systems. (A) Rapid prototyping is the generation of a high-resolution transparency to be used as a photomask. (B) Fabrication for the master involves spin-coating photoresist onto a silicon wafer and developing the photoresist through a photomask. If three-dimensional structures are desired, an additional step involving spin-coating of the photoresist, mask aligning, and UV exposure can be performed. The uncross-linked photoresist is then dissolved, leaving a master with a positive relief feature. (C) Replica molding involves pouring a mixture of PDMS prepolymer and curing agent onto the master, curing at ~70^{o}C for one hour, and peeling off the master. Unlimited numbers of replicas can be made from the same master [5].

The transparency film is then treated with a photo curable epoxy (SU-8) and exposed to ultraviolet light to polymerize areas that are exposed. Once the dissolving effect of the unpolymerized photoresist has been accomplished, a positive release of the reaction remains on the wafer acting as a mold for future castings of PDMS channels. Multilayered structures of this device can be accomplished by repeating the process for a two level photolithography, but instead of dissolving the unpolymerized photoresist following its initial exposure, a second photoresist layer is spun atop of first exposure. Following this step a second mask is setup in alignment with the photoresist layers and then the second layer is polymerized, resulting in the dissolution of the unpolymerized photoresist resulting in a multilayer channel structure. A silane solution containing fluoride functional groups is then used to treat the surface of the master fabricated wafer. The use of the silane prevents bonding between the PDMS and the silicon. A negative relief of the original master structure is made in PDMS by replicating the molding (Fig. 1.3C). Replica molding involves pouring PDMS prepolymer over the master, curing the polymer at 40-80^{o}C for ~ 1 h, and peeling it off of the master. Channel inlets and outlets are drilled into the PDMS using a borer (a small drill will do), and the channel is sealed (reversibly or irreversibly) against a flat substrate [5], [9].

Expenses are reduced by using rapid prototyping and replica molding which reduces future time required for designing, additional fabrication, and the necessary final testing of any new channel configurations. Additional cost reductions equate to a lower overhead for operating a microfluidics research program and the reduction in need for cleanroom and mask writers.

1.5: PDMS Surface Chemistry and Sealing Techniques

The chemical structure of PDMS is made up of repeating groups of $–O\text{-}Si(CH_3)_2$. Such a chemical structure allows for a hydrophobic surface that is made hydrophobic by bombarding it with air plasma or oxygen. Methyl groups ($Si\text{-}CH_3$) [10], [11] is destroyed when the hydrophobic surface is exposed to air plasma or oxygen. Once these channels have been treated with the plasma they can be kept hydrophobic indefinitely by simply keeping the surfaces treated with water or polar organic solvents. Lack of water or the necessary polar organic solvents will result in surface rearrangements that will result in new hydrophobic groups coming to the surface to lower the surface free energy. Using silanol groups allows surfaces of PDMS to react positively to a wide selection of silanes (Si-R) which are terminated with important functional groups (i.e., $R=NH_2$, COOH, SH). Tailoring the surfaces of PDMS to be hydrophobic or hydrophilic is accomplished through the use of the aforementioned functional groups, reducing the no specific absorption of proteins [12].

1.5.1 – Irreversible Sealing

Channels made in silicon thermoplastics or glass are much more difficult to seal then PDMS channels. Sealing PDMS channels does not require the use of high temperatures, high voltages, or high pressurization. Air or oxygen plasma exposed to both the surface PDMS and the surface of the substrate allows the PDMS channels to be irreversibly sealed to glass, silicon, silicon nitride, polystyrene, or polyethylene [13]. Oxidation using plasma produces silanol groups on PDMS, and –OH-containing functional groups on the other materials; these polar groups form covalent –O-Si-O-bonds with oxidized PDMS when these surfaces are brought into

contact [14]. Sealing the two slabs of PDMS can also be accomplished by the inclusion of an excess amount of the monomer to one slab and the inclusion of excess of the curing agent to the other slab. When cured the result is an irreversible seal that is indistinguishable from the bulk properties of PDMS [15]. On the other hand to seal glass to glass or silicon to silicon demands very high temperatures (`600^{o}C for glass; > 800^{o}C for silicon) or voltages (500-1500 V for anodic bonding of glass) [15], this differs greatly from sealing PDMS to glass or to itself.

1.5.2 – Reversible Sealing

Another positive advantage PDMS has over silicon, glass, and hard plastics is that it allows the reversible van der Waals contact to smooth surfaces. This leads to demountable microfluidic PDMS devices and are useful in patterning surfaces with biomolecules, proteins, or cells by using fluid flows [16]. The use of silicone adhesive tapes makes a convenient sealing agent for PDMS channels allowing for a reversible seal. Such tapes are flexible, and will allow for the incorporation of non-sealing layers such as membranes and filter papers, and the tape is very easy to cut as needed for various purposes. The particular silicone adhesive tapes are very useful because they form stronger bonds (that are still reversible) than those between PDMS and other flat surfaces [9].

1.6: Three Dimensional Fabrication of PDMS

Fabrication of three dimensional features in hard materials in prototyping and manufacturing requires an expensive process such as stereolithography, laser-chemical 3-D

writing, or modular assembly. An inexpensive method is to fabricate 3-D channels in PDMS, which is a versatile method of making complex geometries at cost savings. This has been demonstrated by three methods of fabricating 3-D microchannel structures: (A) the use of two-level photolithography, (B) the "membrane-sandwich" method, and (C) solid-object printing [5].

1.6.1 – Two-Level Lithography

When thinking about making topographic surface features within microfluidic channels, two-level photolithography comes to mind. In two-level photolithography fabricating process, two steps of mask alignment and polymerization of SU-8 photoresist (Fig. 1.3). This method makes grooved structures inside channels for chaotic mixing [5].

1.6.2 – Membrane Sandwich Method

When working with hard materials layering is possible, but thermal stress, mechanical stress, and adhesion failure can occur when bonding the various layers. Using soft polymers as the layering component eliminates these problems because a simple chemical process seals the layers. This process also allows for good contact between the surfaces by using low pressure. The "membrane sandwich" was a method developed for fabricating topographically complex 3-D channel structures in PDMS (Fig. 1.4) [8]. The "membrane sandwich" consisting of three levels of features within a single thin layer of PDMS (approximately 100 μm) is place between two thicker pieces of PDMS resulting in a very strong structural support. In this process two masters are fabricated with the use of the membrane. The top master is made by replicating

molding and silanized that contains a single level of the features. The bottom master is made in silicon and photoresist by two-level photolithography containing two-levels of features (Fig. 1.4A). Fabrication of the membrane is accomplished by placing PDMS prepolymer between the two masters and applying a small amount of pressure [5]. The pressure allows the masters to be in contact while at the same time the prepolymer is being expelled from the area of the initial contact. Possessing complimentary microscopic alignment tracks allows both masters to be slipped into one another without any form of magnification needed to accomplish this task. Following the curing process of the prepolymer the resulting silicon master is easily removed from the PDMS allowing the membrane to remain attached to the silanized PDMS master. Exposure of the membrane and a PDMS flat are then oxidized by plasma-treatment and brought into contact with one another. Once this step is completed the PDMS master is peeled away from the opposite side of the membrane and the membrane is sealed against another PDMS flat [5], [8].

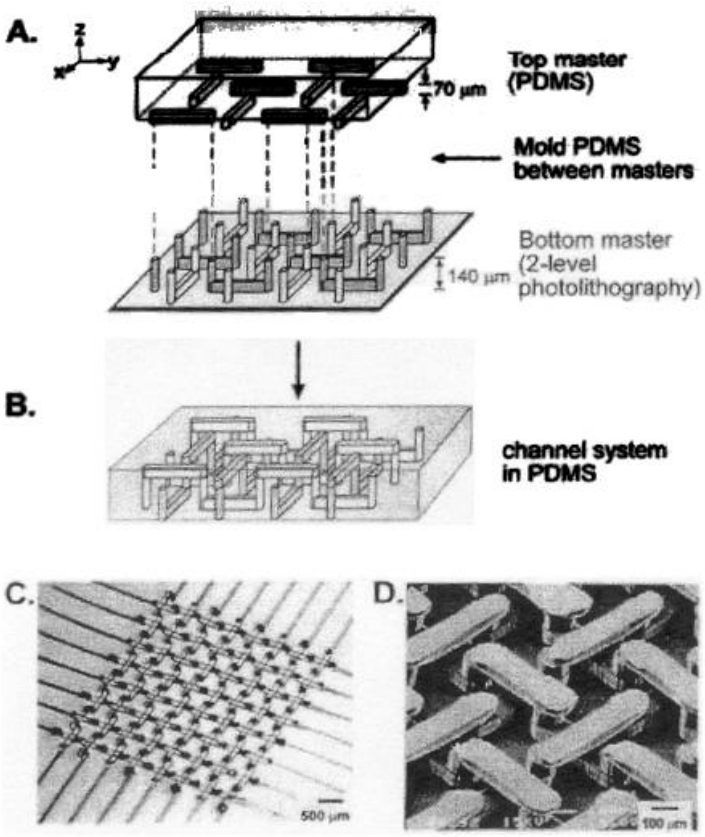

Fig.1.4. The membrane sandwich method for making a three-level channel system in a single membrane. (A) The top master contains one level of features and is made in PDMS by molding against a master. The bottom master is a positive relief of photoresist containing two levels of features, and is made using two-level photolithography. The channel system is made by placing PDMS prepolymer between the two masters, aligning the masters, and applying pressure until the masters are in contact by excluding the PDMS. For clarity, features on the master oriented in the y-direction are depicted with a darker pattern than those in the x-direction. (B) Schematic diagram of the three-level channel system in a PDMS membrane. (C) Optical image (looking down the z-axis) of the PDMS membrane alone, which contains an 8 x 8 channel system. The channels are 100µm wide (x- or y-direction), and each of the three levels used in the fabrication is 70µm high (z-direction), but is not enclosed. To make the final channel structure, both sides of the membrane are sealed to PDMS flats (not shown). (D) Scanning electron micrograph of the channel system in epoxy polymer. The microstructure was formed by filing the channels with epoxy prepolymer, curing under ultraviolet light for ten minutes, and dissolving the PDMS casing in tetrabutylammonium fluoride [5].

1.6.3 – Solid-Object Printing for PDMS Devices

Solid-object printing (SOP) [17] is an alternative process to creating masters for molding microfluidic channels. In this process a 3-D channel system is designed using a CAD program. Once the CAD file is made it is easily read by any commercial solid-object printer resulting in a fabrication of a master directly in a thermal plastic material without the use of a mask. The alignment steps associated when 3-D structures are fabricated using membrane sandwich method or the two-level photolithography are eliminated with the use of the CAD file. Following the completion of the master PDMS prepolymer is dispensed over the mold, allowed to cure, and is then peeled from the mold. Use of the SOP method for generating microfluidic devices allows the devices to be distributed over a larger area up to 250 x 190 x 200 mm in the xyz plane, with increased height in overall features. However, the resolution of the printer is low, 300 x 400 x 600 dpi, in the xyz plane). Therefore, the resolution limits this method to fabrication of features $\geq$ 250 μm, and generates masters who surfaces are rough (~8μm) [5],[17].

1.7: Interfacing of PDMS Microfluidic Devices

Microfluidic systems made in hard materials are very difficult to interface within the realm of the world as a whole. An example is making a watertight seal between the device and tubing for sample introduction often requires either inserting a polymer interface or using expensive high precision micromachining, reactive ion etching, or related techniques [18]-[20]. Microfluidic devices that are fabricated in PDMS will interface with both internal components and the outside world. This method has been demonstrated through the encapsulation of components such as optical fibers, photodiodes, optical filters, glass capillaries, and silicon tubing in PDMS [9]. Electrodes that are electroplated or evaporated on a substrate can also be easily integrated because PDMS conforms to the electrodes if they are thing (<200 nm) [21].

PDMS elasticity allows various objects such as glass capillaries, polyethylene tubing, and sippers to be tight, and at the same time easily inserted into holes made in PDMS by press fitting. These particular holes must be fabricated to be roughly twenty to fifty percent smaller than the actual diameter of the object being inserted. This will allow for the inserted object to fit securely against the walls of the hole providing a leak proof seal. The simplistic ease associated with the placement of an object into a predetermined hole allows for simple removal and ease of operation in PDMS systems. The most commonly used tubing for connecting to PDMS devices is polyethylene tubing. Polyethylene tubing allows easy connection to objects such as syringe needles and is highly praised for its ability to allow fluids to be pumped through channels. The access holes also fit micropipette tips for manual injection of samples [5].

1.8: Advantages and Disadvantages of PDMS

PDMS based microfluidic systems offer advantages over hard materials. Advantages include low cost and the time necessary to fabricate a small number of devices. The nature of PDMS allows for ease in modification and fabrication designs using soft lithography and replica molding. The ability to produce compact sealing interfacing with optical fibers and inclusion of organic membranes were made easy through the use of soft lithography with PDMS. Other components or counterparts that are required to build functional devices are compatible with PDMS. At times some properties associated with PDMS may be affected when working with features less than twenty millimeters. Problems such as shrinking or sagging associated with PDMS can be eliminated with features greater than or equal to twenty millimeters. In the near future polymeric systems such as PDMS will replace glass and silicon systems for many biological analyses. Soft lithographic technology is expected to become more commercialized in the near future. Accompanying the projected commercialization of soft lithographic technology the cost associated with current methods is expected to drop.

1.9: Specific Objectives

The overall research goals for the PDMS micropump are achieved through the following objectives. Develop the PDMS microfluidic pump with two fabrication methods. Fabrication Method I utilizes the VMC Microelectronics Laboratory. This method will utilize microelectricalmechanical systems methodology, lithography, and sealing processes. Fabrication Method II will use design optimization and rapid prototyping to optimize the manufacturing process for the micropump. These two methods will be compared with to determine the best method that will quickly produce this device. Develop a method for testing and characterization. This involves methods for actuation of the pump that possibly involve electrostatics actuation, magnetic actuation, piezoelectric actuation, pneumatic (mechanical motor) actuation, and pressurized flow actuation. Experimental results can then be compared to theoretical results.

CHAPTER 2 – Literature Review of Micropump Technologies

2.1: Introduction

Presently in today's technology micropumps can be divided in to two distinctive categories: displacement micropumps and dynamic micropumps. Displacement micropumps are commonly referred to as mechanically actuated pumps. These types of micropumps apply an oscillatory, periodic, and/or rotational pressure force on the fluid through the use of a moving boundary. The boundary layer can be a solid to fluid boundary, such as a vibrating diaphragm, rotary, and/or a peristaltic pump, or a fluid to fluid boundary layer, similar to a phase change, ferrofluid, or gas permeation pump. In some cases involving phase change and pneumatic actuation methods the pressure will not necessarily be periodic. Aperiodic displacement pumps in most instances will only pump a volume that is fixed. This form of actuation is similar to the action of a syringe. Dynamic micropumps are classified as a micropump that continuously adds energy to the working fluid to either increase its momentum (i.e., centrifugal micropumps) or its pressure directly (i.e., electrohydrodynamic, electro-osmotic, electrowetting, , acoustic, etc.). Due to the continuous energy transfer that is exhibited, dynamic pumps can generate constant, steady flows.

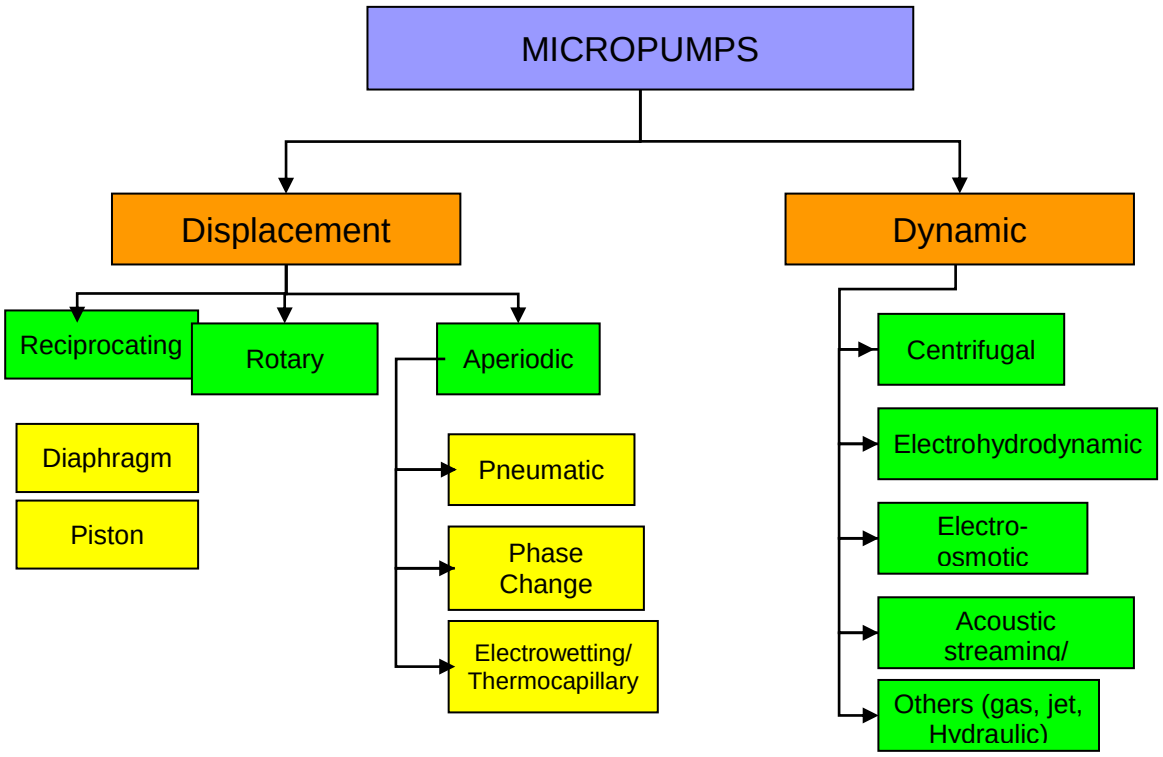

Figure 2.1: Current Micropump Classification based on Laser & Santiago (2004)

Micropumps can be broken into sub-categories based on their actuation method. Figure 2.1 illustrates the current micropump classification investigated by Laser & Santiago (2004). The research that is currently being investigated will revolve around displacement micropumps and their different actuation methods. Attention will be focused on the volumetric flow rate, Q_{mzx}, and the maximum measured differential pressure, Δp_{max}. Other parameters that may be of interest are the operating voltage and frequency. In the following sections the categories of micropumps will be discussed in more detail.

2.1.1 - Displacement Micropumps

Displacement (reciprocating) micropumps utilize a rotational or oscillatory movement of mechanical parts to move fluid from an inlet to an outlet. Early development of micropumps began with reciprocating piston actuation similar to peristaltic micropumps and diaphragm micropumps that still make up the main representatives of the MEMS environment. The principle that is most commonly utilized involves a pumping chamber that is sealed with a flexible diaphragm on one side of the micropump (figure 2.2).

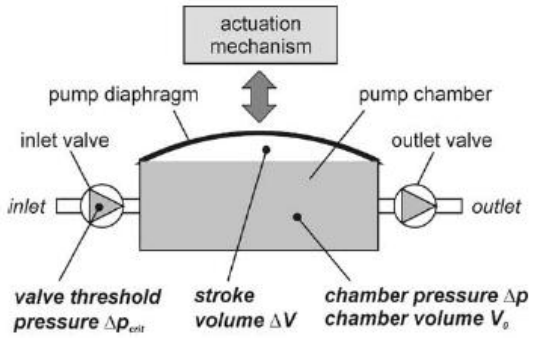

Figure 2.2: Configuration of piston-type micropumps

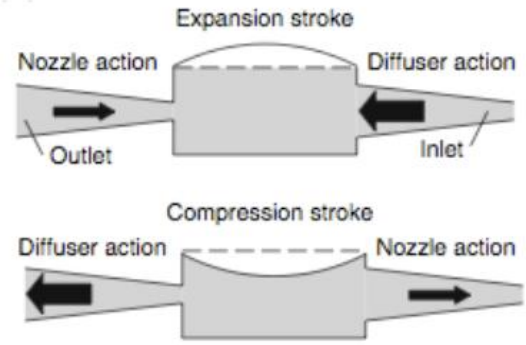

Figure 2.3: Structure and Operation of reciprocating pump, Iverson & Garimella (2008)

Oscillating movement of the diaphragm generates a two-phase pump cycle with periodic volume changes that result in under/overpressure transients Δp in the pumping chamber. As the pump is being actuated it will experience a supply phase. The supply phase is when the under-pressure in the pumping chamber sucks fluid through the inlet into the chamber of the micropump. When this phase is reversed the micropump will experience a pumping phase. The pumping phase is defined as an over-pressurization within the pumping chamber that allows transfer of liquid into the outlet (figure 2.3). Valves that are usually located at the inlet and outlet will block unwanted reverse flow during the respective pumping phases. These valves mimic fluid rectifiers that guide and direct the bi-directional fluid flow generated internally within the pumping chamber towards a desired unidirectional flow. The fluid (liquid or gas) is delivered in a series of discrete fluid volume whose magnitude is dependent upon the actuator stroke volume ΔV (net volumetric displacement during one cycle).

Currently it has been illustrated and determined through biological evolution that this concept has been perfected in micro dimensions long before technical studies were investigated. There are predaceous bugs, the Graphosoma Lineatum, [22], [23] utilize piston type micropump designs at the end of their picking stylet for the external digestion of their insect prey (figure 2.4). This type of micropump operates with the use of a muscle operated piston and passive flap valves as inlet and outlet check valves. One micropump dispenses saliva filled with digestion enzymes through the picking stylet into the blood of the prey. A second micropump removes (sucks) the digested food back.

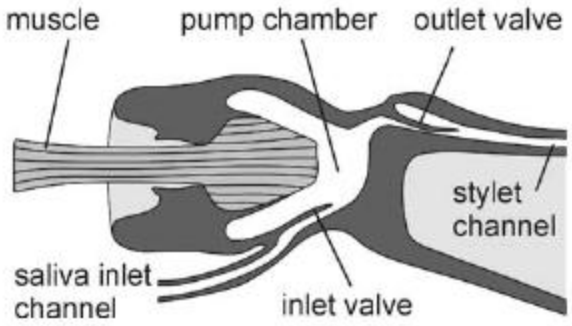

Figure 2.4: Schematic of Graphosoma Lineatum Saliva Dispensing Micropump [22]

2.1.2 - Dynamic (Continuous flow) Micropumps

Dynamic micropumps are based on a direct transformation of mechanical or nonmechanical energy into a continuous fluid movement. These types of devices have been currently developed focusing on ultrasonic, magnetohydrodynamic (MHD), electrohydrodynamic (EHD), electroosmotic, or electrochemical actuation methods. The design principles being vastly different depends upon the respective physical or chemical principle which will be discussed within this chapter.

2.2: Early Research of Reciprocating Micropumps

In the beginning of micropump technology basic designs were based on an actuation of both the valves and the pump diaphragms, instead of utilizing passive valves, which was presented by Spencer et al. [25] in 1978. Spencer's approach to design this type of micropump is illustrated in figure 2.5. It is shown by the diagram that a

cylindrical micropump body was fabricated from stainless steel and sealed with a piezoelectric actuated stainless steel shim to mimic a pump diaphragm.

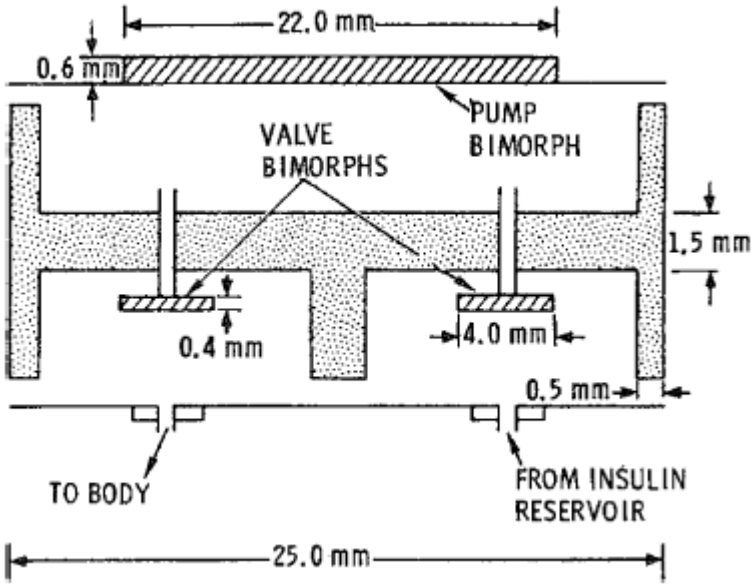

Figure 2.5: Diagram of Cross-sectional cutaway of a micro-diaphragm pump with active valves [25].

Activation flap valves were fabricated from piezoelectric bimorphs with dimensions of 0.4 mm x 4 mm x 20 mm. To avoid electrical short circuits during submersion in liquid the bimorph valves were coated with an electric resistive material. Utilizing a high voltage actuation of 100V a theoretical stroke volume of 1.94 microliters and an output pressure maximum of 100 mmHg were achieved. Measurements of various data points were tested and a maximum stroke volume of 1.5 microliters with 90V actuation and a maximum pressure of 60 mmHg at 70V actuation were determined [25]. It must be noted that only unidirectional flow was utilized, but this form of

micropump was capable of bidirectional fluid transport by changing the valve actuation method.

In 1990 a similar silicon based device was realized by Smits [26] with a planar peristaltic micropump design. The particular micropump was fabricated from an anisotropically etched silicon wafer that housed valve seats on its topside and connected to microchannels on the bottom surface (figure 2.6). For this design the silicon wafer was sealed with glass by anodic bonding from both sides. On top the glass wafer was left unattached to the three silicon valve seats which converted it into three pump/valve diaphragms by gluing piezoelectric disks at each of these points. To eliminate the issue of liquid wetting of the actuators the planar construction developed allowed for the separation of the piezoelectric actuator from the fluid flow. This planar peristaltic micropump exhibited a maximum pumping rate of 100 microliters per minute with an operation frequency of fifteen hertz coupled with a maximum outlet pressure of 60 mbar at zero flow [25], [26].

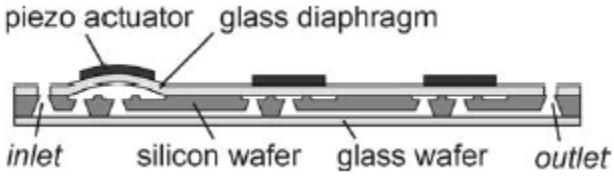

Figure 2.6: Planar Peristaltic micropump [26]

One of the first microdiaphragm pumps with passive check valves was presented in 1988 by Van Lintel et al. [27]. This type of pump utilizes a three layer configuration that incorporates two glass sheets that encase an anisotropically etched silicon wafer

(figure 2.7). Overall dimensions that were characteristic of this device were 12.5 mm for the pump diaphragm diameter and 7 mm for the diameter of the membrane valves. Through experimental testing it was determined that a stroke volume of 0.21 microliters was achievable with an actuation voltage of 100V. At this actuation level a maximum flow rate of 8 microliters per minute at 1 Hz operation frequency and a maximum pressure of 100 mbar were achieved.

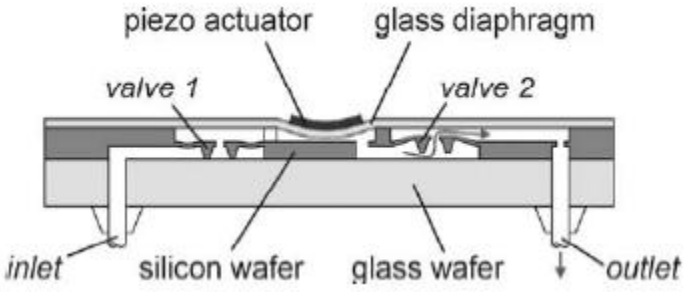

Figure 2.7: Microdiaphragm pump that utilized piezoelectric actuation [27]

Although the early contributions of Spencer and Thomas were widely unknown, the publications of Smits and Van Lintel firmly established the beginning of extensive micropump research and fabrication in MEMS technology. As of late an astounding amount of diaphragm and peristaltic micropumps are being developed. These micropumps are developed with varying valve configurations and geometries, fabrication technologies, and actuation principles. Numerous features and trends can be studied concerning the functional elements and properties of these devices that will be discussed in the following subsections.

2.3: Principles of Actuation

Currently and in past applications a wide-variety of actuation techniques for micropump technology has been available. Most principles that are common consist of piezoelectric [32-36, 38, 19, 21], thermopneumatic [28-31], electrostatic [39-41], and electromagnetic actuation [37-38]. Some other methods that are in the beginning stages revolve around shape memory alloys [23] and magnetostrictive effects. Each of these topics will be discussed in detail in the following subsections.

2.3.1 – Piezoelectric Actuation

Piezoelectric actuation is the most commonly utilized actuation method for micropump technology. This method was the first to be tested due to its attractive characteristics. This type of material provides a comparatively high stroke volume, a high actuation force, and a quick mechanical response. Also on a fabrication level piezoelectric material, such as PZT, is commercially available for quick integration into the particular fabricated device. Disadvantages of the piezoelectric material involve the high actuation voltages required and the procedure for mounting the piezo to the surface of the micropump device. It has been theorized that a systematic optimization of mounting procedure could significantly improve yield and reliability of this form of actuation [43-44]. Currently for hybrid integration procedure to be completed a very well defined gluing is performed. The procedure is crucial for proper optimum actuator performance, which is usually difficult to complete with minimal reproducibility. Due to

the difficulty in the placement of the piezoelectric material through gluing other studies have been performed involving screen printing [45-46] and thin-film deposition of PZT material as an alternative quasi-monolithic integration technique. Even though these techniques prove to be feasible, the results ranging from 1 micrometer displacement at 100V [45] are relatively small as compared to glued PZT bulk material with 15 micrometers at 100V [32]. Optimization techniques have been utilized for the geometric design to achieve higher strokes at lower voltages [32, 47]. In most instances in literature the actuation voltages of the optimized designs are in the range of approximately 100V with 130 voltage peak-to-peak [33]. This form of actuation demonstrates a vast improvement as compared to other micropump actuation methods that sometimes utilize commercial piezo buzzers without optimization. These types of devices demonstrate results of 400 volts peak-to-peak [34]. Studies that have been completed involving piezoelectric actuation that incorporate design optimization have provided lower actuation voltages. These optimized designs assist for the development of highly miniaturized electronic drives that allow low-power operation from a battery source.

2.3.2 – Thermopneumatic Actuation

Thermopneumatic actuation was first introduced and demonstrated by Van de Pol et al. [28] with a micropump fabrication similar to Van Lintels device (figure 2.8). As previously discussed the Van Lintels device utilized a piezoelectric disk of PZT. In the case of thermopneumatic actuation the PZT disk is removed and an air-filled chamber with an internal heat resistor was fabricated on the topside of the pump diaphragm. The

heat resistor is characterized as a free-hanging structure [28-30] achieving better thermal efficiency or simply attached to the pump diaphragm [31]. This form of actuation is a representation of a low voltage alternative to the piezoelectric actuation and eliminates the high voltage deflections associated with the electronic drive [28].

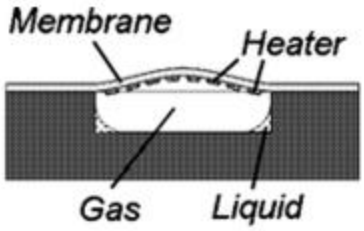

Figure 2.8: Thermopneumatic Micropump Actuation

An advantage of thermopneumatic micropumps is the capability of making a compact, small design, while generating displacements of the membrane up to several 100 micrometers resulting in high flow rates throughout the pump [29]. Fabrication and integration in silicon technology is easily achievable [30]. One of the main disadvantages of thermopneumatic actuation is the relatively long thermal time constant, which is especially crucial during the cooling process. Due to this constraint a limitation is imposed on the upper actuation frequency that tops out around 50 hertz. This actuation exhibits a power consumption that is in the range of several watts, which most of the time excludes the portable operation from a small voltage source. Operation and actuation at these power ranges cause a large amount of heating the transport medium that is problematic.

2.3.3 – Electrostatic Actuation

Illustrated in figure 2.9 is the first successful micropump encompassing electrostatic actuation from Zengerle et al. [40]. This method incorporates the first vertically-stacked modular micropump fabricated and designed in silicon. This actuation method is created from two silicon chips that incorporate the flexible pump diaphragm and rigid counter electrode in a capacitor-like configuration. Application of a high voltage to the capacitor electrodes provides an electrostatic attraction of the pump diaphragm, resulting in deflection of the membrane. After discharging of the electrodes the pump diaphragm returns to its original state. Utilizing this type of rapid actuation principle bidirectional fluid flow was observed at high operation frequencies. These frequencies were created by a time delay associated between the diaphragm movement and the slower valve switching [40].

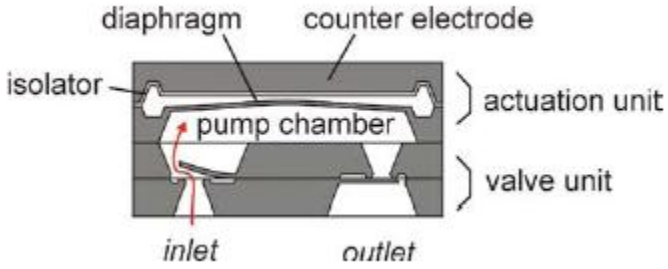

Figure 2.9: Electrostatic actuation principle for micropumps

This periodic motion of the membrane changes the volume and thus the pressure inside the micropump caused the fluid to propel in one direction. Preference of direction is accomplished by similar flow rectification techniques as previously discussed in the piezoelectric actuation methods. Capacitance between the diaphragm membrane and the electrode can be calculated as follows:

$$C = \frac{\varepsilon \pi d^2}{4l}$$

The force being developed by the electrostatic actuation to achieve the attraction between the two electrodes is given by:

$$F = \frac{1}{2}\frac{\partial C}{\partial l}V^2 = -\frac{\varepsilon \pi d^2}{8l^2}V^2$$

where V is the voltage applied between the electrodes, ε is the permittivity of the medium, d is the counter electrode diameter, and l is the distance separation between the two electrodes. It must be noted that since the force is dependent upon the medium, appropriate selection of the medium must be considered. A medium with appropriate high permittivity facilitates the usage of the electrostatic actuation even when the plates are far apart, due to the fact that force created will be sufficient to pump the fluid throughout the pumps entirety.

Forms of various electrostatic actuation methods provide operation frequencies up to several kilo-hertz, an extremely low power consumption, and full MEMS compatibility [39-41]. Results studied and tested involving electrostatic actuation principles have yielded major disadvantages. The major drawback is the significantly small actuator stroke (displacement) that is usually limited to displacement values of five micrometers actuated at 200V. Another disadvantage is the degradation of the electrode after long-term high voltage operations. The reason this deterioration occurs is due to the build up of surface charges on the insulator within the capacitor. This in turn reduces the internal electric field strength, thus diminishing the stroke (displacement). To overcome this problem studies are being conducted involving bipolar operation which is resulting in studies involving more complex electronic drive systems.

2.3.4 – Electromagnetic Actuation

Actuation of micropumps utilizing electromagnetism and metallic particles has been investigated briefly. This technology is in its early development stages and in most instances not very compatible with micropump technology [37, 38]. In theory when an electrical current flows through a wire under the action of a magnetic field, Lorentz forces come into action. This phenomenon is utilized for electromagnetic actuation by attaching a permanent magnet to the diaphragm and generating a current in the coil that surrounds the diaphragm. Lorentz forces deflect the diaphragm based on the electric and magnetic field interaction. This form of actuation requires voltages that are relatively low (~5V) and the actuator designs are simplistic as compared to previous actuation

methods which could be a possible advantage. Early researchers of this phenomenon such as Chang et al. (2007), Su et al. (2005, 2006) have attempted to improve and optimize the micropump diaphragm deflection characteristics. To do so the integration of permanent magnets and coils directly into the fabricated device has been accomplished (figure 2.10).

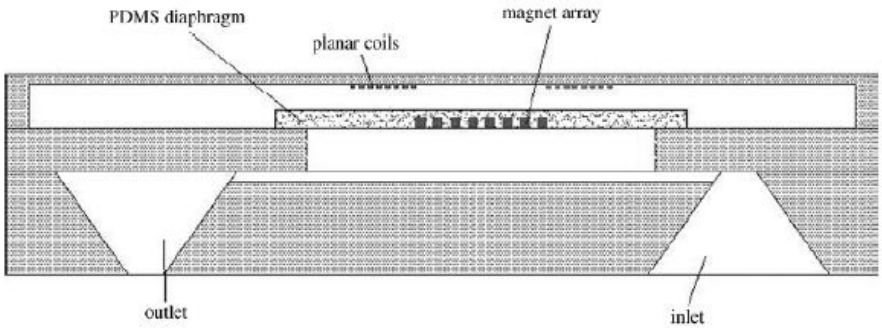

Figure 2.10: Electromagnetic micropump described by Su et al. (2005)

Several concepts have been investigated and tested. Yamahata et al. (2005) developed a permanent magnet cast where flow rectification was created by the incorporation of ball valves. Similar to this design, Pan et al. (2005) utilized a magnet attached to a DC motor coupled with relatively large induction coils. It was determined that the maximum flow rates ranged from 0.7 – 1.0 milliliters per minute with back pressures up to 30 kilopascals. Transgressions from these designs as of late researchers have been developing composite diaphragms that are embedded with magnetic particulates (Yamahata et al., 2005, Nagel et al., 2006). As of late Haeberle et al. (2007) has designed a micropump that requires attractive forces between a permanent magnet and steel disk to actuate the device. Currently, electromagnetic fluids have been utilized

to study the flow characteristics with certain micropump devices. The fluids possess magnetic particulate contained within a micropump design to study movement (Sim et al., 2006). Suspension of the magnetic particles is stable and preserves their material properties even after environmental and long actuation exposures. Through several tests and studies it has been concluded that electromagnetic actuation may be plausible. The overall mechanical electrical properties are comparable to thermopneumatic actuators with advantages of quicker mechanical response actuation.

2.4: Valve Design (Flow Rectification)

As previously discussed MEMS devices have been tested with various actuation methods. In most instances mechanical check valves such as moving membrane or flaps were utilized. Presently, there is an effort to design and fabricate such devices with the elimination of such valves. A host of drawbacks are present when such check valves are removed from the devices. Internal properties exhibited during fluid transport such as backward flow (reverse flow), pressure drop, and switching speed must be considered to achieve a working valveless micropump. External properties consisting of wear and fatigue are a critical issue to maintain a working device, which is becoming more predominant in polymer fabricated micropump devices. Lately, pushes toward filtering of particles is becoming a new idealistic approach for manufacturability and marketing. This is pushing the pumps to a new technology where valves would be non-existent to eliminate particulates blocking fluid flow, resulting in degradation of pump performance.

These new ideas of filtering are now making previously studied valve-based micropumps obsolete and less effective.

As of late consideration of a valveless micropump is being investigated. Eliminating valves can help avoid problems related to sorting particles contained with the fluid flowing through the micropump device. A device that eliminated valve control was first introduced by Stemme and Stemme [48]. The device utilizes a combination of nozzle/diffuser elements with flow-rectifying properties to imitate the function of a check valve (figure 2.11). According to Stemme and Stemme a maximum achievable forward-backward flow ratio of 2.23 can be tested and calculated for this configuration. This design allows for sufficient pumping characterization. A prototype illustrated in figure 2.11 was fabricated from a cylindrical brass body consisting of an outside diameter of 29 millimeters and evaluated with two different nozzle/diffuser geometries. Theoretically it was calculated that the forward-to-backward flow ratios 1.48 and 1.67 matched with the experimental data. It was reported that a maximum outlet pressure around 100 mbar was found for water dependent upon the nozzle/diffuser geometry configuration. Also it was noted this micropump was capable of pumping different gases.

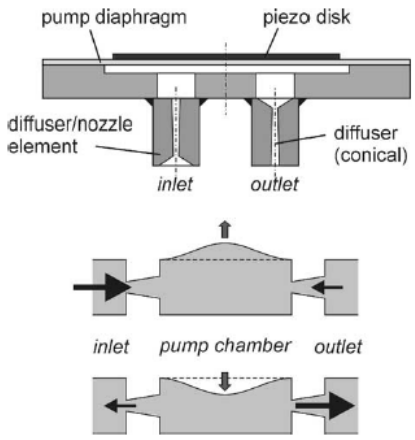

Figure 2.11: Valveless micropump actuated with piezoelectric material [48]

From this prototype various planar silicon micropumps have been the new plateau on which to develop these new valveless micropumps. In most instances to reduce inlet and outlet pressure pulses while increasing the pump flow performance a setup of two valveless micropumps was determined by Olsson et al. [49-50]. An additional planar design was developed by Foster et al. [51] on the foundation of a more complicated flow rectifying valve design proposed by Tesla [52]. Recently vertically stacked devices are beginning developed based on the works of Gerlach et al. [53] and Koch et al. [46]. They make use of the conical sidewalls of anisotropically etched silicon cavities to create a nozzle/diffuser element with minimal effort in fabrication processes.

Advantages of valveless micropumps revolve around the simplistic construction as compared to the micropump designs consisting of active valves and check valves. Pumping of particulate loaded mediums is more simplistic to achieve based on the open flow structure. As with advantages there is always a host of disadvantages with every device. If any overpressure at the outlet occurs a reverse flow of the fluid will become

predominant when the micropump ceases to operate, i.e. cutoff. To combat this phenomenon Stehr et al. [56-57] improved the blocking capability of the valveless micropump. Stehr discovered and tested the pumping effect of a bossed silicon diaphragm valve that was actuated periodically with the use of a piezoelectric bimorph. Based on the modulation of the gap width between the boss and valve seat resulted in a flow-rectifying behavior for the device. The pumping device was capable of transporting liquids and gases, while being able to reverse the direction of the fluid flow by varying the actuation frequency. It must be noted that reverse flow was still present during operation.

Currently, a new design and concept for a valveless micropump has been theoretical studied by Su and Pidaparti [58] utilizing the experimental fabrication methods from Cartin and Pidaparti [59]. The theoretical and fabricated micropump can be visualized from figure 2.12.

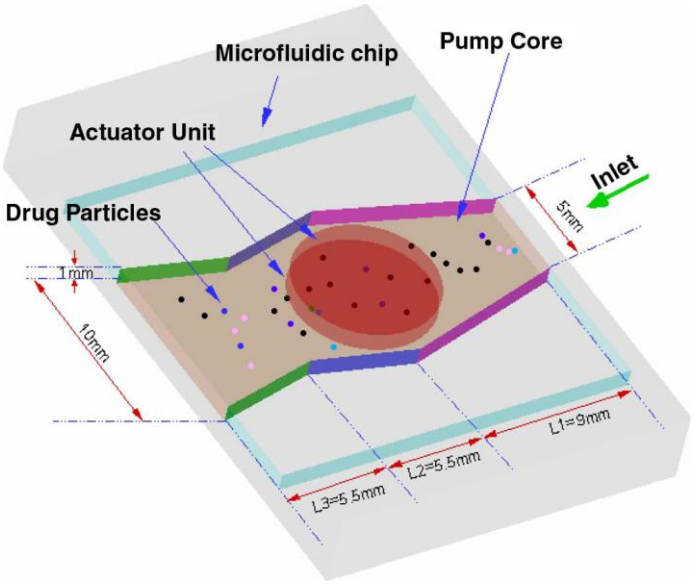

Figure 2.12: Schematic diagram of pump chamber [58]

Su and Pidaparti theoretically reported the relationship among the actuation frequency and the net mass flow rate and the time the particles took to exit the micropump which is illustrated in figure 2.13 [58]. To compare particle/fluid transport under steady-state flow conditions, the time interval during the particles passing through the static micropump is also reported in figure 2.13 [58]

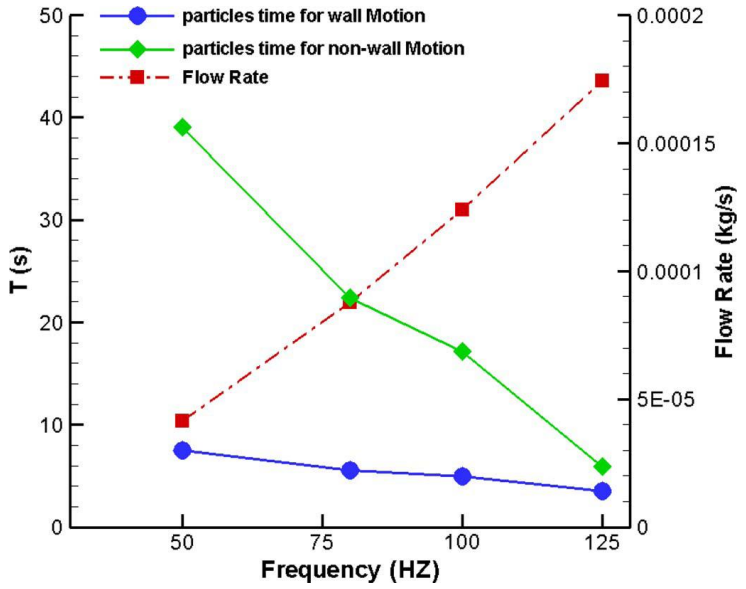

Figure 2.13 – Residing time, average mass flow rate versus the actuating frequency of the micropump [58]

It can be seen from figure 2.13 that the net mass flow rate is linearly proportional to the actuating frequency of the micropump. This characteristic is important for drug delivery applications as a means to estimate the time for the drug to be delivered through the micropump in correspondence to the specific actuation frequency.

For particle and fluid transport, the time that the particles move throughout the static micropump passageway nonlinearly depends on the flow condition. On the other hand, it was reported that the particle and fluid transport time versus the actuation frequency of the micropump tended to possess a linear property. This relationship is important for manipulation of particle drug delivery flow and estimation of the drug delivery time [58]. These theoretical results presented for novel actuation of the proposed valveless micropump may be suitable for both liquid and particle drug delivery systems.

Power consumption was another study investigated by Su and Pidaparti. Figure 2.14 illustrates the power input for the micropump at multiple operating frequencies for the present micropump with three nozzle-diffuser elements [59]. The power consumption required for the micropump is utilized to operate the actuator, and the energy is consumed during vibration of the fluid flow through viscous dissipation [58]. Through these theoretical studies of Su and Pidaparti it was discovered that more viscous dissipation is associated with the higher frequency vibration of flow, and the energy consumption is increased with the increase of the actuation frequency as illustrated in figure 2.14 [58]. To illustrate the advantages of the current micropump design the average net flow rate and power consumption for the Anderson micropump [60] were also calculated. It can be seen that the Anderson design provides less flow thus consuming more energy, while the current design is capable of pumping more fluid with less energy consumption.

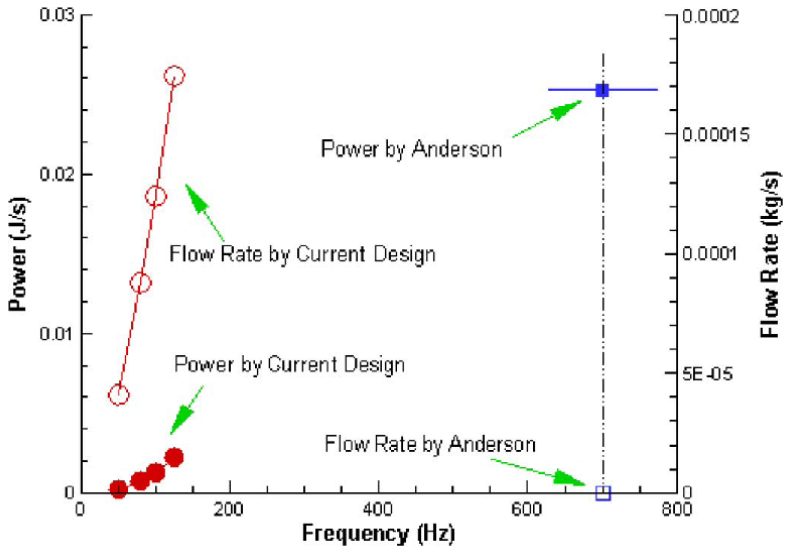

Figure 2.14: Power required, average mass flow rate versus the actuating frequency of the micropump [58]

In conclusion from Su and Pidaparti [58] a systematic theoretical computational study was completed investigating the flow and particle transport characteristics through a valveless micropump utilizing combined computational fluid dynamics and discrete particle transport methods. Results obtained from their studies demonstrated the feasibility of the valveless micropump for the transport of fluid and particulate drugs. It was concluded that the novel micropump design with vibrating actuation could transport fluid faster than previously studied micropumps. For fluid transport the complex flow pattern within the micropump results in relationships between mass flow rate of the fluid and actuation frequency which was linearly proportional. This proportionality depicts that fluid flow will continue to increase with actuation frequency, thus providing more and more flow. Additionally, the micropump exhibited less energy consumption during actuation as compared to other pumps.

2.5: Dosing (Operating) Properties

Common characteristics of the dosing properties are similar throughout the large number of micropump concepts and designs. Figure 2.15 and 2.16 illustrate the typical behavior of the pump rate as a function of the actuation frequency as well as the typical influence of varying outlet overpressure [32].

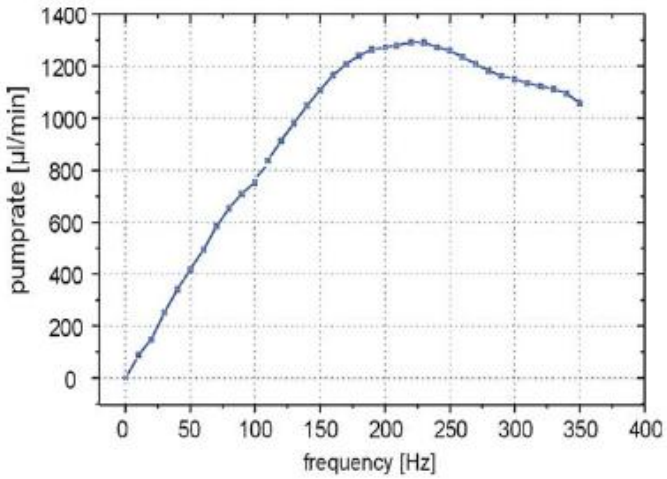

Figure 2.15: Typical Dosing Rates of a Micropump Diaphragm Pump
Pump rate as a function of the operation frequency [32]

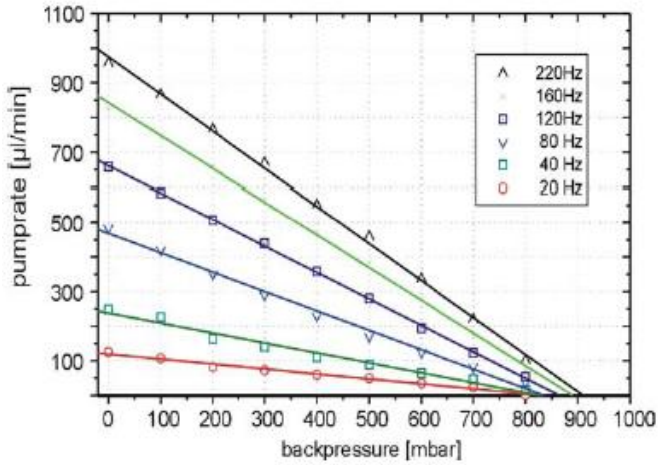

Figure 2.16: Typical Dosing Rates of a micropump diaphragm pump
Pump rate as a function of the applied outlet backpressure [32]

In most instances the rate of pumping (microliters per minute) is linearly increasing with operation frequency until a certain value is reached (figure 2.15 depicts ~150 Hz). Studying the linear behavior allows calculation of the stroke volume ΔV of the diaphragm actuator (approximately 120 nanoliters in figure 2.15). In the linear regime the actuation diaphragm possesses the capability to deliver the full stoke while the duration of the pumping cycle is still long enough to allow a full relaxation of the valve movement and all pressure-flow transients. Beyond the 150 Hz frequency it is observed that flow saturation is occurring. Flow saturation results from an increasingly insufficient relaxation and other effects associated with the individualized micropump design. The drop in the curve indicates that an increased energy loss is apparent (e.g. squeeze film damping) and the increasing time lag between the diaphragm and valve movement will lead to reverse pumping [40]. Figure 2.16 illustrates a backpressure curve that is similar among micropump devices. This curve illustrates a linear degradation of the present flow rate as soon as the outlet pressure begins to increase. At a particular value, approximately 800~900 mbar in this example, the pressure generated within the pump can no longer be high enough to open the outlet valve, thus ceasing operation. Similar characteristics have been studied for underpressure at the inlet.

Influence of varying pressure can pose a limit to the dosing accuracy of the micropump. In certain applications the utilization of high force actuation assists to extend the maximum backpressure values well beyond the operational values typically expected. For these types of cases the pressure dependency flow curve may become significantly flat ensuring an accurate dosing. Furthermore metric dosing can be made available through design considerations. In literature studies have been performed

concerning a precision micropump with a mechanical double limiter that allows for the setting of the diaphragm movement to a predefined value. This method allows for only a certain amount of liquid to be transported during pump operation. Coupling this concept with metric dosing studies have been tested depicting a flow range of 0-2 milliliters per hour and outlet overpressures and inlet underpressures of 200 and -100 mbar.

Previous micropumps described in the literary review were neither self-priming nor bubble-tolerant. Bubble tolerance means that even small gas bubbles within the pumping chamber could severely deteriorate the performance of the micropump devices. Many pump designs ceased actuation as soon as a gas bubble arrived at the inlet valve [63]. To eliminate this phenomenon complicated and unreliable manual priming procedures have to be performed initially. To resolve this issue a more practical approach was discovered by using a carbon dioxide to purge the dry device [61]. Carbon dioxide residuals contained within the pumps were easily dissolved when an aqueous priming solution was introduced, thus achieving complete filling of the device. However, the bubbles traveled through the inlet tube of the pump, which still remains an issue and cannot be eliminated.

These types of problems were discussed quite early during the beginning phase of micropump technology [27, 28, 62] especially the debate that a microdiaphragm pump with passive valves would be unable to self-prime due to several physical characteristics [56-57]. In 1996 the first self-filling polymer fabricated micropump was discussed by Dopper et al. [34]. The first theoretical study was performed in 1998 by Richter et al. To study self-filling characterization the basic laws of thermodynamics and fluid compression were utilized. Minimal values for the compression ratio, ε, which is the

ratio of the stroke volume ΔV, and the pump chamber volume V_o were calculated and validate with experimental data [63].

Typical compression ratio values for a liquid micropump were discovered to be on the order of 10^{-6}, whereas a gas operated pump currently requires a significantly higher compression ratio on the magnitude of 10^{-2}. Higher compressions must be achieved for a gas pump with wetted inner structures which is similar to the case of bubble-tolerance and self-priming pumps.

The aforementioned design procedures were consistently followed in the first and up to the smallest self-priming and bubble-tolerant silicon micropump that was discovered in 1996 by Linnemann et al., Woias et al. and published in 1998 [32-33]. A depiction of the micropump is illustrated in figure 2.17. The internal volume of the pump chamber was drastically reduced by combining chemical and mechanical fabrication methods of the middle wafer.

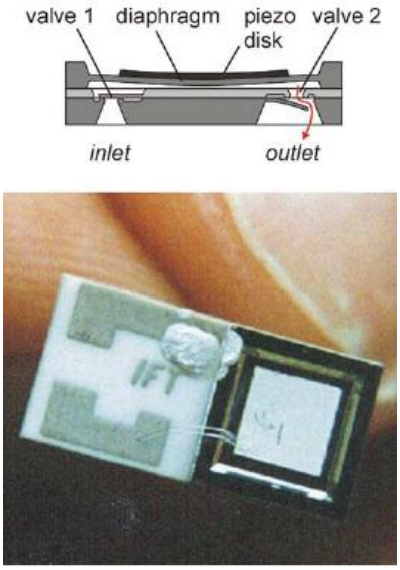

Figure 2.17: Self-priming and bubble-tolerant silicon microdiaphragm pump [32, 33].

As seen in figure 2.17 the micropump is actuated with a piezoelectric disk. Careful optimization was considered involving the piezoelectric actuator. The actuator was designed with the capability to perform comparatively high strokes at low chip dimensions. The first design exhibited a compression ratio of 1:9.4 that proved to be significantly high for self-priming and bubble-tolerance [63]. As testing progressed, later versions were continually optimized to achieve a compression ratio of 1:2 which is relatively high in relation to the small chip size of 7 mm x 7 mm x 1 mm [33]. Many other effective self-priming and bubble-tolerant designs have been discussed in literature [29, 34-35, 38, 65-66]. Some approaches turn out to be only self-priming from the dry state but no fully bubble-tolerant that results in a limited practical application [56 – 57].

2.6: Materials and Fabrication Technologies

From the early designs of micropumps that were designed via conventional fabricating methods [22, 23], micropump development has recently become an exclusive and novel domain for silicon microfabrication. In recent years microfabricated silicon and glass have been utilized successfully for pump designs, because these processes present high geometric precision. The drawback to micropumps in general is the long term fatigue, wear, and failure of mechanical moving parts, such as valves or flaps, which has been reduced by utilizing silicon micropump fabrication [33, 43]. Due to this discovery many high performance silicon micromachined devices have been recently demonstrated in industry [64, 65]. Even though positive advantages have been discovered, disadvantages do exist. As with most manufacturing processes, the

drawbacks center on the high fabrication costs and limited material choice, thus extending the search for a more affordable, effective, and efficient approach. Currently strides are being made in polymer microfabrication techniques such as injection molding [31, 34, 66], polymer hot embossing, and mainly stereolithography [36, 37]. Although the goal of a true low-cost efficient micropump is promised the aforementioned microfabrication techniques fall short of satisfactory results. Currently problems exist for these fabrication techniques due to the complexity of fabrication, expense of the procedures, and the material-aspect ratio that limits the life span of the device.

Since there has been high cost and complexities associated with silicon and glass microfabrication techniques, an intriguing concept has been presented by Piet Bergveld's group with the work of Bohm et al. [35, 38] who has completed research on electrochemical pumping principles. As an alternative to polymer microfabrication his research has utilized a conventional polymer molding process as a true low cost method to manufacture microdiaphragm pumps with electromagnetic and piezoelectric actuation. Currently research in this field is using established printed circuit board technology for microfluidic device development [29]. These relatively new ideas will not provide the performance of thoroughly designed silicon devices, but will provide an experimental result that is acceptable with moderate costs associated with fabrication. These techniques appear to be a popular choice among moderate performance and low cost applications, but still lack other requirements such as reproducibility and functioning stability.

2.7: Continuous Flow Micropumps

Continuous flow micropumps provide a direct energy transfer and steady flow. Several principles can be found in literature such as ultrasonic, magnetohydrodynamic (MHD), electrohydrodynamic (EHD), electrochemical displacement, and electrokinetic micropumps. The common characteristic that occurs between these micropumps is the easiness of the microstructures involved since there are no moving parts. Performance on the other hand is mainly influenced by the properties of the particular fluid which limits selection and narrowing the fluid field. For most continuous flow pumps a gas is not a possibility for fluid transportation through these devices.

Electrohydrodynamic (EHD) principle for fluid transportation was proposed in the 1960s and later researched in the 1990s by Bart et al. [68] and Richter et al. [69, 70] for their fabricated electrohydrodynamic micropump design. Bart and Richter utilized the EHD induction effect [68]. This effect revolved around the concept of generating and moving induced charges through at fluid-fluid or fluid-solid boundary layer and the EHD injection effect that is based on the electrochemical formation and movement of charged ions [69, 70]. Richter developed a micropump that consisted of silicon chips with identical grid electrodes fabricated with the use of anisotropic etching and sputter deposition of gold, sealed together in pairs, and placed into a flow channel (figure 2.18). High voltages were applied to the electrodes to inject ions into the fluid, which allowed the transportation of ions within the electric field between the electrodes to induce fluid movement through the electrode grids.

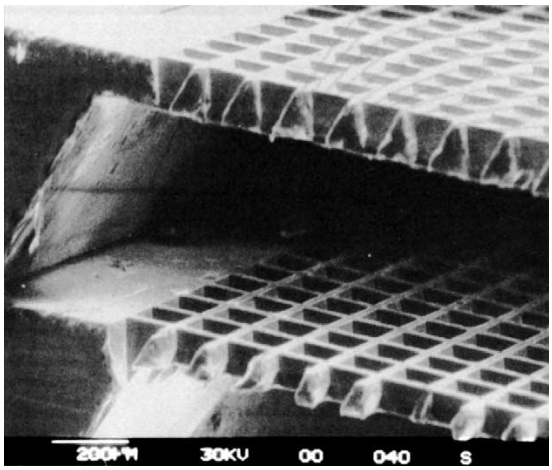

Figure 2.18: EHD Micropump [69].

Voltages applied to the EHD device ranged from 0 to 800 volts. At 800 volts it was observed that a net flow approximately 14 milliliters per minute was achieved utilizing ethanol as the transport fluid. Maximum outlet pressure was observed and recorded at 24 mbar with 700 volts of actuation. Pumping bidirectional was tested by simply reversing the polarity of the electrodes being applied to the grid [69].

Mostly all of the EHD pumping principles depend upon one critical factor, electricity. The electrical properties associated with this concept are permittivity and conductivity to transport the fluid through the microchannels. In most instances the electrical conductivity for this device must remain within the range of 10^{-14} and 10^{-9} Siemens (S) per minute, which crucially limits the EHD device to non-conducting and/or non-ionic fluids such as solvents [71].

Electrokinetic micropumping is the foundation for capillary micro-electrochromatography that has seen much progress in recent years. This concept has been studied and pushed forward in fabrication due to the lab on a chip concept in most

MEMS technologies. An interesting paper on this concept was published by Paul et al. [75] who studied electrokinetic transport of fluids in microporous media. The research focused on incorporating a fused silica capillary filled with porous glass beads with a platinum electrode affixed at either end. This technique allowed flow rates to be observed at a range of 0.1 microliters per minute with pressures of 200 atm, which is an astonishing record for most high-pressure micropumps (figure 2.19).

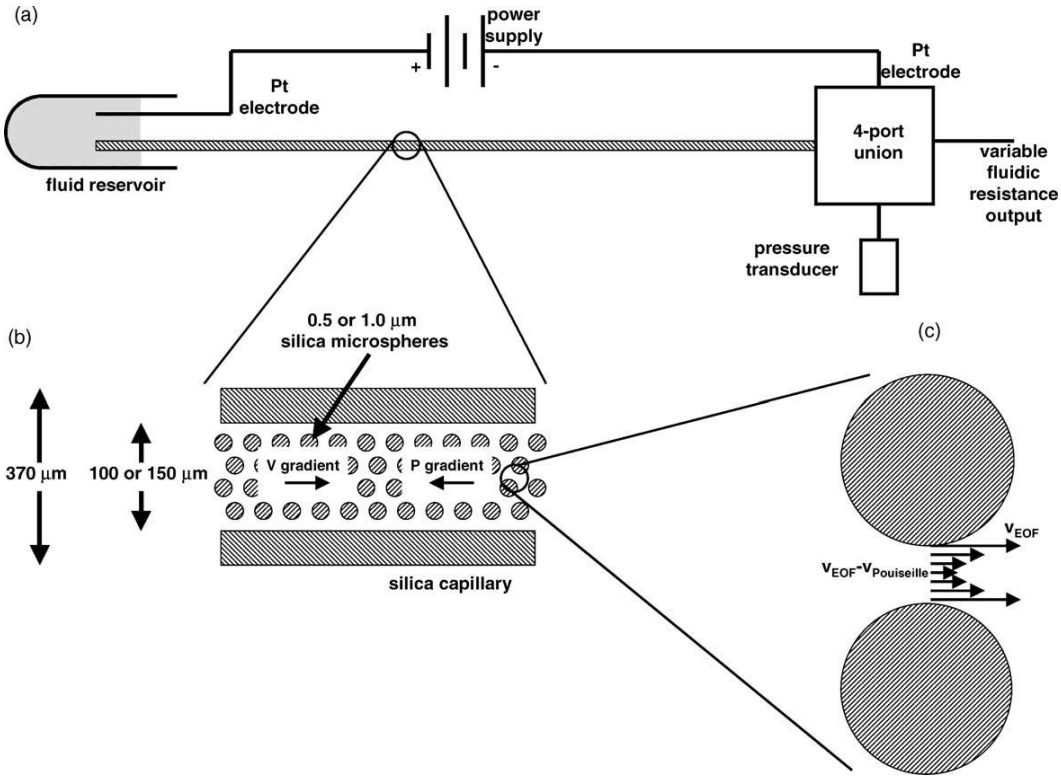

Figure 2.19: Electrokinetic Micropump [75]

Ultrasonic and RF pumping demonstrate the dragging force of a progressive mechanical wave [76, 77] or the "quartz wind" of a vertically oscillating surface [78] that is excited at a liquid-solid interface (sidewalls or endwalls of the micropump device). Devices such as the lamb-wave, piezoelectric ultrasonic, or RF transducers [76–78] have

been utilized for power generation resulting in frequencies reaching an ultrasonic range up to 10 MHz. These principles share one common property in literature which is a small flow rate in the range of microliters/minute coupled with minimal outlet pressure of roughly 0.13 Pa [76–79]. Most recently these applications are being pursued more extensively for fluid positioning or micromixing rather than the main search for fluid transport.

Magnetohydrodynamic (MHD) pumping incorporates the Lorentz effect in magnetic field theory. This method is focused on the use of an electric current that is induced between two electrodes located at side walls facing each other within the microchannel. The injection of charge helps create a transversal ionic current in the microchannel walls that is concurrently subjected to a magnetic field oriented at an angle of 90 degrees to current direction and microchannel axis. Based on the Lorentz effect, a Lorentz force will be generated acting on the ionic current in the solution thus creating a fluid flow within the microchannel of the device. By nature this pumping technique can be reversed simply by reversing the magnetic field vector or the electric current connections. Most micro-MHD pumps can only generate small values associated with flow rate in the range of microliters per minute and pressures in the range of 1~2 mbar. The flow rates depend strongly upon the ionic conductivity of the fluid being studied. In some cases electrolytic bubble generation can occur during DC operation where the injection electrode is placed. To correct this problem, further studies have concluded that the issue can be resolved with AC current injection that uses electromagnetism rather than a permanent magnet [81]. By operating both the magnetic coil and the current injector from synchronized alternating current sources, the Lorentz vector and fluid flow

direction remain in the same direction. Another issue is gas bubbles forming during operation, which currently is being prevented by driving the pump with high frequencies. The electrolytic generation of gas bubbles in turn has been presented in a study as a way to actuate a micropump to allow for high precision dosing systems within drug delivery devices. The concept of utilizing gas bubbles for dosing of drug delivery was first noted in publication of Bohm et al [83, 84]. He created a reservoir filled with electrolytic fluid with two immersed electrodes to create gas bubbles through current injection. Due to the gas bubble generation the volume increases within the microchannels thus generating a continual or cascading displacement that allows the fluid to be dispensed (figure 2.20). With the use of a closed-loop control for the gas bubble generation [63] this dosing capability allows for drug delivery quantities as small as 100 nanoliters with at least five-percent accuracy.

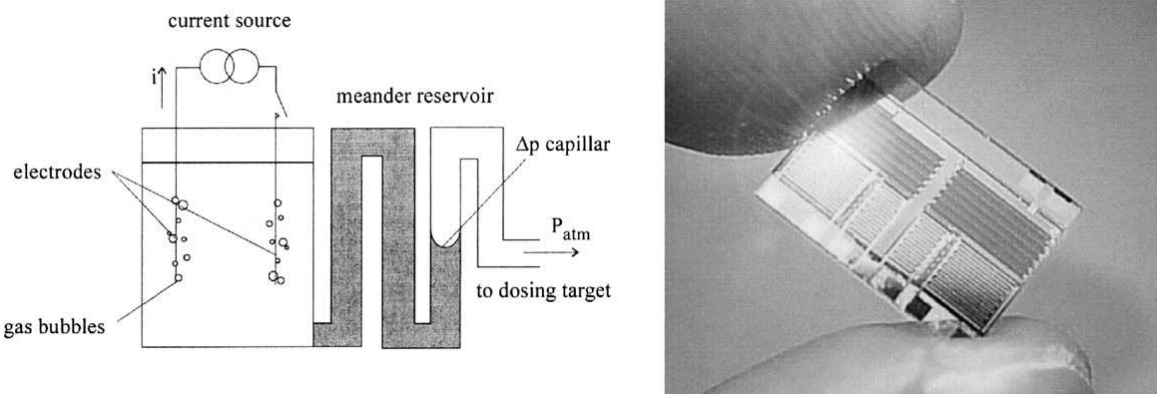

Figure 2.20: Electrochemical Displacement Micropump [83]

The newest of the continuous flow micropumps is the concept of centrifugal pumping. This particular method incorporates the force exhibited in a rotating microchannel system, usually an integrated disk, to transport fluid from center to outside perimeter [85, 86]. Fluid flow within these micropumps is manipulated and controlled by capillary stop valves within the fluid pathway that can be changed by a stepwise controlled increase of the rotation speed. The most distinct advantage of this type of pump is the concept concerning the presence of a single technological platform, usually a plastic disk with a fabricated microchannel, allowing a host of fluid transport procedures to be changed or integrated through design. A flow through chemical analysis is feasible without any additional efforts in fabrication. In most instances varying fluid density will influence the overall flow characteristics, because it is directly related to the centrifugal forces from the disk. Additionally, the other main factor is the surface to liquid interaction between the walls of the microdevice and the fluid, which requires a thorough control of the surface properties during the fabrication process to achieve results that can be reproduced.

2.8: Viscous Flow Micropumps

Growth and development of new drug delivery systems, microfluidic mixers, pumps and valves, devices for cell or protein patterning, microfluidic switches, and other various microfluidic devices have become more predominant in recent years. The development of these devices was brought about due to the need of circulatory fluid movement requirements to fulfill requirements of specific usages. Presently, micropumps are readily and easily obtainable to meet almost any need. The non-

mechanical version of the micropump does not have moving parts, which in turn improves the long term reliability of the pump. Pumps which are non-mechanical are limited by reduction in flow rate and pressure rise capabilities, the working fluids that can be pumped, the application of the pump, and the high voltage supply requirements. On the other side of the spectrum, mechanical pumps such as peristaltic pumps, membrane pumps, and rotary pumps have a vast variety of possible applications and working fluids. The drawback of mechanical pumps is that they are believed to be feasible only when they are larger than a particular size, because of the large viscous forces in the fluid at small pump geometries. Viscous forces are considerable at small scales, resulting in expanded pressure drops over small lengths for flow through a channel. Presently efforts are directed at developing a miniature pump that will produce controllable, constant flow rates from large viscous forces.

Viscous pumps are idealistic for such applications where pressure rises greatly and moderate to low flow rates are required. Currently several pumps have been developed that utilize the viscous shear to produce a pumping action. One such pump was developed which uses a spinning disk rotating over a spiral channel, resulting in a pumping action [87]. Conclusions from a large scale version of this particular pump are consistent with an analytic expression for flow rate and pressure rise [88].

Development and creation of a new viscous micropump has been created and is referred to as the Single-Disk viscous pump. This pump is capable of achieving easily controlled flow rates and pressure rises while maintaining simplicity and ease of manufacturing. Analytical equations, such as Navier-Stokes, are utilized to relate pressure rise and flow rate based on the pump geometry, rotational speed, and working

fluid properties. The single disk viscous pump is distinctive because it utilizes a viscous stress to create a pumping effect by employing one disk and a C-shaped channel [88], [89]. Figures 2.21, 2.22, and 2.23 illustrate the external and internal views on how the single-disk viscous pump operates.

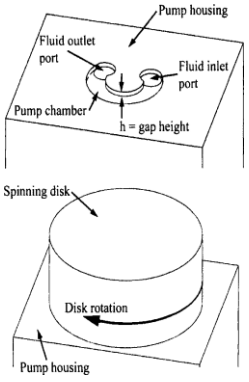

Figure 2.21: External and Internal Views of the Single-Disk Viscous Pump [88]

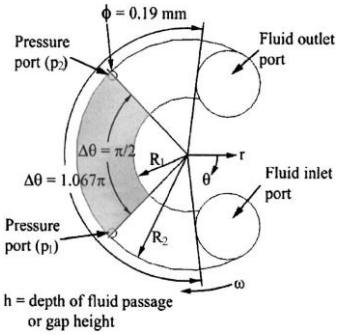

Figure 2.22: Configuration of the Single-Disk Viscous Pump. The shaded region of the pump chamber is used for flow analysis [88]

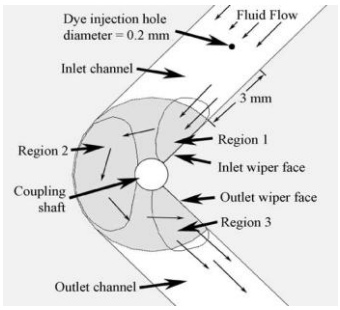

Figure 2.23: Top view of the Single-Disk Pump. Arrows indicate flow direction. Disk rotates counter clockwise [89].

The rotation of the single-disk creates a net movement of fluid due to viscous stresses imposed on the fluid due to the spinning disk. If the height of the channel that the fluid is flowing through decreases the Reynolds number reduces and the viscous forces become much more significant than inertial forces. This leads one to employ an assumption that allows the advection or inertial term in Navier-Stokes to be insignificant as compared to the diffusion of momentum terms.

Flow analysis of the single-disk viscous pump requires the use of Navier-Stokes equations. This involves derivation of an expression for pressure rise and flow rate in terms of pump geometry, rotational speed of the disk, and fluid properties required to properly design, develop, and analyze a function viscous single-disk pump [88]. The analysis that was performed for the single-disk viscous pump resulted in an expression for pressure rise and flow rate dependent on pump geometry, rotational speed of the disk, and the fluid properties (refer to figure 2.22).

For the single-disk viscous pump, an incompressible, steady flow of a Newtonian fluid, with constant viscosity and density was considered. Assumptions about height of the fluid passage were made as follows: $h << (R_2 - R_1)$. This assumption allowed for edge effects near the inner radius and outer radius to be ignored. It was also assumed that gravity was negligible and the rotational speed of the disks was slow enough such that the body force due to centrifugal acceleration is negligible compared to the forces produced by gradients of viscous stresses, and gradients of pressure (which is valid for low Reynolds numbers) [88], [89]. It must be noted that the gradients of viscous stresses are assumed to be more significant than the inertial or advection terms in the Navier-Stokes equation because the fluid motion is produced by viscous forces, and because the flow

passage height is small [88]. This results in the following Navier-Stokes equation, where inertial or advection terms are ignored, in cylindrical coordinates:

$$\frac{1}{r}\frac{\partial p}{\partial \theta} = \mu\left[\frac{\partial}{\partial r}\left(\frac{1}{r}\frac{\partial}{\partial r}(rv_\theta)\right) + \frac{1}{r^2}\frac{\partial^2 v_\theta}{\partial \theta^2} + \frac{\partial^2 v_\theta}{\partial z^2} + \frac{2}{r^2}\frac{\partial v_r}{\partial \theta}\right] \qquad Equation(1)$$

From equation (1) one can see that the circumferential pressure gradient (left hand side) is equivalent to the diffusion of circumferential momentum terms (right hand side). Therefore, it can be determined that the pressure gradient changes as the viscous stress imposed on the fluid by the spinning disk changes. It can also be noted that as viscous stressed increase then the pressure gradient will increase as well. An example of this would be increasing the rotational speed of the disk or increasing the viscosity of the particular fluid.

For the single-disk viscous pump analysis, flow in the pumping regime is (indicated by the shaded region in figure 2.22) considered. When dealing with a cylindrical coordinate system, the velocity $v_\theta >> v_z$, in order to allow for the z component of velocity at every location to be approximated as v_z goes to zero ($v_z = 0$). Additionally, if an assumption is made that $h << 3R_1(p/2)$ (circumference of the inner radius of the pump chamber), then the fluid flow in this region can be approximated as fully developed flow in the θ-direction. Since it has been assumed that the single-disk viscous pump is dealing with an incompressible, steady, fully developed flow, the continuity equation can be expressed as the following:

$$\frac{1}{r}\frac{\partial}{\partial r}(rv_r) = 0 \qquad \textit{Equation (2)}$$

From equation (2) the value of rv_r is equal to a constant. Also it can be stated that r = R_1 (inner radius wall), $v_r = 0$, this implies that $v_r = 0$ in the entire regime is being considered. Pressure gradients for the z and r directions can thus be given by the following:

$$\frac{\partial p}{\partial z} = 0 \quad \textit{Equation (3)} \qquad \textit{and} \qquad \frac{\partial p}{dr} = 0 \quad \textit{Equation (4)}$$

These equations (3 and 4) illustrate that the pressure gradient is variant in the z and r direction.

As the height of the fluid channel becomes thinner, when h / (R_2 – R_1) << 1, notable changes of v_θ across the z-direction over the distance h are much greater than the changes of v_θ in the r-direction over the distance R_2 – R_1. This result allows the first term on the right hand side of equation (1) to be ignored. Also, the second term on the right hand side of equation (1) is ignored due to the fact that fully developed flow was assumed earlier. Lastly, the fourth term on the right hand side of equation (1) is ignored, because $v_r = 0$. This allow for the following simplified equation:

$$\frac{1}{r}\frac{\partial p}{\partial \theta} = \mu\frac{\partial^2 v_\theta}{\partial z^2} \qquad \textit{Equation (5)}$$

The circumferential velocity (v_θ) does not change with circumferential position based on the fully developed and incompressible fluid assumptions previously stated. Therefore, since mass must be conserved, the pressure gradient on the left hand side of equation (5) must be constant in the θ-direction, which creates a linear rise in pressure in the θ-direction. The pressure gradient in the θ-direction is approximated utilizing the following equation:

$$\frac{\partial p}{\partial \theta} \approx \frac{\Delta P}{\Delta \theta} \quad \textit{Equation (6)}$$

Equation (6) the ΔP is the rise in pressure over the angle $\Delta\theta$. The rise in pressure between the two pressure ports ($p_2 - p_1$) illustrated in figure 2.22 and 2.23 is denoted as $\Delta P_{2\text{-}1}$, and the rise in pressure between the fluid inlet and outlets (figure 2.22 and 2.23) is denoted as $\Delta P_{\text{out-in}}$. Additionally, $\Delta\theta$ is the angle between the pressure ports ($\Delta\theta$=p/2) or between the inlet and outlet ports ($\Delta\theta$ = 1.067p) (figure 2.22 and 2.23) [88].

The velocity profile $v_\theta(r,z)$ is found by solving the ordinary differential equation given by equation (5), with the following boundary conditions for the single-disk viscous pump:

$$v_\theta(r,h) = 0 \quad \textit{and} \quad v_\theta(r,0) = r\omega$$

Thus the resulting velocity profile is given by:

$$v_\theta(r,z) = \frac{h^2}{2\mu}\frac{1}{r}\frac{\Delta P}{\Delta\theta}\left[\left(\frac{z}{h}\right)^2 - \frac{z}{h}\right] + \frac{r\omega}{h}z \qquad \textit{Equation (7)}$$

The volumetric flow rate is then determined by integrating the velocity profile over a radial cross section of the pump chamber, from z = 0 to z = h and from r = R_2 to r = R_1 as given by:

$$Q = \int_0^h \int_{R_1}^{R_2} v_\theta(r,z)\,dr\,dz = \frac{h^3 \ln(R_1/R_2)}{12\mu}\frac{\Delta P}{\Delta\theta} + \frac{\omega h(R_2^2 - R_1^2)}{4} \quad \textit{Equation (8)}$$

Equation 8 above defines the flow of the single-disk viscous pump as being dependent upon the pressure rise (ΔP), the pump geometry (R1, R2, $\Delta\theta$, and h), the disk angular velocity (w), and the fluid viscosity (μ) [88], [89].

This single-disk viscous pump has been developed and tested utilizing von Karman principles for viscous pumps. The single-disk viscous pump in question consisted of a 10.16 mm diameter disk that rotated above a C-shaped channel with inner and outer radii of 1.19 and 2.38 mm respectively. The channel heights were varied from 40, 73, 117, and 246 micrometers. Fluid ports were located at each end of the viscous pump to allow for entry and exit of the fluid. Advantages of the single-disk viscous pump are analytic tractability, a vast range of possible rates of flow, simplistic design, constant flow, flow rate independent of fluid viscosity, planar structure, well controlled flow rate, and the ability to pump delicate fluids with disruption or damage [88]. Design and fabrication of single-disk pumps are quite simple and can be possibly fabricated through injection molding technology or microfabrication techniques. The chamber for the viscous pump is symmetric, allowing for easy reversal of the flow direction simply by changing the direction of rotation. Flow rates and pressure rises were well represented

by equation (8) for rotational speeds of 100 – 5000 rpm, fluid viscosities of 1 – 62 mPa s, flow passage heights of 40 – 246 micrometers, pressure rises of 0 – 31.1 kPa, and flow rates of 0 – 4.75 ml/min. It must be noted that deviation between equation 8 and experimental data increases for Reynolds numbers that exceed 110 [88], [89].

The theoretical and experimental rises in pressure show a nearly linear relationship for variation in flow rate. Pressure rise increases as the flow passage height reduces for a particular speed of rotation. When $\Delta P = 0$, maximum volumetric flow rate is achieved and is found to vary linearly with rotational speed. Volumetric flow rate for the single-disk viscous pump is independent of the fluid viscosity. Also, the pressure rise through the pumping chamber can be raised by increasing the span of the circumference of the shear channel or by reducing the height of the fluid passage. On the other hand, flow rate in the pumping chamber can be increased by increasing the height of the fluid passage, increasing the width of the pumping chamber, or by increasing the speed of rotation [88].

The overall efficiency of the single-disk viscous pump was determined using the equation $\eta = \Delta PQ / T\omega$. Usually a typical efficiency of 0.25 or 25% occurs at a rotational speed of 1000 rpm, a pump chamber height of 117 μm, and water as the working fluid. Such a value does not take into account for any type of motor losses [88], [89]. This type of pump can be utilized for an array of applications such as mixing fluids, transport of chemical and biomedical fluids, drug delivery, electronic cooling, and sorting particles.

2.9: Micropumps and Micro-Total Analysis Systems

Micro total analysis systems (μTAS) is a concept first introduced and proposed by Manz et al. [90] that has created widespread research to incorporate chemical sensors and sample processes into highly fabricated miniaturized self-sufficient analytical systems. Stepping away from the microfabrication (miniaturization) idea and focusing mainly on the integration of fluid flow analysis and chemical sensors has provided several advantageous ideals. Combining ion-sensitive field-effect transistors (ISFETs) and micropump fabrication technology with micro total analysis systems research has helped develop these issues.

In the 1990s Gumbrecht et al. [91] established a microfluidic concept that became quite popular and well known in the micro-total analysis systems research dealing with an ISFET based pH detection system for clinical monitoring. The approach was founded on the combination of microchannels, syringe pumps, and monolithic ISFET arrays. This approach utilizes the excellent pairing of chemical and electrical properties within a monolithic sensor array coupled with an appropriate liquid handling component to suppress the common noise disturbances. Additionally, a stable electrochemical reference potential is matched that permits the application of metal reference electrode as opposed to the fragile, redundant maintenance of glass reference electrodes.

These fabrication techniques have been studied and evaluated. The fabrication studied [92] used ISFET sensors coupled with Si_3N_4 gate insulators that are identified as possessing relatively high drift and hysteresis properties. Even though these gate insulators exhibited such traits, it turned out that a pH detection accuracy of 0.002 was able to be achieved in series measurements with a constant sample pH. As the study was

evaluated using alternate pH steps of +/- 1 unit, which provided a worst case scenario, the hysteresis effect of the ISFET sensor was still greatly reduced to approximately 0.01 – 0.02 pH degrees. This type of behavior is highly favored during the study and was also tested under more practical conditions, such as organ systems, where pH deviations of 0.04 could easily be detected [93].

Besides the high measurement precision exhibited, Gumbrecht's principle does not require a physical contact between the solution sample and the micropump. His approach is well suited for a realization with micropump technology which is more frequently prone to contamination from external sources. This advantage was first studied by van der Schoot et al. [94] with a hybrid micro total analysis system fabricated from two microdiaphragm pumps and potassium (K^+) sensitive ISFET as the sensing element. Based on measurement curves established from this research the systems were capable of measuring potassium concentrations with high precision and consistent reproducibility [94]. A number of similar micro total analysis systems have been studied recently in the 1990s, based either on micropump technology [95, 96] or on conventional pumps [97]. The vast rise of research on such devices created the foundation for a dedicated conference series on micro total analysis systems in the mid-1990s. During this conference some predominant results were concerning the micro-total analysis system concept as a combination of mechanical micropumps, microchannel systems, and chemical sensors resulting in similar concepts of flow-through chemical analysis [98, 99]. From these studies a major drawback came to be known involving performance deficiencies associated with these devices. Several of the studies at this time were not including basic requirements such as self-priming, bubble tolerance, high system

complexities, interferences between sensors and actuators, and problems associated with hybrid or monolithic integration. These factors that were overlooked and not well presented have slowed the progression toward fully integrated systems.

Currently the focus on micro-total analysis systems research has begun to progress towards electrochromatography. Advancement in this direction has prompted further development of electrokinetic microfluidic pumping in association with all microfluidic devices. Traditional flow-through analysis ideas of centrifugal fluid transport have become a better alternative to mechanical micropumps [100, 101]. Although recent studies have focused toward micro-total analysis systems, it must be noted that research involving fluid handling, fluid transport, and chemical analysis through microdevices has provided a very effective and constant simulation of microfluidic research.

2.10: Conclusions

It can be seen from the literary review of micropumps that an amazing multitude of pump designs have been fabricated with various technologies. The beginning research and development of these devices began in the 1970s and was pushed toward the MEMs technology in the early 1990s. The main component of this research focuses on the exploration of new ideas concerning the conceptual design of these micropumps. Research that has been conducted provides a positive view on the whole spectrum of micropump concepts, fabrication technologies, actuation principles, and valve designs for these types of devices. The overall goal of each investigation was to obtain a novel

microfluidic device while improving the performance. As discussed, the combination of microactuation, microfabrication, microfluidics, and applications presented in history have developed a platform for a wide array of MEMS research.

From the research conducted during the early stages of micropump technology in the 1970s a host of advantages and disadvantages were observed. As the technology progressed into the 1990s, studies began to focus on alternative fabrication technologies and significant micropump related issues. Resulting from these studies the performance of specific micropumps has been consistently increased. Features such as self-priming, bubble tolerance, high flow, pressure capabilities, and precision dosing have been addressed and solved in a particular manner.

The biggest issue as the history of micropumps is studied is the commercialization process that is still in the beginning stages. Through the years it has been understood that MEMS devices as well as other technical products in the realm of pump design require an astonishing long duration of time from the conceptualization to the manufactured product [102]. Therefore, it is most important to understand the positive aspects that have been researched, while improving upon the negative drawbacks that have been discovered. Currently, the positive points for pump design focuses upon the mature multidisciplinary knowledge that has been published through research in the past four decades. It has been noted that the optimization and fabrication processes have already reached a high level [44]. Since the first micropumps the availability of such devices have been focused in areas of life science and biochemical analysis, while other designs are reaching that point [64-65].

Presently and in the future the main concern for the devices to be acceptable and readably useable relies on two main points. The first is the fabrication techniques and the second is a combination of performance and reproducibility. Utilizing an optimum fabrication process coupled with a fast, precise, reproducible process will assist in obtaining a micropump device that will possess high performance characteristics. Even though perfection and constant reproducibility through manufacturing is still needed a strong focus is still required within the commercialization and basic research. There is still a vast amount of knowledge required to understand the fundamentals processes occurring within micropumps and microfluidic devices such as influences of medium properties, liquid-surface interactions, and long term effects from usage. While micropump technology appears to be almost forty years old it is still a relatively new idea. Micropump technology is still in its infancy requiring more research concerning the design, fabrication, actuation, and manufacturability techniques to make this type of device a commercialized product that is effective globally in the technological field.

As discussed in this chapter micropumps, part of most microfluidic systems, typically control the movement of small fluid volumes. A number of micropumps have been designed, fabricated and investigated for use in many applications including drug delivery systems [22-24], insulin injectors [25], artificial prostheses [26, 27], liquid cooling systems [28, 29], fuel cells [30], space missions [31, 32], as well as macromolecular and cell analysis [33]. In general, micropumps consist of two nozzle/diffuser elements, which transport fluids from an inlet to an outlet, through pumping action, and have been successfully employed in many applications. One of the drawbacks of the nozzle/diffuser micropump is the back flow resulting from the operating

cycle [34]. This back flow results in decreasing the flow rate, and leads to an increase in power/energy consumption.

Several studies have been carried out to improve the performance of nozzle-diffuser valveless micropumps. In addition to geometric arrangement, several types of actuations including electrostatic, piezoelectric, pneumatic, thermo-pneumatic, magnetic and shape memory alloys have been used in micropump designs [35-42]. Experimental tests and numerical simulations of valveless micropumps with diffuser-nozzle elements have also been completed to assess their performance. Stemme and Stemme [48] manufactured and experimentally tested valveless micropumps driven by an oscillating diaphragm. Olsson *et al.* [49, 50] manufactured the diffuser element of valveless micropumps and investigated the influence of the shape associated with the length of diffuser, the width of the throat, and the divergence angle of the diffuser on the performance of the micropump. Anderson *et al.* [60] evaluated the influence of density and viscosity of the fluid on the pump performance with implications for biochemistry.

To examine the versatility of the nozzle-diffuser configurations, and to improve the backflow conditions, a new micropump design consisting of three nozzle-diffuser elements was designed, fabricated and tested to evaluate its performance in this research. The effect of fluid viscosity and actuator location was also investigated and the results are presented and discussed.

CHAPTER 3 – Fabrication and Manufacturing Methods

3.1: Overview of PDMS Micropump Design

The proposed design of the micropump is shown in Figure 3.1 in the beginning stages as an idealized concept shown in SolidWorks. This micropump has gone through several different design concepts. Initially the first design (Figure 3.2) consisted of four walls.

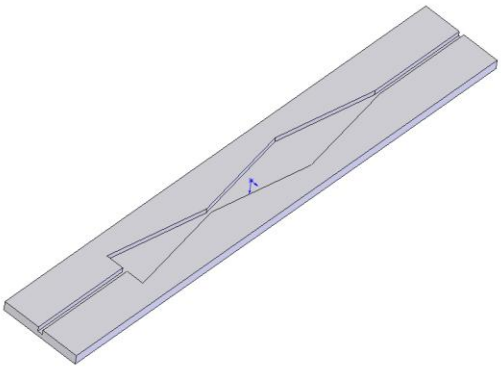

Figure 3.1: Three-wall Micropump Design Concept

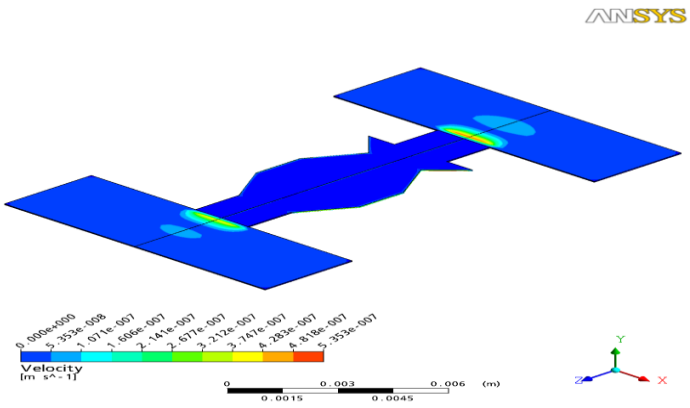

Figure 3.2: Fluid Velocity of Four Wall Micropump

From the analysis of the four wall micropump it was determined that the fluid velocity was very minimal from the inlet to the outlet side of the micropump. From this simulation it was determined that a four-wall pump would not give the proper flow that is desired. Also the height that was tested was approximately one-hundred micrometers. At this height the micropump would collapse from pressure applied to the top. Sidewall actuation was studied and the walls were not high enough to give proper deformation to provide the proper fluid flow. To generate optimal fluid flow it was determined that a three-wall micropump should be designed with inlet angles between 5 ~ 20 degrees. The height of the micropump chambers must be approximately four-hundred micrometers or greater to eliminate collapsing of the pump.

Studies of the three-wall micropump were initially tested and results were formed with the use of ANSYS as previously explained in chapter 2. From this analysis it can be determined that the flow rate will be optimal and the micropump will possess good flow characteristics. An example of this analysis is shown in figures 3.3 and 3.4.

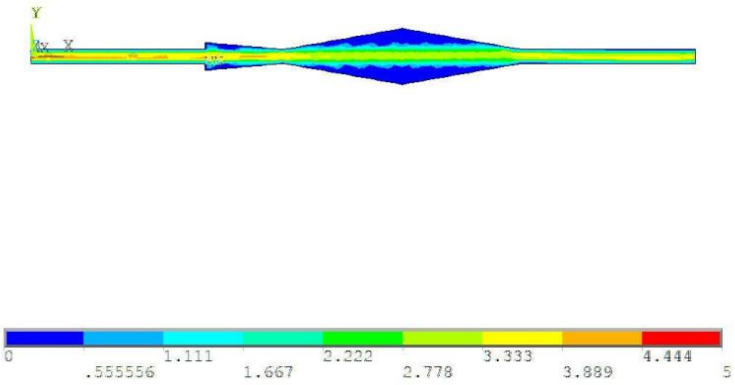

Figure 3.3: Fluid Velocity Plot

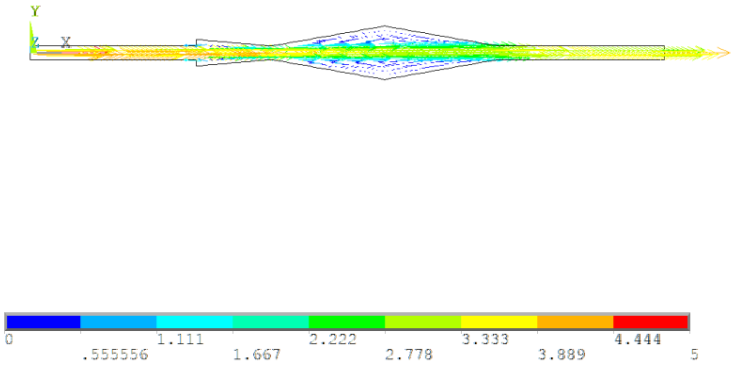

Figure 3.4: Fluid Vector Plot

Two methods for fabricating and designing the micropump have been initiated and completed. The first process involves the VMC Microelectronics Laboratory at VCU, and the second involves Design Optimization and Rapid prototyping Techniques. In the VMC Microelectronics Lab, an IC Station file of the micropump design was created and used in the clean room to create a mask. A silicon wafer was then chosen to begin the build of the micropump. On the wafer a layer of SU-8 negative photoresist was applied with an overall thickness of fifty micrometers. Diffusion lithography was then performed to create the micropump pattern in the photoresist layer. PDMS was then successfully poured into the pattern, resulting in the desired micropump in Figure 3.5.

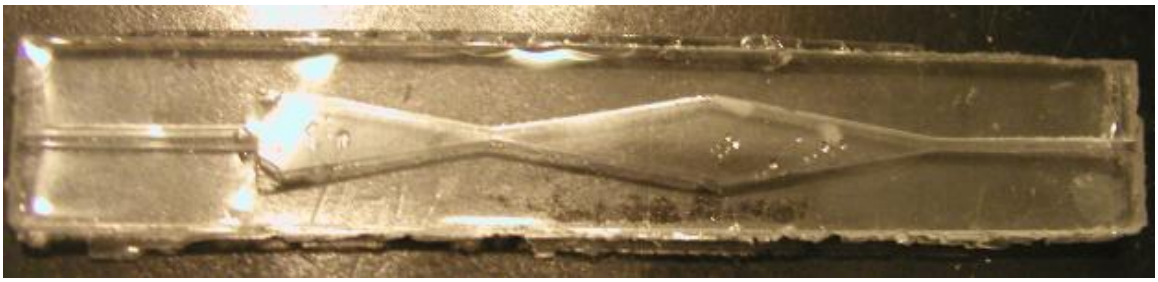

Figure 3.5: PDMS Micropump

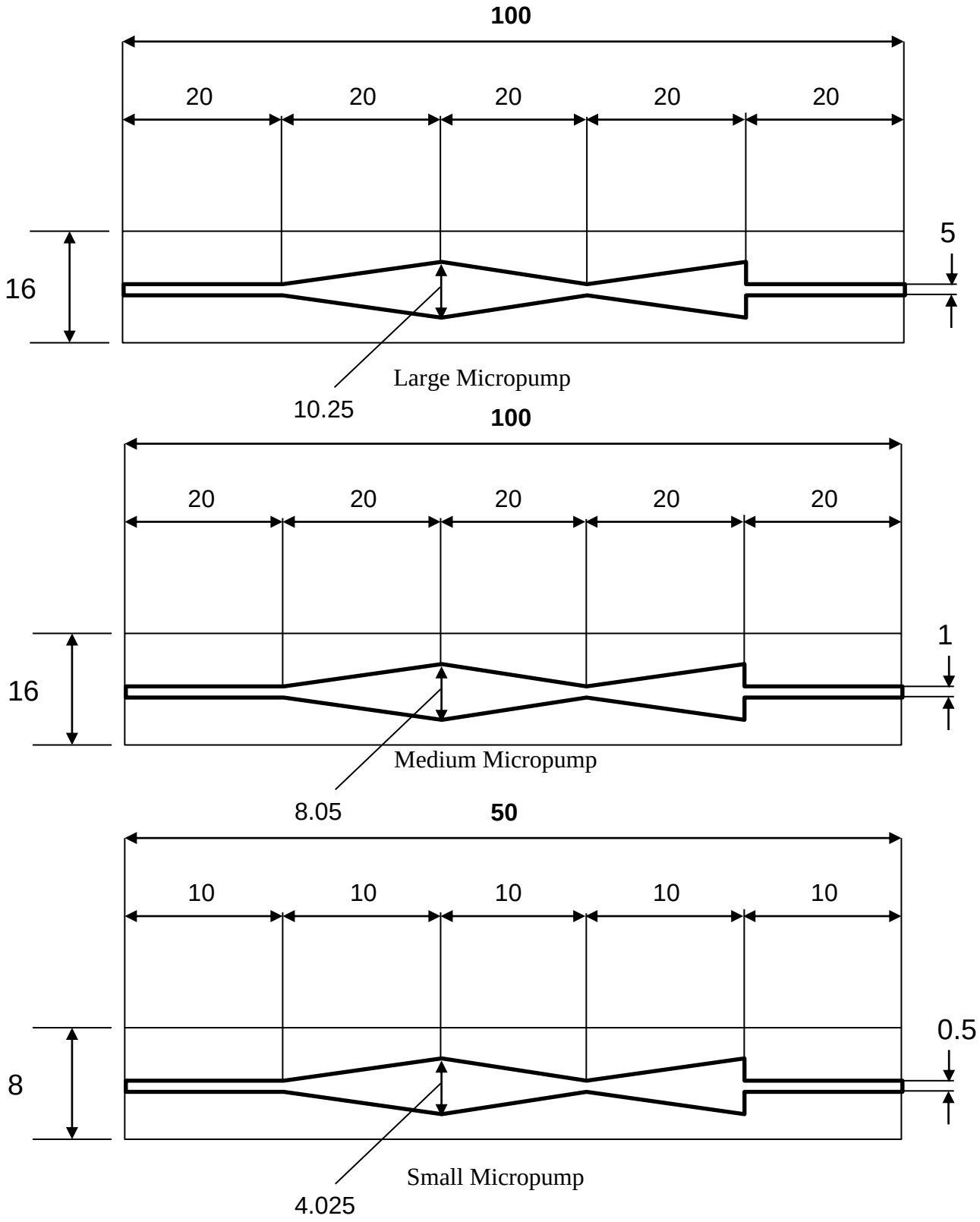

Figure 3.6: Dimensions of PDMS micropumps

The second fabrication process involves SolidWorks and Rapid Prototyping Machinery. A particular rapid prototyping machine was utilized in the fabrication, which involves stereolithography. Stereolithography is a common rapid prototyping technique used for producing parts with high accuracy and good surface finish. This form of rapid prototyping is performed by a Stereolithography Apparatus (SLA). Stereolithography is an additive fabrication process that utilizes a vat of liquid UV curable photopolymer "resin" and a UV laser to construct parts or models one layer at a time. For each layer, the UV laser beam traces a part cross-section pattern on the surface of the liquid resin. The exposure to the UV laser light solidifies and cures the pattern traced on the resin, thus, adhering it to the previous layer below it.

Once a pattern has been outlined (traced), the Stereolithography's Apparatus elevator platform descends by a single layer thickness, typically 0.05 millimeter to 0.15 millimeter (0.002" to 0.006"). After the platform has descended into the resin, a resin filled blade squeegees across the part or model's cross-section. This allows the part or model to be recoated with fresh resin material. Once the part or model has been recoated with a new resin layer, the subsequent layer pattern is traced, thus adhering to the previous layer. A complete three-dimensional part or model can be formed by this process. After the parts are built, they are removed and cleaned of excess resin by simply immersing the part in a chemical bath. Once the part has been fully clean it is then cured in an ultraviolet oven.

Stereolithography requires the use of support structures to adhere the part or model to the elevator platform. These support structures also prevent certain part geometries from deflecting due to gravity as well as accurately holding the two-dimensional cross sections in place to resist lateral pressure from the re-coater squeegee blade. Supports are usually generated automatically during the preparation of the three-dimensional CAD files for use in the stereolithography

machine, even though the supports can be changed manually by the user. Once any part or model is produced using stereolithography all supports for the part must be removed manually by the user.

Utilizing SolidWorks and SLS provided a mold for the micropump in question. The SolidWorks file developed is shown in Figure 3.7.

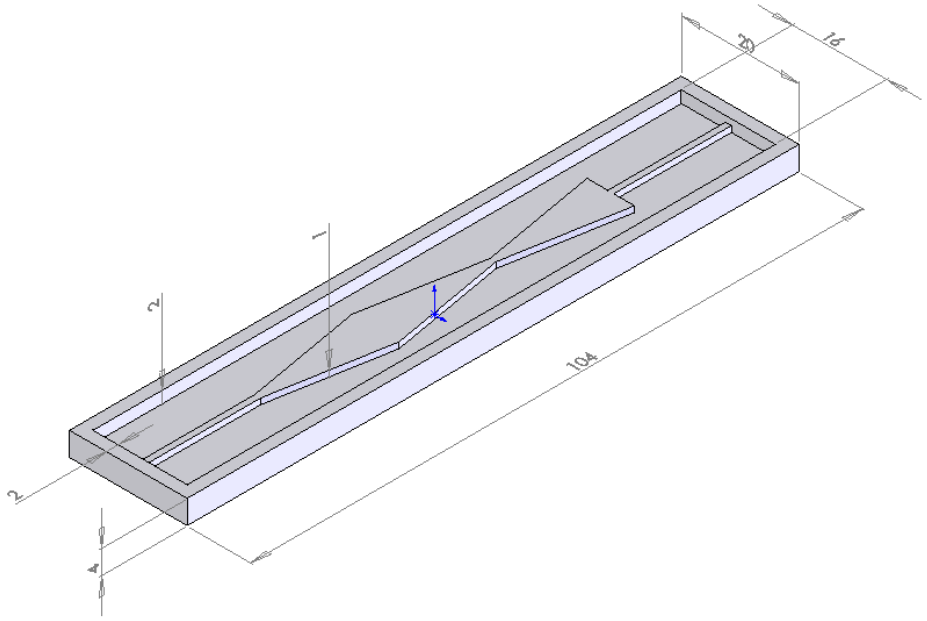

Figure 3.7: Dimensions of Micropump Mold

After this mold is created, PDMS material can be mixed and poured into the mold. Once cured and developed, the PDMS micropump can be removed. This process proves to be less time consuming and consists of minimal steps.

3.2: PDMS Micropump Fabrication Method I - VMC Cleanroom MEMS Process

3.2.1 – Fabrication and Manufacturing of an Electrostatic Actuated Micropump

Fabrication of an electrostatic actuated micropump has been proposed and is illustrated in figure 3.8. The flow region of the micropump is actuated by six electrostatic pump chambers. Each pump chamber will exhibit a thin flexible wall separating it from the central fluid flow region. These pumping chambers will consist of an electrode on top and bottom surfaces. The top surface will consist of PDMS which will allow flexibility of the chambers during actuation. Each of these electrodes can be actuated with independent voltage sources to drive the pump. As voltage is applied the electrostatic phenomenon will attract the two electrodes together. This movement will allow pressure to increase within the chamber and result in the thin wall surrounding the chamber to expand into the flow regime. The flow region is divided into three walls with chambers for pumping located on each side to apply a pulsating sequence of activation. Actuation electrostatically will exhibit a cascading motion for moving the fluid.

Fabrication processes which are the main focus of the research are centered on a novel fabrication technique for microfluidic devices based on a common polymer material polydimethylsiloxane (PDMS). The micropump will be created, constructed, and fabricated from a generated wafer procedure in the VMC cleanroom. Metal electrodes will be placed upon the PDMS fabricated pump and sealed to another glass wafer with electrical connections. This process will be discussed in detail within this section.

3.2.1.1 – Overview of the Electrostatic Actuation PDMS Micropump

The top view of the micropump design is illustrated in Figure 3.8 below. In this illustration, the micropump utilizes an electrostatic actuation method. The pump consists of a flow channel with three successive chambers, with each section of the flow channel possessing actuation chambers on each side. These actuation chambers consist of a thin wall (lining the flow channel), three thicker walls, and electrodes on the top and bottom. Electrodes are on the top and bottom of each actuation chamber. Voltage applied to the electrodes provides electrostatic attraction, compressing the actuation chambers and causing the thin sidewalls to bulge into the flow channel, pressurizing each section of the pump. Successive sinusoidal actuations of the three chambers will cause a net fluid flow through the pump.

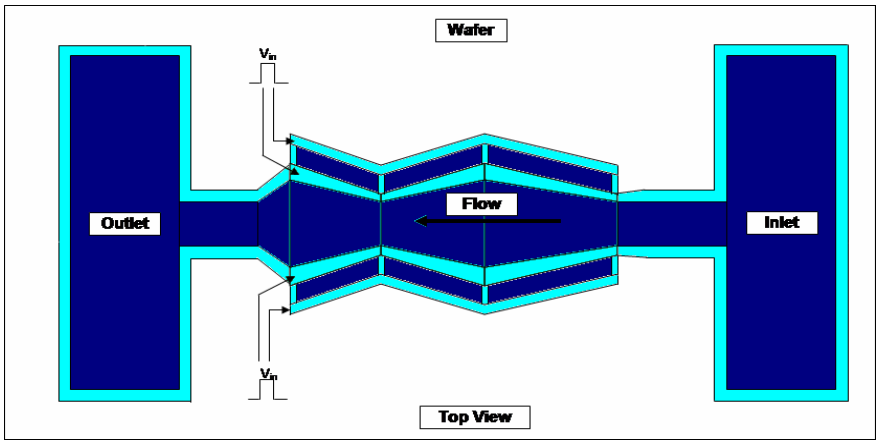

Figure 3.8: Proposed Micropump Design with Nozzle/Diffuser Elements

3.2.1.2 – PDMS Micropump with Electrostatic Actuation Fabrication Process

The PDMS micropump is fabricated in two parts: one molded PDMS layer and a second metalized glass substrate. The PDMS molded layer contains the flow channel, actuation chambers with top electrodes and inlet and outlet reservoirs. This molded PDMS layer was created and peeled from a silicon wafer with an SU-8 negative resist pattern. The bottom substrate is a glass wafer with the lower electrode pattern. Bonding both wafers together creates a sealed, functional micropump.

3.2.1.3 – Photo Mask (IC Station) Method

Layouts for the micropump design were generated using the Mentor Graphics layout tool (IC Station) and a mask set for the micropump design was created using an Electromask pattern generator. Integrated Circuit (IC) station is UNIX based software that allows the user to design the particular layout for microelectronic devices. Illustrated below in figure 3.9 below is the IC station software with the electrostatic PDMS micropump design layout. This particular layout consisted of a reference layer (utilized to align all layers), PDMS layer, Metallization Layer, and Wafer Metallization layer. Each of these layers required a separate photomask generated and created in the VMC cleanroom. The photomask generator that must be operated with care and the photomasks that were generated and created are shown in figures 3.10, 3.11, and 3.12.

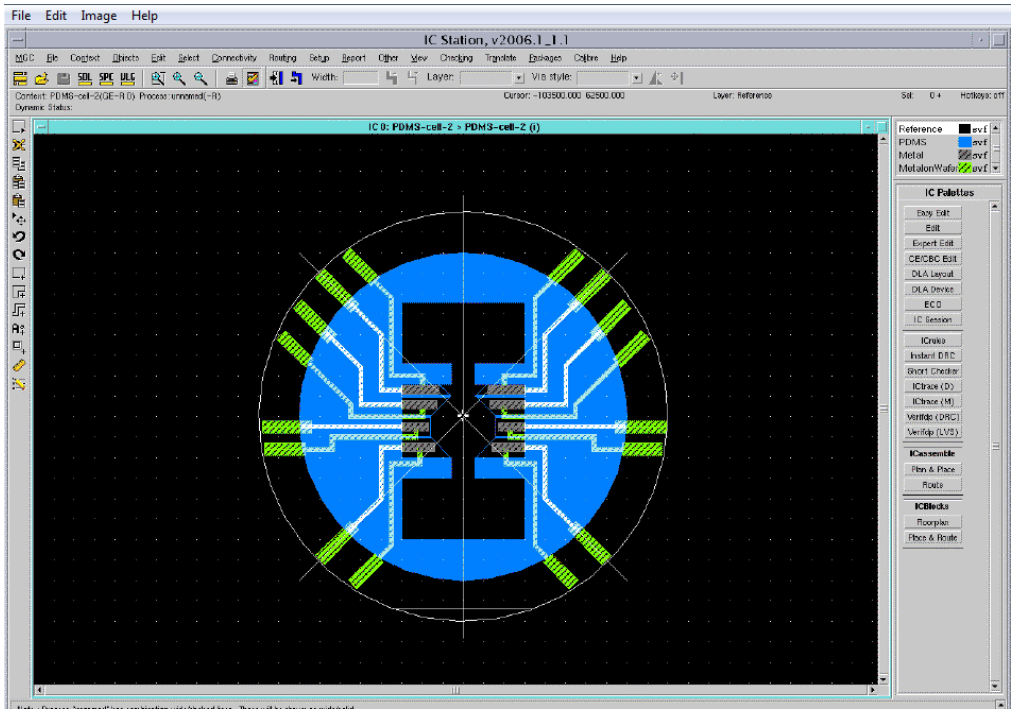

Figure 3.9: IC Station Software depicting Electrostatic PDMS Micropump

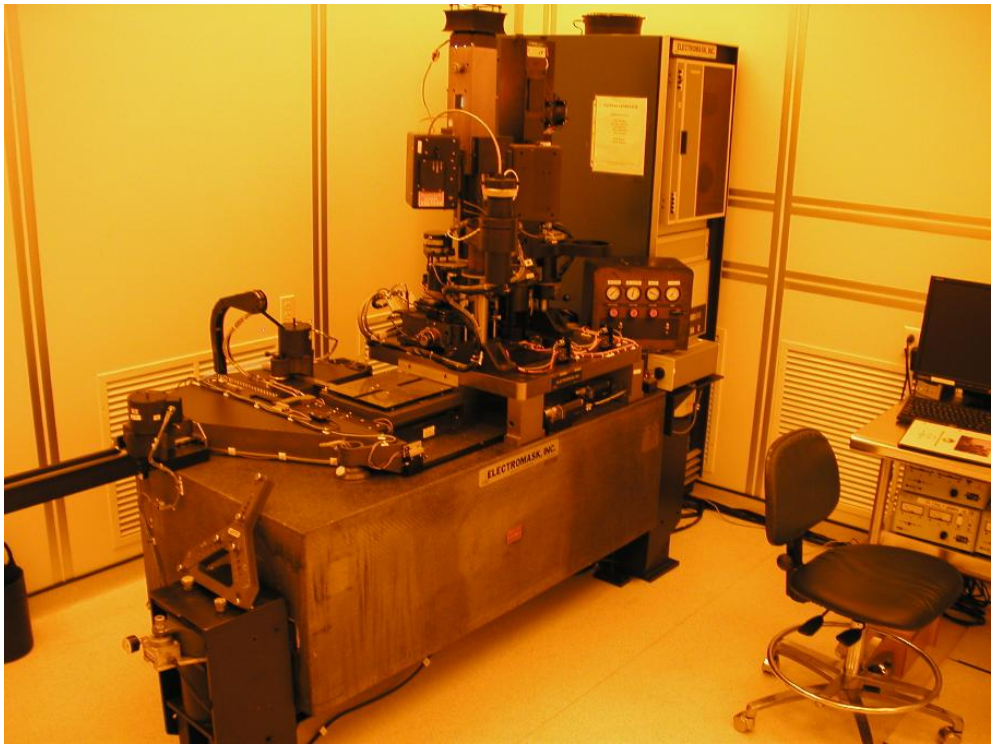

Figure 3.10: Photomask generator in VMC Cleanroom

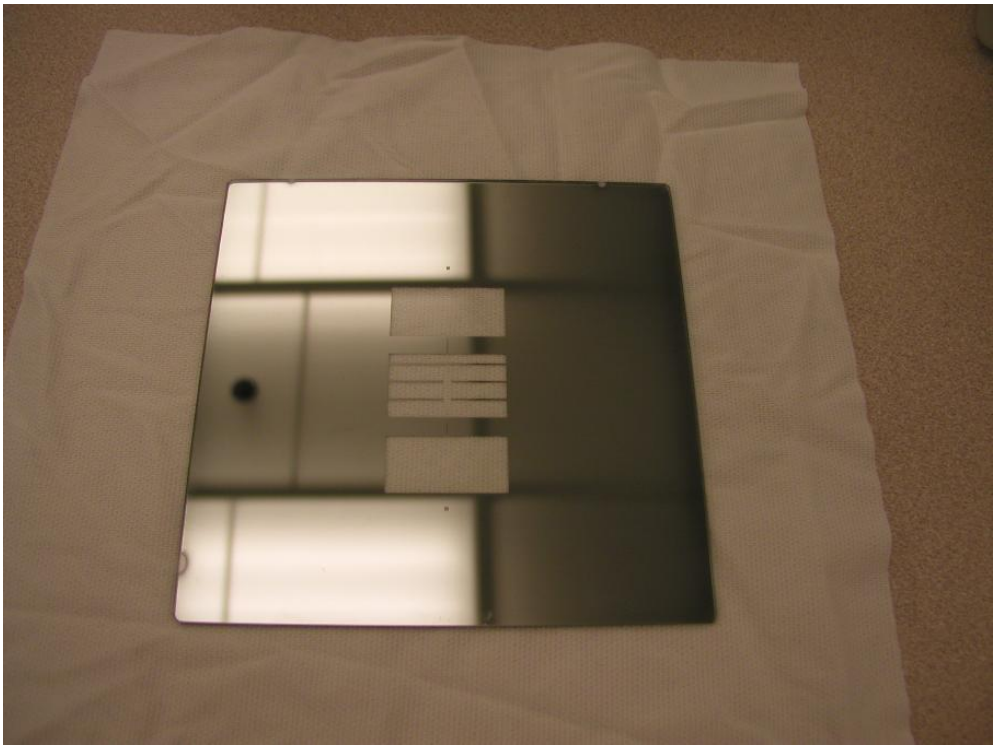

Figure 3.11: Photomask generated for PDMS application

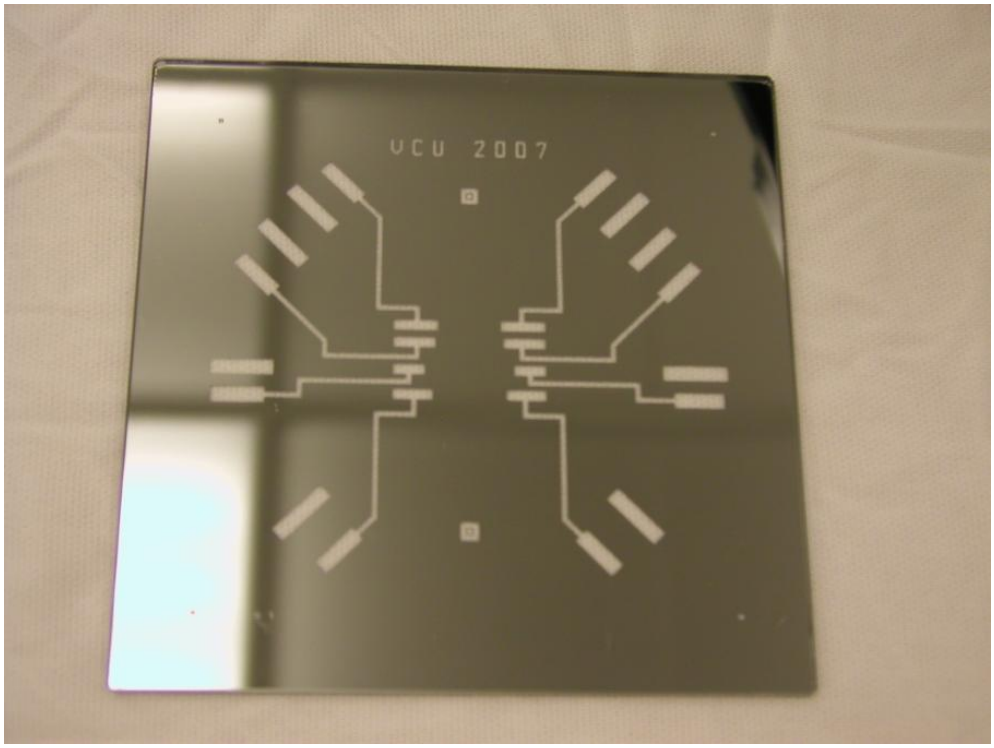

Figure 3.12: Photomask generated and created for Electrostatic Connections

3.2.1.4 – Wafer Identification and Cleaning

Fabrication of the PDMS micropump is initiated by first identifying and cleaning the proper wafer size for the MEMS device trying to be developed. In the design for the electrostatic PDMS micropump a four-inch silicon wafer was selected. The cleaning process is a vital step necessary to acquire proper adhering of the selected photoresist and the PDMS to the wafer. If cleaning of the wafer is neglected several negative effects may occur such as photoresist cracking, non-adherence, or contamination to the device being fabricated. Negligence of cleaning will result in lost time in fabrication and testing which may consist of several days, weeks, or months.

3.2.1.5 – SU-8 Negative Photoresist Application

Following the completion of the first step, a layer of SU-8 negative photoresist is dispensed onto the silicon wafer (figure 3.13). One milliliter (mL) of SU-8 photoresist is applied for each inch of a wafer. Applying this formula to a four-inch wafer results in approximately four milliliters (mL) of photoresist dispensed. Once the resist is dispensed it is spun at two different cycles. First, in the spread cycle, the photoresist is spun at 500 rpm at an acceleration of 100 rpm/second for approximately eight seconds. Second, in the spin cycle, the photoresist is spun at 500 rpm with an acceleration of 300 rpm/second for thirty seconds. This particular spin cycle gives a photoresist layer thickness of approximately seventy to eighty-five micrometers. After application of the photoresist the wafer undergoes a six minute softbake at sixty-five degrees Celsius and then a twenty minute softbake at ninety-five degrees Celsius.

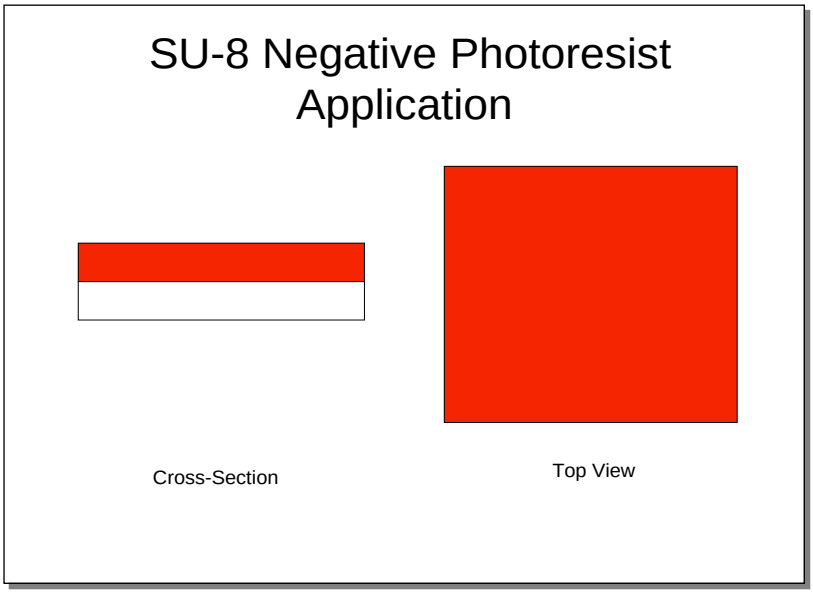

Figure 3.13: SU-8 Negative Photoresist Application

3.2.1.6 – Diffusion Lithography

Next the wafer undergoes contact lithography. A photomask (which was developed using IC station and a mask generator) is utilized to pattern the desired PDMS micropump into the SU-8 photoresist. The photomask is placed over the SU-8 photoresist utilizing a contact lithography machine and then subjected to UV light for approximately fourteen seconds before being removed. Upon removal the wafer then undergoes a post-exposure bake consisting of two phases. First, the wafer is baked on a hotplate at sixty-five degrees Celsius for one minute. Second, the wafer is then baked at ninety-five degrees Celsius for nine minutes. This procedure is done to make sure that the photoresist is fully cured, hardened, and solidified before it undergoes development.

Once the two phase post-exposure bake is completed the photoresist is then developed. Since SU-8 negative photoresist was used to pattern the PDMS micropump an SU-8 developer was used to pattern and develop the micropump design in the photoresist (figure 3.14). The wafer was developed in SU-8 developer for six minutes and then rinsed, revealing the desired micropump pattern. To promote proper curing and development of the SU-8 micropump pattern the wafer underwent an additional five minute oven bake at one-hundred seventy-five degrees Celsius.

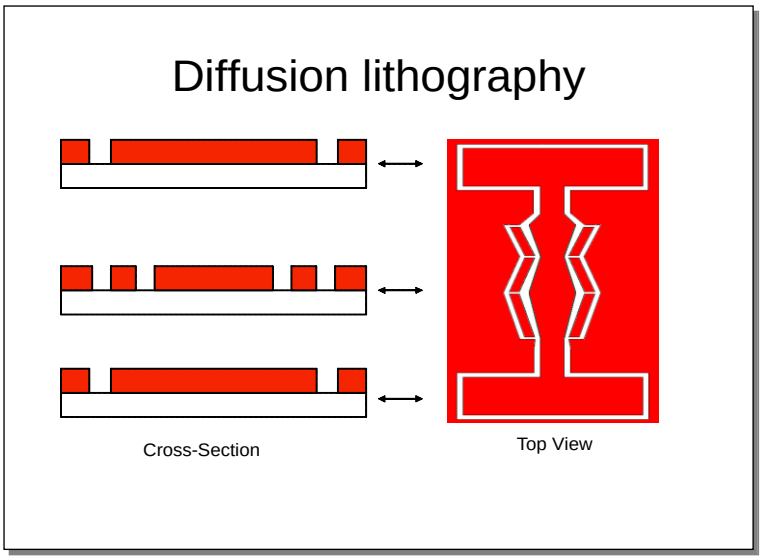

Figure 3.14: Contact Lithography of SU-8 Negative Photoresist Application

3.2.1.7 – Dispensing of PDMS Material

After contact lithography the PDMS is poured directly onto the SU-8 micropump mold (note: the mold is dipped in Liqui-Nox cleaning detergent and left to dry in order to have easy removal of PDMS). The PDMS consists of a two part mixture (polymer and hardener/cure) with a ten to one ratio mixture. To provide the PDMS with a more solid and rigid structure, since it will be undergoing mechanical stresses due to the electrostatic pump, silica (clay) particles are introduced into the PDMS mixture. The mixture was then poured onto the mold developed from the SU-8 photoresist (figure 3.15). The PDMS is then baked at seventy-five degrees Celsius for approximately an hour and forty-five minutes.

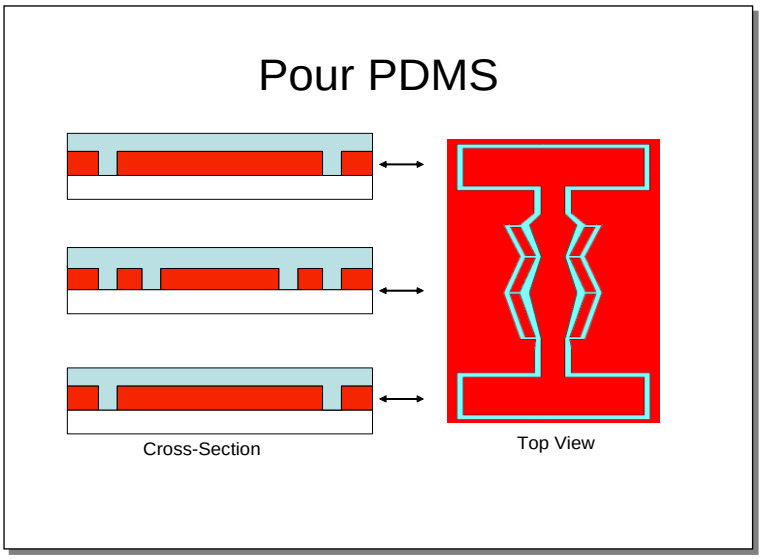

Figure 3.15: Application of PDMS to photoresist mold

3.2.1.8 – Removal of PDMS from Mold

Once the PDMS has cured, it can be safely removed. The removal process is quite simplistic. The PDMS can be easily peeled from the mold and prepared for metallization (figure 3.16 and 3.17). As previously mentioned the PDMS mold was treated with Liqui-Nox. If this step is neglected the PDMS removal process will result in negative side effects such as ripping, tearing, and bubbling of the PDMS substrate. Negligence of applying Liqui-Nox results in loss of time and waste of materials.

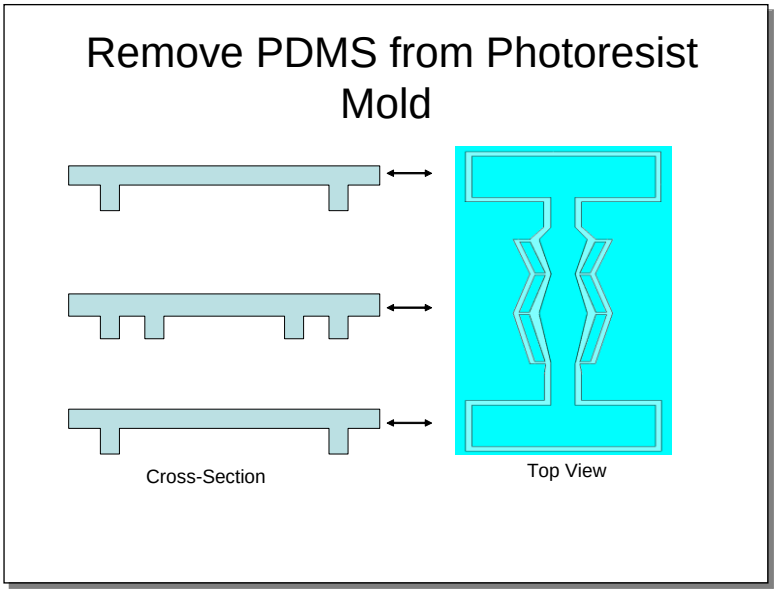

Figure 3.16: PDMS Removal

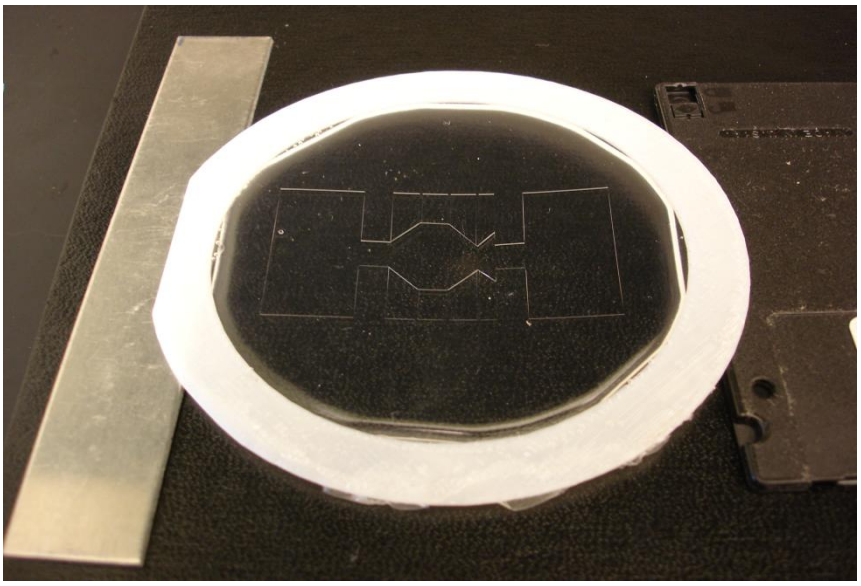

Figure 3.17: PDMS Micropump Removed

3.2.1.9 – Metallization of PDMS

Metallization is produced with the use of an evaporator (figure 3.18 and 3.19). To place metal connections on the PDMS a rapid prototyping mold was developed (figure 3.20). The mold is placed on top of the PDMS micropump as a shadow mask for the metal evaporation process. It must be noted that the shadow mask must be fitted and checked vigorously against the fabricated PDMS micropump to prevent misalignment. Several shadow masks were created via rapid-prototyping to make sure all connections aligned properly to match connections on wafer. If this step is not followed hours of fabrication and metallization are lost and result in restarting the procedure from scratch.

Figure 3.18: VMC Cleanroom Evaporator for Metallization

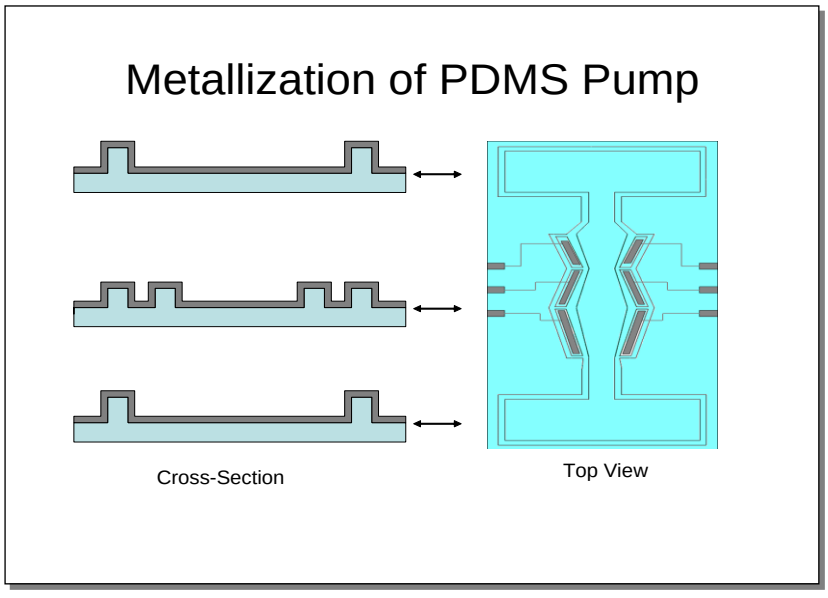

Figure 3.19: Metallization of PDMS

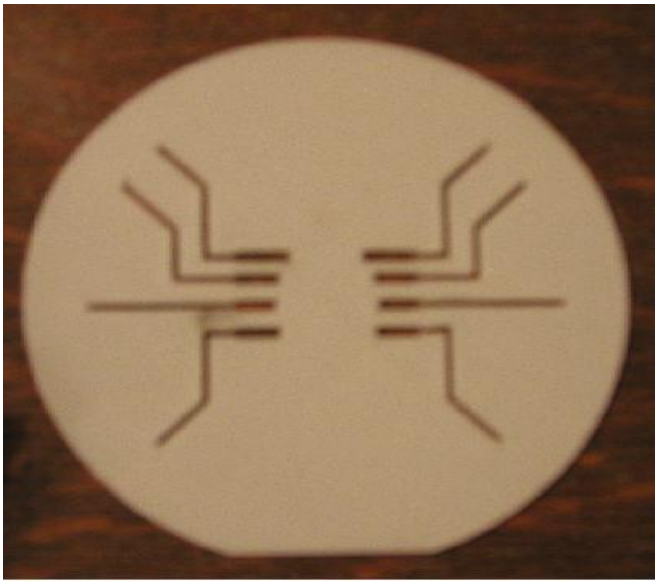

Figure 3.20: Shadow Mask to Metalize the PDMS Material

3.2.1.10 – Metallization of Glass Wafer

3.2.1.10.1 – SPR-3012 Resist Application

A second glass wafer will have voltage connections placed on it in a manner in which it will initiate the proposed electrostatic pump. Approximately four milliliters (mL) of SPR3012 photoresist is dispensed onto the glass wafer. The wafer is then softbaked at ninety-five degrees Celsius for ninety seconds.

3.2.1.10.2 – Diffusion Lithography

Once the softbake is complete, the wafer undergoes an eight second exposure to UV light to pattern the photoresist. The photoresist is then developed, leaving a pattern in the SPR3012 photoresist that allows for lift-off metallization (figure 3.21).

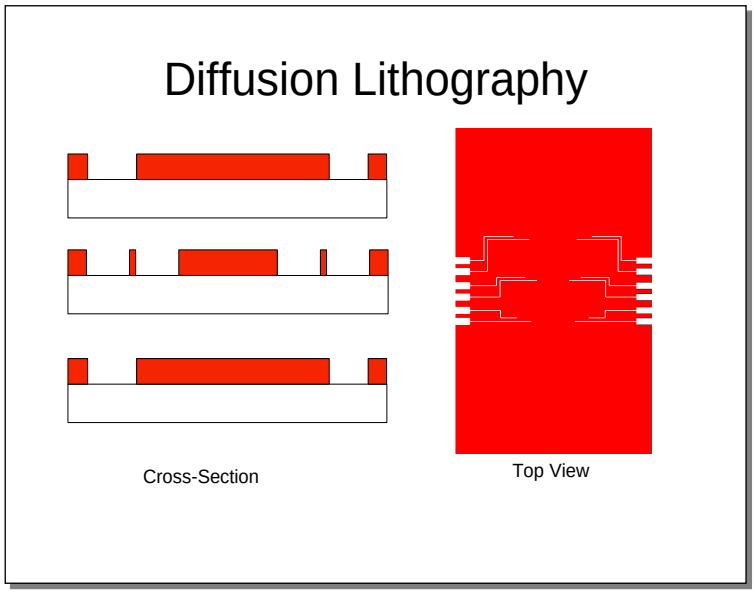

Figure 3.21: Metal Connection Pattern in SPR3012 Photoresist

3.2.1.10.3 – Metallization of Glass Wafer

Following completion of the mold for the metal connections on the glass wafer, the wafer can then be placed in the evaporator in the clean room to undergo metallization (figure 3.22). The metallization lift-off process is completed by placing the metalize glass wafer into an acetone bath. The acetone bath removes the photoresist and the excess metal that is not needed.

This process leaves the desired metal connections (figure 3.23) required for the electrostatic pump (note: all metal connections on both wafers consist of the following: first layer 200 kÅ Titanium and second layer 1000 kÅ Gold)

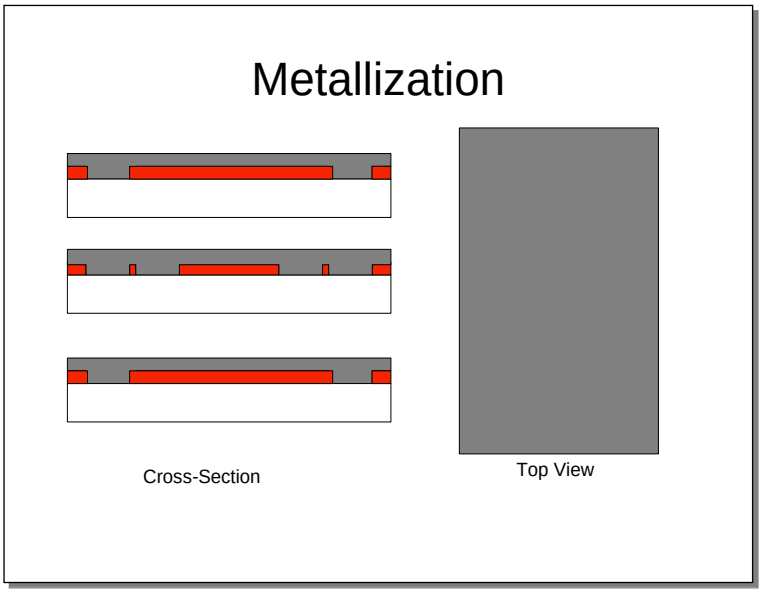

Figure 3.22: Metallization of Connection Pattern in SPR3012 Photoresist

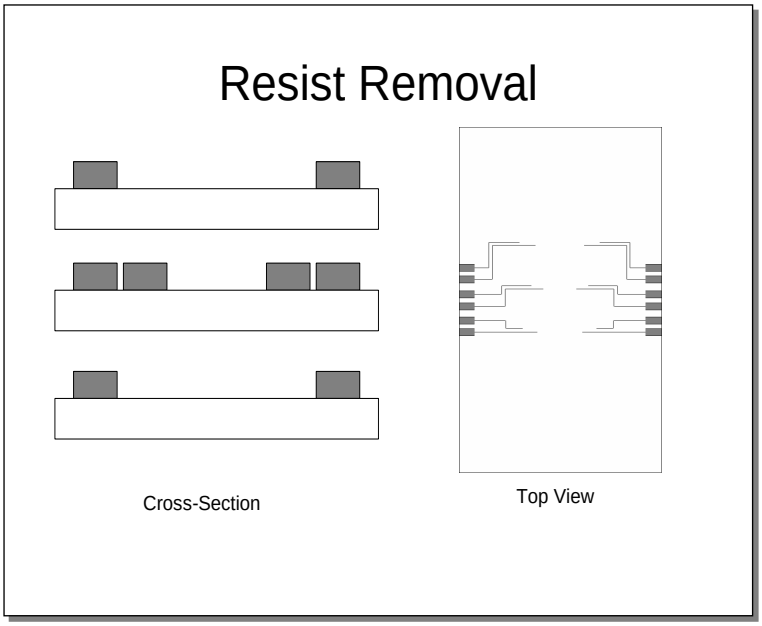

Figure 3.23: Metal Connections on Glass Wafer

3.2.1.11 – Bonding of Structures

Connections on the outside edges of the wafer are exposed and utilized to actuate the PDMS pump with a voltage source. Once both components are fabricated, the molded PDMS layer is bonded to the patterned glass substrate by cleaning both parts exposing them to a low voltage/high pressure oxygen plasma and bringing them into contact forming a permanent, irreversible seal (figure 3.24 – 3.25).

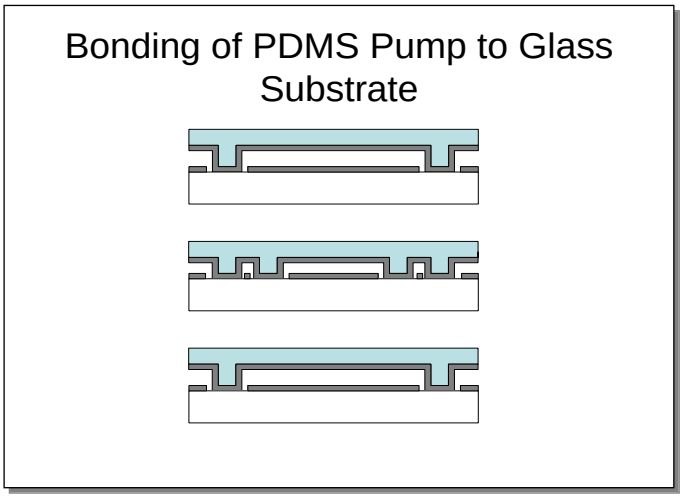

Figure 3.24: Bonding of Both Wafers

Figure 3.25: Complete Fabricated Electrostatic Actuated PDMS Micropump

3.2.2 – Top Actuation Micropumps

3.2.2.1 – Wafer Identification and Cleaning

Fabrication of the PDMS micropump is a very complex process. The first step (Figure 3.26) involves identifying and cleaning a four-inch silicon wafer. The cleaning process is a key step in order to acquire proper adhering of the selected photoresist and the PDMS to the wafer.

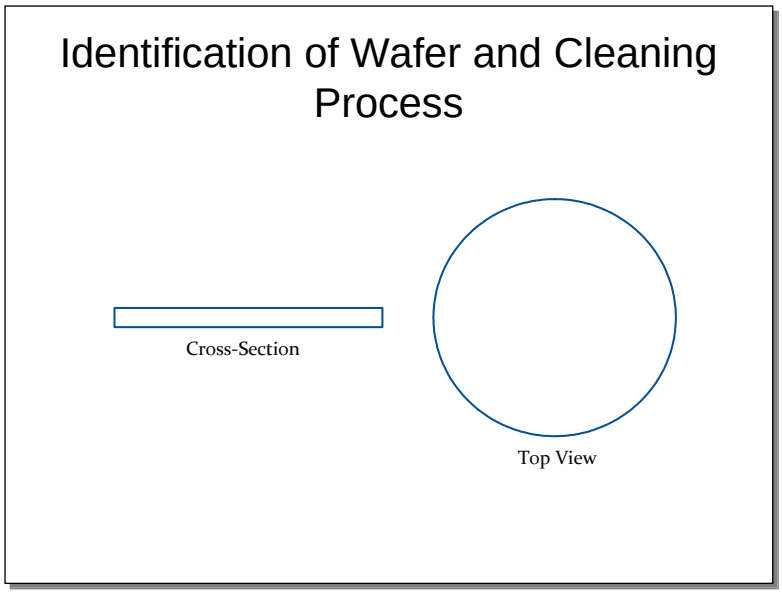

Figure 3.26: Wafer Identification and Cleaning

3.2.2.2 – SU-8 Negative Photoresist Application

After the first step is completed, a layer of SU-8 negative photoresist is dispensed upon the silicon wafer (Figure 3.27). One milliliter (mL) of SU-8 photoresist is applied for each inch of a wafer. In this instance using a four-inch wafer results in approximately four milliliters (mL)

of photoresist dispensed. Once the resist is dispensed it is spun at two different cycles. First, the spread cycle, the photoresist is spun at 500 rpm at 100 rpm/second for approximately eight seconds. Second, the spin cycle, the photoresist is spun at an acceleration of 300 rpm/second for thirty seconds. This particular spin cycle gives a photoresist layer of approximately fifty to seventy micrometers. After the photoresist has been applied it undergoes a six minute softbake at sixty-five degrees Celsius and then a twenty minute softbake at ninety-five degrees Celsius.

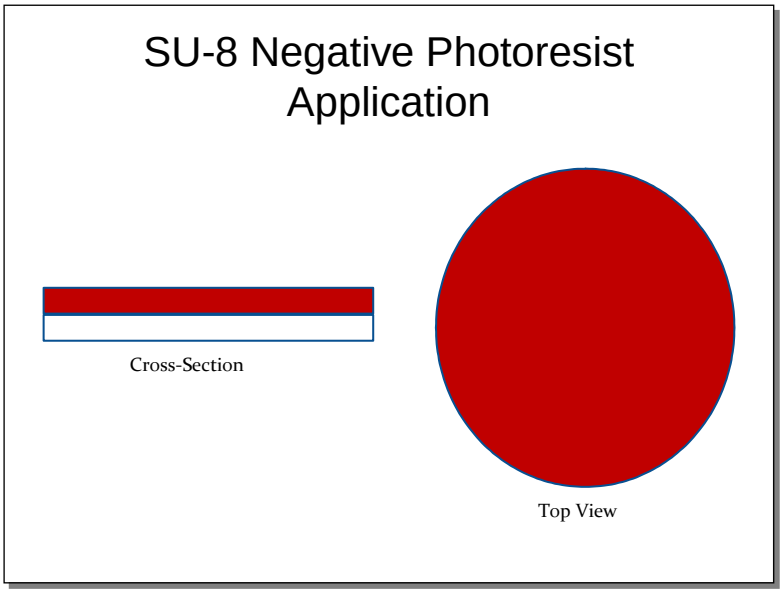

Figure 3.27: SU-8 Negative Photoresist Application

3.2.2.3 – Diffusion Lithography

Following step 2, the wafer then undergoes diffusion lithography. This is where a mask (which was developed with IC station) is utilized to pattern the desired PDMS micropump into the SU-8 photoresist. The SU-8 photoresist is exposed to UV light for approximately fourteen

seconds and removed. After removal the wafer then undergoes a post-exposure bake, which consists of two phases. First, the wafer is baked on a hotplate at sixty-five degrees Celsius for one minute. Second, the wafer is then baked at ninety-five degrees Celsius for 9 minutes. This procedure is done to make sure that the photoresist is fully cured, hardened, and solidified before it undergoes development.

Once the two phase post-exposure bake is accomplished the photoresist undergoes diffusion lithography. Since SU-8 negative photoresist was used to pattern the PDMS micropump, an SU-8 developer was utilized to pattern and develop the micropump design in the photoresist (Figure 3.28)

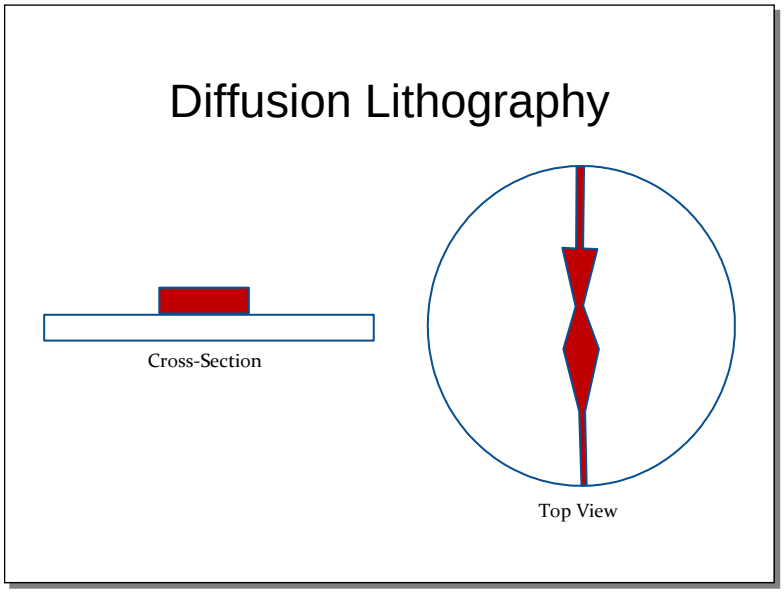

Figure 3.28: Diffusion Lithography

3.2.2.4 – PDMS Pouring

After diffusion lithography the PDMS was poured into the mold that was developed in Figure 3.28. The PDMS is a two part mixture (polymer and hardener/cure) with a ten to one ratio mixture. To give the PDMS a more solid and rigid structure, due to the fact that it will be undergoing mechanical stresses due to the electrostatic pump, silica (clay) particles were introduced into the PDMS mixture. The mixture was then poured into the mold that was developed (Figure 3.29). The PDMS is then baked for approximately one hour between sixty-five degrees Celsius up to eight-five degrees Celsius. It was then left to cure for approximately twenty-four hours (or longer) to allow the PDMS polymer to chemically cross-link and form a solid structure. After it has cured it can be removed by peeling the PDMS away from the micropump mold.

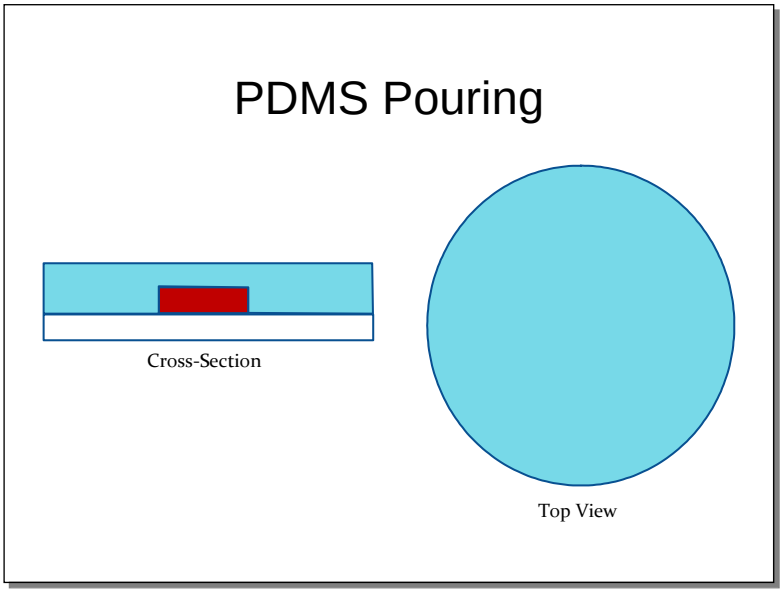

Figure 3.29: Pouring of PDMS

3.3: PDMS Micropump Fabrication Method II Rapid Prototyping Process

In today's engineering world it is vital to use the method of rapid prototyping. Rapid prototyping allows an engineer to physically construct and test a design that he or she has developed through hours of research. Using this method allows an engineer to determine if the design will withstand and hold up to the design criteria that revolves around a particular design. This is why in engineering and in the real world it is important to prototype an idea or design to determine if it will be able to function for worldwide marketability and meet the standards of the consumer.

Rapid prototyping is defined as being the automatic construction of physical objects using solid freeform fabrication. Techniques for rapid prototyping began to evolve in the late 1980s and were utilized to prototype parts and models. In today's society, rapid prototyping is used for a wide range of applications such as manufacturing quality production parts in relatively small numbers. Also, outside of the engineering spectrum, artists (such as sculptors) use rapid prototyping to produce complex shapes for fine art exhibitions.

The technique of rapid prototyping uses virtual designs from computer-aided design (CAD) or solid modeling software (SolidWorks), transforming them into virtual, thin, horizontal cross-sections and creating each cross-section in physical space (one after another until the prototyped model is completed). This type of process where the virtual model and the physical model correspond identically is referred to as the WYSIWYG process.

Additive fabrication allows the rapid prototyping machine to read data from a CAD drawing and lay down consecutive layers of liquid, powder, or sheet material. This is the process that allows the model to be constructed through a series of cross-sectional layers. Each

of these layers correspond to the virtual cross section from the CAD model and are joined or fused together automatically to create the final prototyped part or model. A primary advantage of using rapid prototyping technology is the ability it has to create any shape or geometric feature with ease.

Standard data interface between the rapid prototyping machines and the CAD software is use of STL file format. STL files approximate the shape of the assembly or model using triangular facets. The smaller these facets, the higher the quality surface of the part or assembly.

When one refers to the word "rapid" in rapid prototyping, it is quite relative. The reason is because construction of a part or model with contemporary methods can take from several hours to several days. This depends on the method used, the size of the part, and the complexity of the model. Additive systems for rapid prototyping typically can produce parts or models in a few hours, even though the time to produce these parts can vary widely depending on the type of prototyping machine that is being used, as well as the size and number of parts being produced simultaneously.

Various solid freeform fabrication techniques use two materials during the construction of parts or models. The first material is the support material, which is used to support the features of the particular part or model during construction, while the second material is the part material. After a part or model is prototyped the support material for the model is usually removed from the finished prototyped part.

Another technique that is used in polymer based processes, which is similar to rapid prototyping, is injection molding. Injection molding is a cheaper, less expensive form of manufacturing plastic/polymer products in high quantities. Even though injection molding

appears to be less expensive, rapid prototyping can be much faster and less expensive when producing relatively small quantities of parts or assemblies.

A vast number of competing rapid prototyping technologies is available in the world market today. With all rapid prototyping technologies, the significant differences are noticed in the way layers are built to create parts or models. Differences in rapid prototyping range from melting or softening material to produce the layers (Selective Laser Sintering, (SLS) and Fused Deposition Modeling (FDM)), where other rapid prototyping techniques lay liquid material thermosets that are cured with different techniques (Stereolithography (SLA), Multi-Jet Modeling (MJM), and Polyjet Modeling).

There are many rapid prototyping techniques that are utilized in today's engineering world. In the case of the PDMS micropump the rapid prototyping technique of Stereolithography (SLA) was utilized. Using the prototyping technique provides smoother part quality, closer tolerances, higher resolution, and ease of processing.

Producing the micropump design with the rapid prototyping method proved to be an easier and simpler way to replicate the desired pump. First, with the use of SolidWorks software (figures 3.30 and 3.31) a three-dimensional mold was designed and created. After utilizing design optimization techniques, this file was downsized to accommodate for quicker production times.

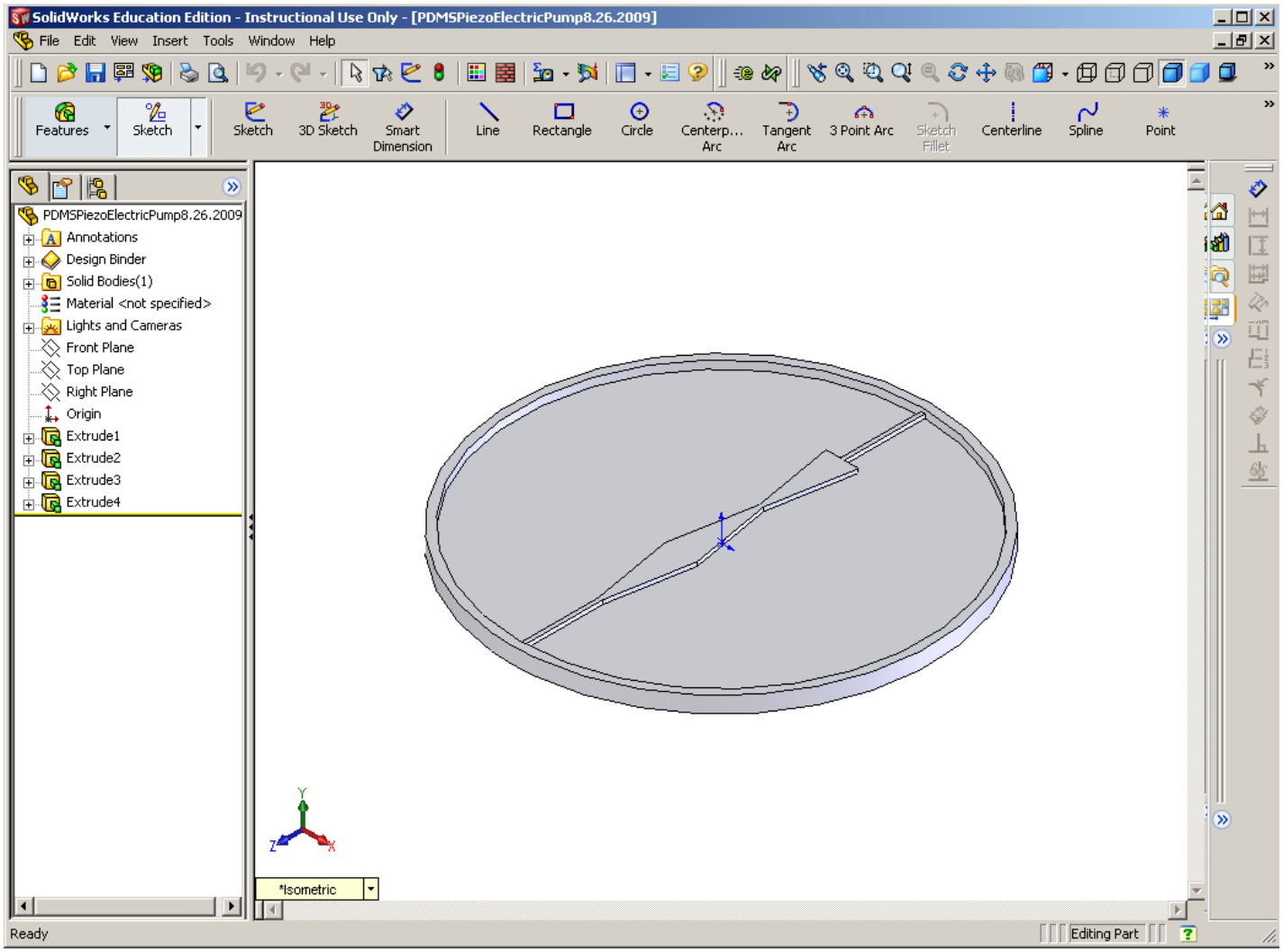

Figure 3.30: SolidWorks Rendition of Micropump

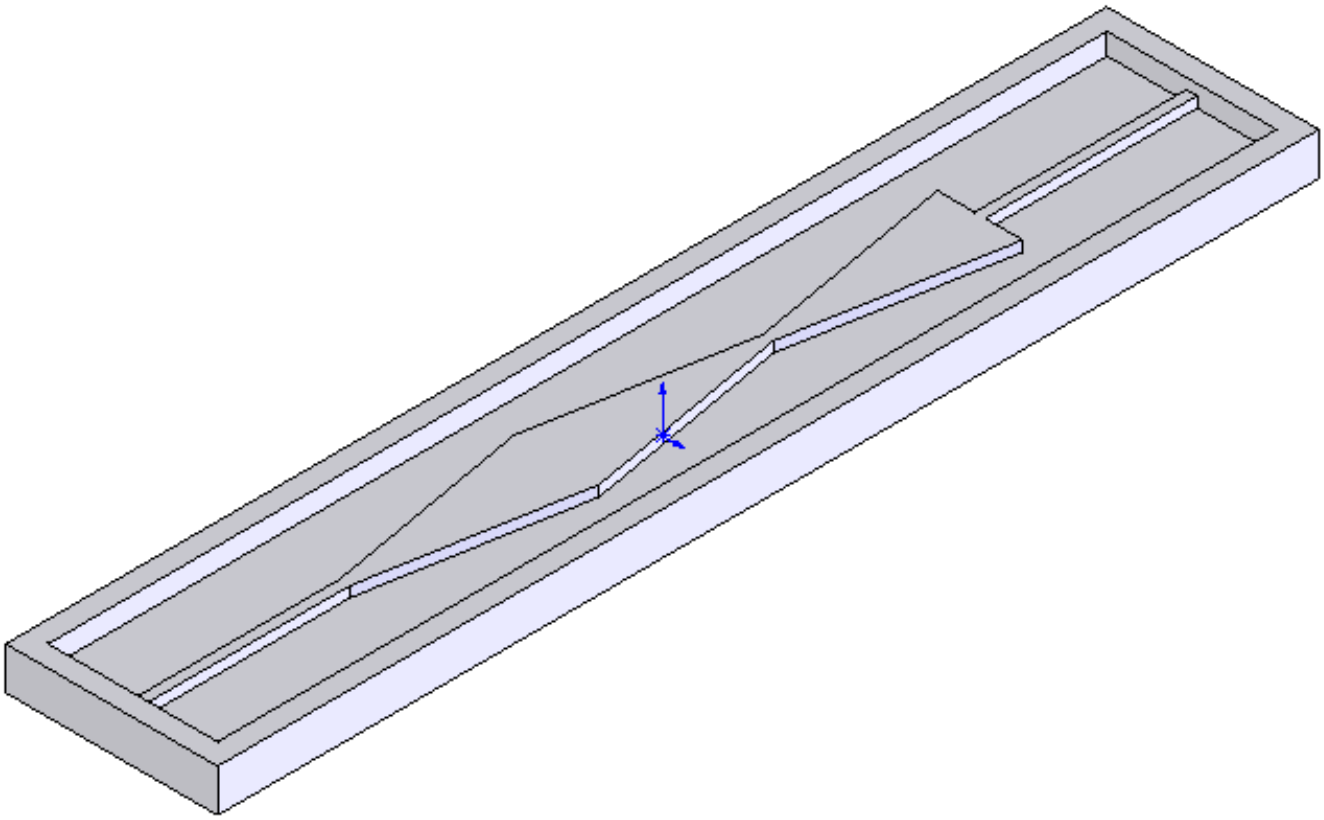

Figure 3.31: SolidWorks Completed Micropump Mold

After the micropump mold has been developed in Solidworks, the file must be saved as an STL file. The STL file is then placed into 3D light-year software that will convert the STL file to readable information the Stereolithography rapid-prototyping machine (Figure 3.32).

Figure 3.32: Stereolithography (SLA) Rapid Prototyping Machine

Once the file has been created the SLA rapid prototyping machine then can be utilized. The file is simply installed, loaded, and ran with the use of this prototyping machine. Depending on the size, resolution, and part quality, the part may take only minutes or possibly days for completion. For the PDMS micropump at this time it only takes a couple of hours. The finished prototype part can be seen in Figure 3.33.

Figure 3.33: Rapid Prototyped PDMS Micropump Mold

After completion of the micropump mold, PDMS can be simply poured and cured with the use of the mold. Once cured it is a simple lift off process illustrated in the following figures 3.34 and 3.35. This process is very simplistic and will be discussed in the next section.

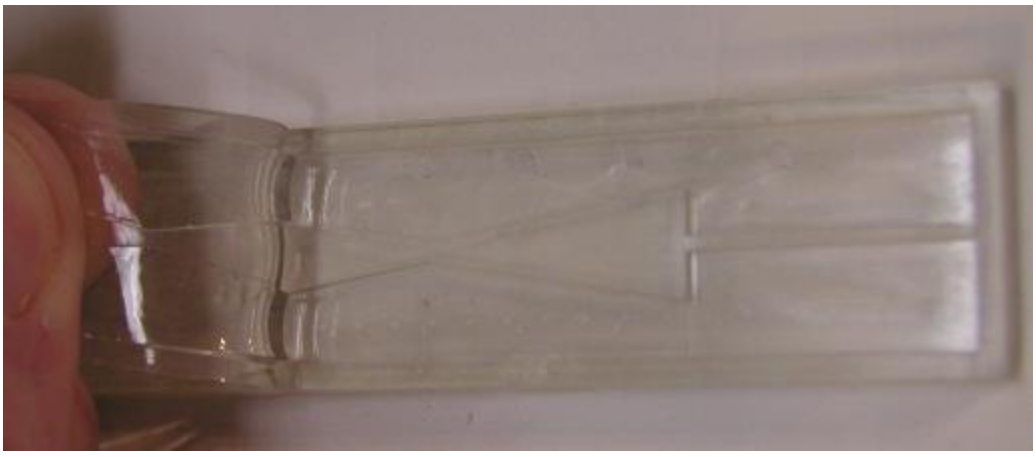

Figure 3.34: Removing PDMS from Mold

Figure 3.35: PDMS Completely Removed from Mold

3.4: Magnetic Actuation Fabrication

3.4.1 – Introduction to Magnetism

Magnetism is a topic that is considered to be relatively difficult to understand in some instances. The main concepts of magnetic field (H), magnetic flux density (B), and magnetization (M) are considered to be the essential concepts within the fundamental theoretical concepts of magnetism in general physics and engineering. Therefore, it is rather important that one understand the concept of magnetism when utilizing it to actuate microfluidic devices.

Magnetism has been present in the scientific and engineering world for thousands of years that involve a phenomenon by which materials assert a repulsive or attractive influence or force on other materials. The theory and principles that explain the magnetic phenomenon are still complex and subtle. Several modern technological devices rely on magnetism and magnetic materials, such devices can range from electric generators, transformers, electric motors, radios, televisions, telephones, computers, and components within sound and video equipment [103 – 105].

Examples of materials that exhibit magnetic properties range from iron, some steels, and naturally occurring minerals. On the other hand, it has been studied that all substances are influenced in some degree within the presence of a magnetic field. This section will discuss the origin of magnetic fields and the various magnetic field vectors and magnetic parameters.

3.4.2 – Magnetic Dipoles

Magnetic forces are developed by moving electrically charged particles. In most instances it is easier to view magnetic force as fields. Imaginary lines of force may be illustrated to show the direction of the force at positions within the vicinity of the field source. The magnetic field distributions are shown below in figure 3.36 with lines indicating the force loop directions.

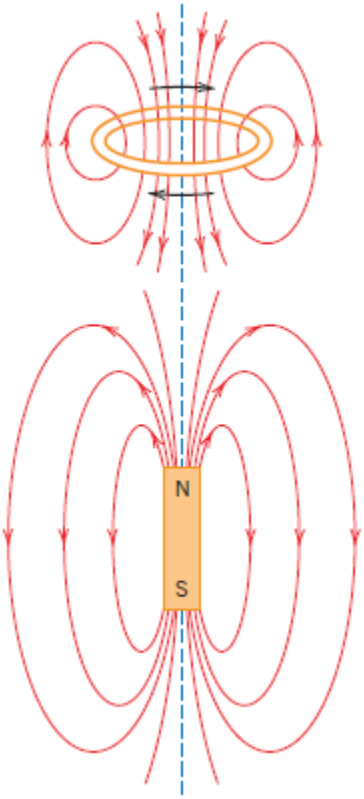

Figure 3.36: Magnetic Field Lines around a current loop and bar magnet [103]

Magnetic dipoles exist in magnetic material and are analogous to electric dipoles. Magnetic dipoles can be thought of as smaller bar magnets composed of north and south poles as an alternative of positive and negative electric charges. Most of the time magnetic dipoles are

represented with the use of arrows as depicted in figure 3.37. Magnetic dipoles are influenced by magnetic fields in a similar manner as electric dipoles are affected by electric fields. When studying a magnetic field, the force of the field itself exhibits a torque that tends to orient the dipoles with the field [103 – 105]. An example of the phenomenon is the needle on a compass aligning itself with the earth's magnetic field.

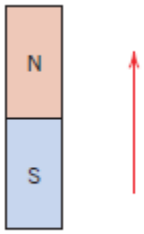

Figure 3.37: Magnetic Moment designated by arrow [103]

3.4.3 – Magnetic Field Vectors

To understand the magnetic moments that occur in solid materials, one must understand the overall magnetic behavior in terms of field vectors. The externally applied magnetic field is referred to as the magnetic field strength, **H**. If the magnetic field is generated by means of a cylindrical coil (i.e. a solenoid) consisting of closely space turns, N, with a length, l, and supplying current of magnitude I, then one can write **H** as:

$$H = \frac{NI}{l}$$

A typical diagram of this common arrangement is illustrated in figure 3.38. The magnetic field that is general created by the current loop and bar magnet in figure 3.36 is referred to as an **H**-field. The SI units that are associated with the **H**-field are Ampere per meter [103 – 105].

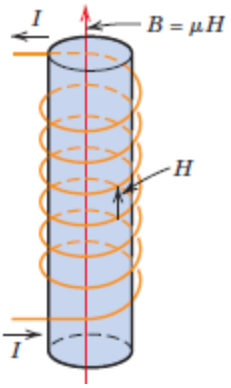

Figure 3.38: The magnetic flux density B is equal to μH [103]

The magnetic induction or magnetic flux density is denoted by the variable **B** which represents the magnitude of the internal field strength within a substance that is subjected to an **H**-field. The SI units for the **B**-field are teslas or webers per square meter. Both the **B**-field and the **H**-field are field vectors and are characterized by both magnitude and direction.

The magnetic field strength and the flux density are related by the following equation:

$$B = \mu H$$

where the variable μ is referred to as the permeability that is a property of the medium through which the **H**-field passes and where the **B**-field is measured as illustrated in figure 3.39. The SI units of the permeability are webers per ampere-meter (Wb/A-m) or henries per meter (H/m).

When the magnetic field is subjected to a vacuum equation 2 can now be written as:

$$B_0 = \mu_0 H$$

where μ_o is referred to as the permeability of a vacuum, a universal constant, that has the value of $4\pi \times 10^{-7}$ (1.257×10^{-6}) H/m [103 – 105]. The variable B_o represents the flux density inside of the vacuum as illustrated in figure 3.39.

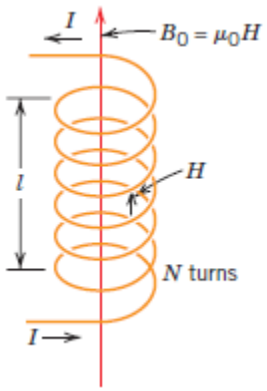

Figure 3.39: The magnetic field H created within a vacuum related by turns N [103]

Many parameters can be utilized to represent the magnetic properties of solids. One of these is the ratio of the permeability in a material to the permeability in a vacuum, and is defined as follows:

$$\mu_r = \frac{\mu}{\mu_0}$$

where μ_r is referred to as the relative permeability and it is unitless. The permeability of relative permeability of a material is a measure of the degree as to which the material can be magnetized or the ease as to which a **B**-field can be induced in the presence of an external **H**-field [103 – 105].

The field quantity, M, is referred to as the magnetization of a solid and is defined with the following expression:

$$B = \mu_o H + \mu_o M$$

In the presence of an **H**-field the magnetic moments within a medium tend to become aligned with the field and attempt to reinforce it by their respective magnetic fields. The term $\mu_o M$ in the above equation is a measure of this phenomenon [103 – 105].

The magnitude of M is proportional to the applied field and is defined in the following equation:

$$M = \chi_m H$$

where χ_m is referred to as the magnetic susceptibility and is virtually unitless. Magnetic susceptibility and the relative permeability can be related in the following way:

$$\chi_m = \mu_r - 1$$

A dielectric analogue for each of the aforementioned magnetic field parameters does exist. The **B**- and **H**-fields are analogous to the dielectric displacement *D* and the electric field ξ,

while the permeability μ parallels the permittivity ε. Another analogy exists between the magnetization M, and polarization P [103 – 105].

3.4.4 – Origins of Magnetic Moments

The magnetic properties of materials are a consequence of magnetic moments associated with electrons. Some of the concepts dealing with magnetism are relatively complex and encompass some quantum-mechanical principles beyond the scope of this research. To be more simplistic, one can view each electron in an atom possessing a magnetic moment that originates from two sources. One is related to orbital motion around the nucleus of the atom. An electron is a moving charge that can be viewed and considered to be a small current loop, thus being able to generate a very minimal magnetic field while simultaneously creating a magnetic moment (figure 3.40).

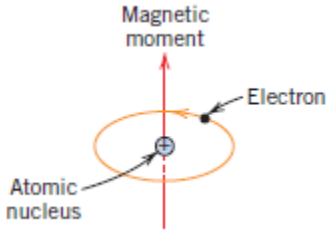

Figure 3.40: Magnetic Moment of an orbiting electron [103]

Every electron can be thought of as spinning around a particular axis associated with it. This spin that an electron exhibits creates a magnetic moment as it rotates along the spin axis (figure 3.41). Spinning magnetic moments may be only in an upward direction or in an

antiparallel downward direction. Therefore, every electron within the atom may be viewed as a small magnet possessing a permanent orbital and spinning magnetic moment.

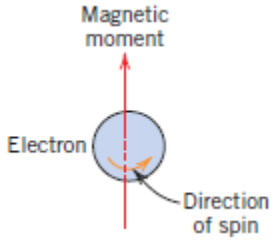

Figure 3.41: Magnetic moment associated with a spinning electron

When magnetic moments are discussed, the most common that comes to light is the Bohr magneton, μ_B which possesses a magnitude of 9.27×10^{-24} A-m^2. For every electron associated with an atom the spin magnetic moment is positive or negative, denoting positive for upward spin and negative for downward spin. Additionally, the magnetic moment contribution is equivalent to $m_l \mu_B$, where m_l is the magnetic quantum number of the particular electron.

Each individual atom has orbital moments consisting of electron pairs that will cancel out, and this is true for spinning moments as well. An example is the spin moment of an electron spinning upward and downward, the spin up will cancel the spin down. Therefore, the net magnetic moment will simply be the sum of the magnetic moments of each constituent electron for both orbital and spinning while taking into account the moment cancellation aspect. If an atom consists of completely filled electron shells or subshells there is a complete cancellation of the orbital and spinning moments. Due to this materials consisting of atoms possessing completely filled electron shells are not capable of being permanently magnetic such as inert gases (He, Ne, Ar, etc.) and some ionic materials. The forms of magnetism include

diamagnetism, paramagnetism, and ferromagnetism. A couple of subclasses of ferromagnetism do exist and they are antiferromagnetism and ferrimagnetism. All materials do exhibit a form of magnetism and the overall behavior is dependent upon the response of electron and atomic magnetic dipoles to the externally applied magnetic field.

3.4.5 – Magnetic Actuation PDMS Micropump

The magnetic PDMS micropump can be fabricated utilizing the methods of microfabrication and rapid-prototyping facilities. The flow region for the PDMS micropump is actuated with the use of magnetic material, Fe_2B (figure 3.42) incorporated into the PDMS mixture.

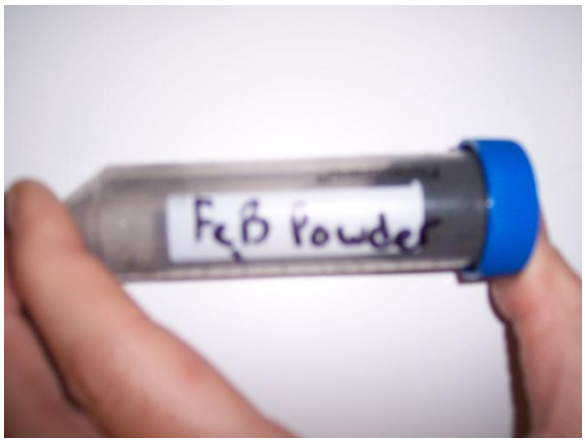

Figure 3.42: Fe_2B Particulates

The procedure for blending in the particulate is the same as previously discussed where varying percentages of the magnetic material was utilized to determine whether or not the magnetic

strength would increase if the particulate amount was increased. After following the mixing and curing procedures a magnetic micropump was developed as seen in figure 3.43.

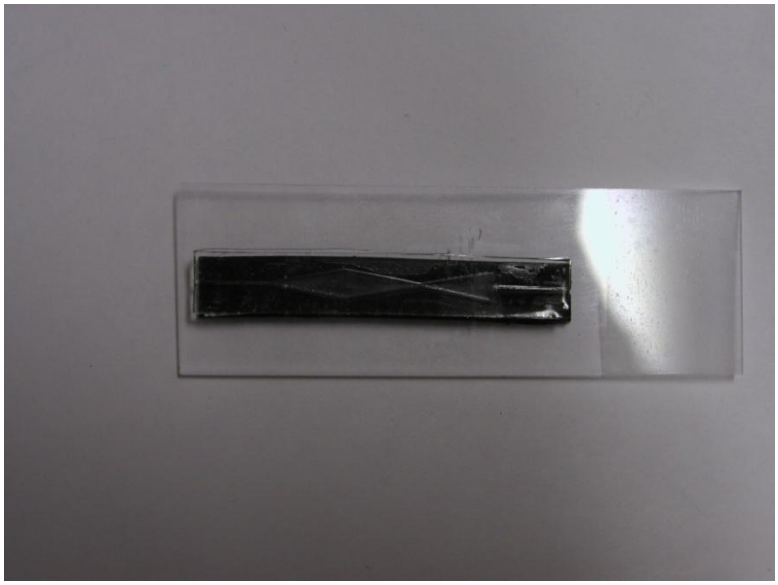

Figure 3.43: PDMS Magnetic Fabricated Micropump

3.4.6 – Magnetic Force

When an object or material is in the presence of a magnetic field, the single-domain magnetic particles suspended in the PDMS begin to feel a magnetic attract or repulsive force. In figure 3.44 a theoretical schematic is shown of the randomly oriented north poles of the Fe_2B particles within the PDMS material before curing and being absent of an external magnetic field.

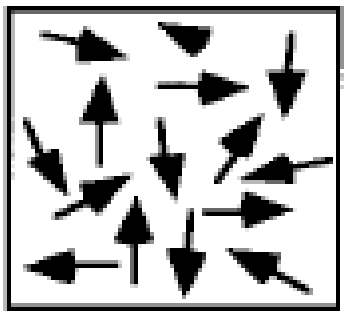

Figure 3.44: Randomly Oriented Fe_2B in PDMS

In theory if the Fe_2B magnetic particles were coupled with a permanent magnet, the magnetic poles would align themselves as theorized in figure 3.45. This would allow the PDMS micropump to exhibit a well-established magnetization as it interacts with an external magnetic field to produce attractive and/or repulsive forces on each Fe_2B particulate within the PDMS mixture.

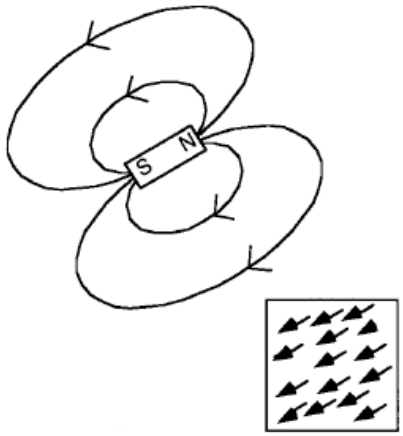

Figure 3.45: External magnetic field applied to PDMS/ Fe_2B Mixture

The attractive/repulsive magnetic forces that are exhibited on the PDMS material acts similar to a body force on the PDMS, similar to the body force on a solid due to gravity. Magnetic force can be defined as follows:

$$F = \mu M \nabla H$$

where μ is the magnetic permeability of free space (Teslas-minute per Ampere, Tm/A), M is the magnetization (A/m), ∇ is the gradient, and H is the magnetic field (A/m) [104], [105].

Magnetization occurs when the Fe_2B become polarized in the presence of an external magnetic field. When the strength of the external magnetic field increases from zero A/m, the Fe_2B particles encapsulated within the PDMS will become magnetized to a degree, ultimately controlled by the strength of the external field being applied as well as the particles utilized (Fe_2B).

3.5: Piezoelectric Actuation Fabrication

Piezoelectric actuation is another method that is currently under investigation. Three types of piezoelectric materials are being investigated, PZT, PVDF (Polyvinylidene Fluoride), and MFC (Macro Fiber Composite). Each of these materials has characteristics that could be possibly utilized for the actuation of the micropump. To affix the piezoelectric material to the micropump it can either be adhered with gluing or fabricated into the PDMS during curing/mixing. An example of the piezoelectric placement on the micropumps can be seen in figures 3.46 and 3.47. After the PDMS underwent the application of the piezoelectric materials testing was done. The testing and characterization methods will be discussed in later chapters.

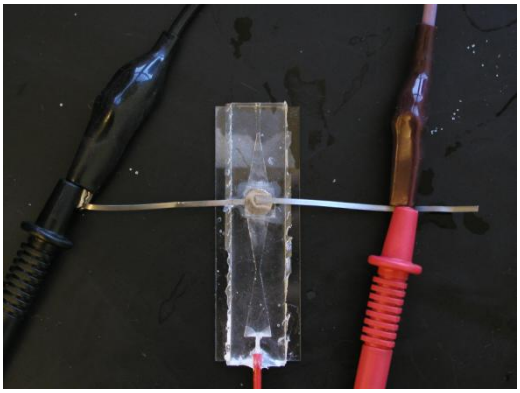

Figure 3.46: Piezoelectric Adhered to PDMS Micropump

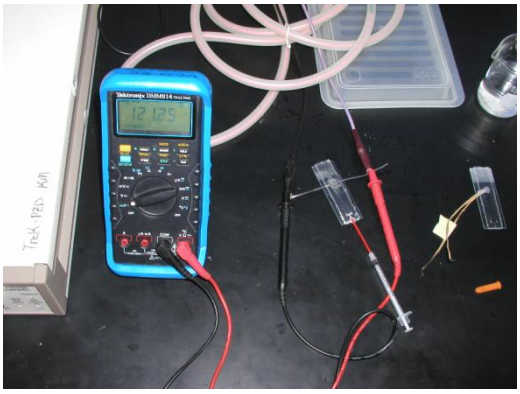

Figure 3.47: PDMS Micropumps with Piezoelectric Material affixed

3.6: PDMS Mixing and Curing Process

The PDMS that is being utilized in this research is manufactured and distributed by Dow Corning under the commercial name SLYGARD 184. SLYGARD 184 is an elastomer kit that comes with a two part mix. The mixture consists of a base and a curing agent. These two items must be mixed with a 10 to 1 ratio, ten parts base and one part cure (Figure 3.48).

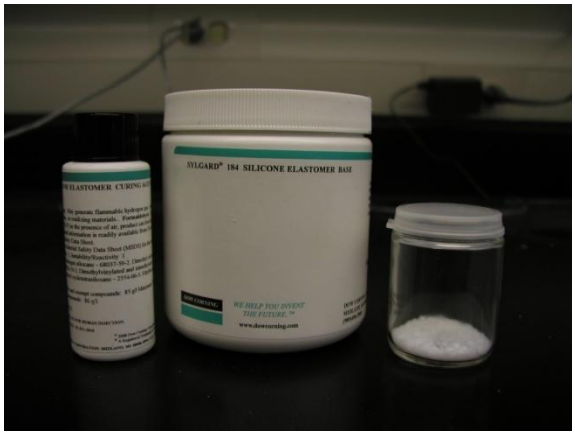

Figure 3.48: PDMS Base and Cure with Microparticles

Before the PDMS can be mixed and poured, the molds for the micropump must be treated in order to provide for easy liftoff of the PDMS material. In order to do so a liquid detergent, Liquinox, is used for this process. Liquinox is an industrial grade detergent cleaner that is utilized for cleaning lab floors, equipment, and various other components found within labs and hospitals. This detergent is mixed with water at a 10 to 1 ratio, ten parts water and one part liquinox. After this mixture is completed, the fabricated pump from the microelectronics and the rapid-prototyping laboratory are then dipped into this solution and left to dry while the PDMS is mixed.

The process for mixing the PDMS (Figure 3.49) is a straight forward procedure, but has some alternate steps depending on how you want the PDMS material to turn out. First, ten parts of base material is dispensed into a glass beaker and one part of the curing agent is then mixed into the base. After the mixture has been thoroughly mixed together it is then placed within a vacuum chamber for approximately forty-five minutes to one-hour. Using a vacuum chamber on the PDMS material allows one to remove all of the air bubbles from the polymer to provide for a smooth, air bubble free surface. Removal of air from the PDMS is crucial to ensure there are not defects that will cause sealing or pumping issues while testing. If air bubbles are present in the PDMS mold it can possibly cause weaknesses within the walls of the pump, a decrease in stiffness and rigidity where needed, and failures in the actuation of the micropump.

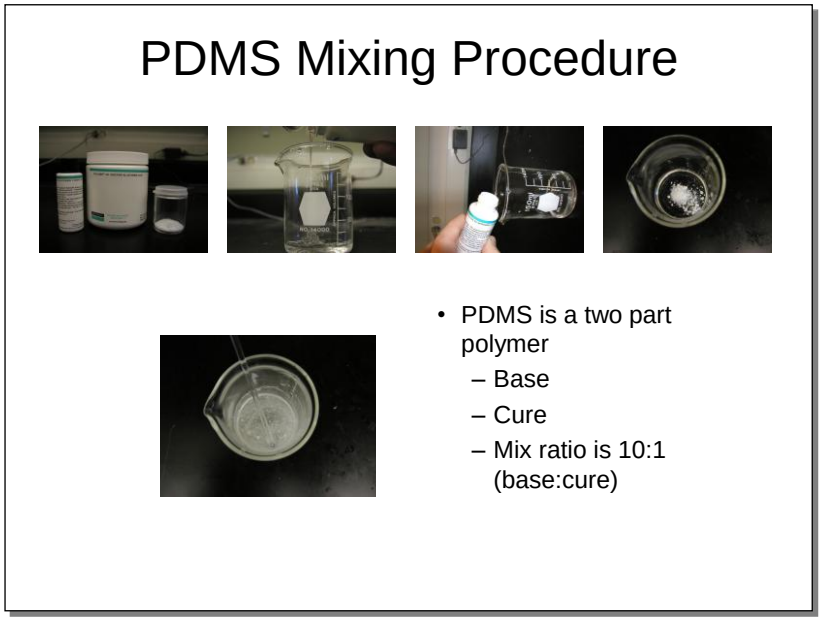

Figure 3.49: Procedure for Mixing PDMS

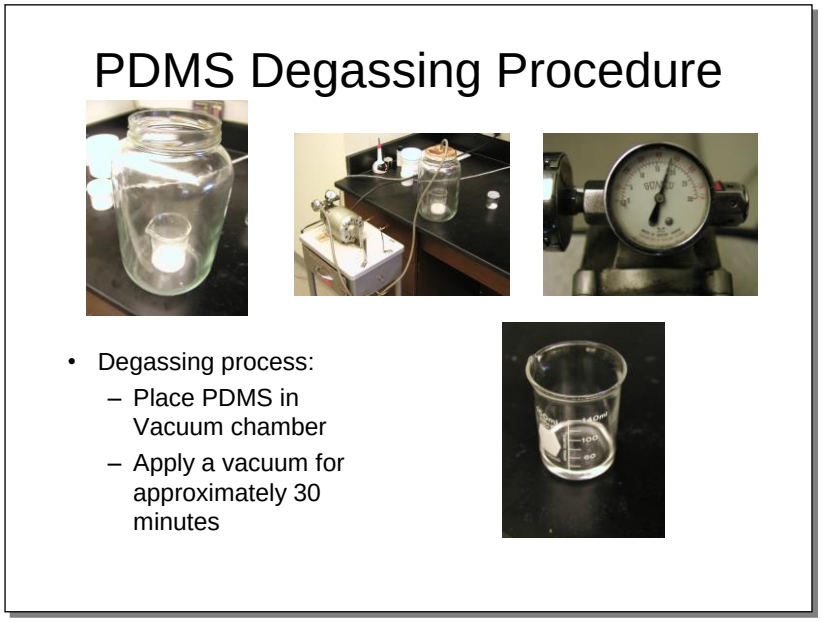

Figure 3.50: PDMS Degassing Procedure

Once the PDMS has been degassed (air-bubble removal, Figure 3.50) it can be simply dispensed onto the fabricated micropump molds (that were treated with Liquinox) until the desired quantity is achieved. After the PDMS has been poured the molds are placed into an oven (Figure 3.51). The oven temperatures can range from seventy degrees Celsius to eight five degrees Celsius. The part is baked for one-hour and then removed from the oven. During a twenty-four hour period it is left to cure at room temperature. Sometimes there have been issues with this procedure, and other possibilities do exist, such as allowing the part to bake twenty-four hours and let it cure at room temperature for another twenty-four hours. Depending on the mixture, temperatures, and other factors the bake times can fluctuate. Incorporation of microparticles can be placed within the PDMS giving the material a more rigid and stronger polymer. This can be done if strength of the PDMS is not sufficient and the material appears weak.

Figure 3.51: PDMS Baking and Removal

Following removal from the oven and curing at room temperature, the PDMS can be removed from the molds. Removing the PDMS from the micropump mold is simple, but care must be exercised because a polymer can rip and tear with ease. Once the fabricated PDMS micropumps have been removed from the molds, they can undergo the sealing process. The sealing process provides an air-tight seal between the pumps, in order to prevent any form of leaking.

Images of the fabricated pump were obtained with the use of a camera attached to a Nokia Microscope in the microelectronics lab. The use of this microscope provided detailed images of the exact dimensions of the PDMS micropump channels and sidewalls. This

microscope allows one to visually inspect and make sure the dimensions of the pump are accurate and precise. Images are seen in figures 3.52 and 3.53.

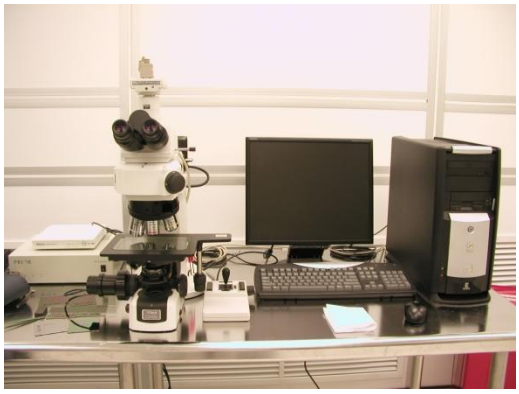

Figure 3.52: Nikon Imaging Microscope

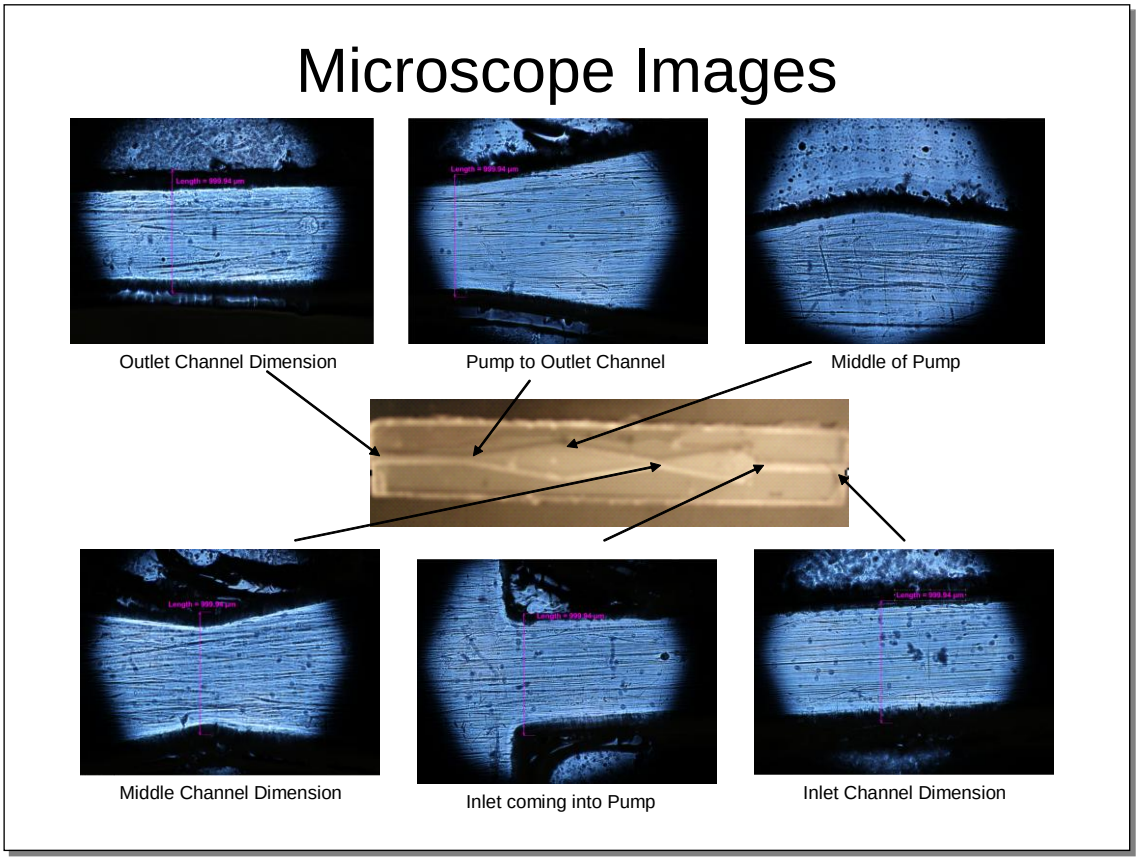

Figure 3.53: Images of the PDMS Micropump obtained from Nikon Imaging Microscope Model LV1000D with magnifications of 5X, 10X, 20X, 50X, 100X

3.7: Sealing PDMS to a Substrate

A process has been developed using the VMC cleanroom microelectronics lab. To seal the PDMS to a surface, whether it is glass or PDMS, it must undergo a cleaning procedure. Two procedures can be utilized for cleaning the PDMS surface prior to sealing.

Figure 3.54: Piranha Etch Materials

Procedure one involves a Piranha etch (Figure 3.54), which is a mixture of sulfuric acid (H_2SO_4) and hydrogen peroxide (H_2O_2) that cleans organic residue off of substrates. Usually the Piranha etch consists of a mix ratio of 4:1, four parts hydrogen peroxide and one part sulfuric acid. After the mixture has undergone a chemical reaction between the acid and base, the PDMS substrate is simply dipped into the Parana etch and removed. Upon removal the PDMS is then thoroughly rinsed and dried with nitrogen.

Figure 3.55: Cleaning Procedure Two

Procedure two involves a serious of chemical bath rinses (Figure 3.55). There is a serious of three chemical baths consisting of Methanol (CH_3OH), Acetone ($OC(CH_3)_2$), and Isopropyl Alcohol (C_3H_7OH) in which the PDMS is dipped resulting in a clean substrate. The PDMS is placed in each chemical bath in the order above, and allowed to sit in each one for approximately thirty seconds. As it is moved from one bath to another it is dried with nitrogen. After the PDMS has undergone the series of chemical baths it is then placed in deionized water and then air dried with nitrogen.

These two procedures can be used on any PDMS surface to provide proper adhesion characteristics. Both cleansing procedures will produce a clean surface that can undergo Oxygen-Plasma treatment. Oxygen-plasma is used to provide an irreversible seal between PDMS and any substrate. Each PDMS micropump and substrate undergoes Oxygen-Plasma

treatment with parameters set at a pressure of 0.600 Torr for thirty-five seconds. The precise recipe for the PDMS treatment is shown in Figure 3.56.

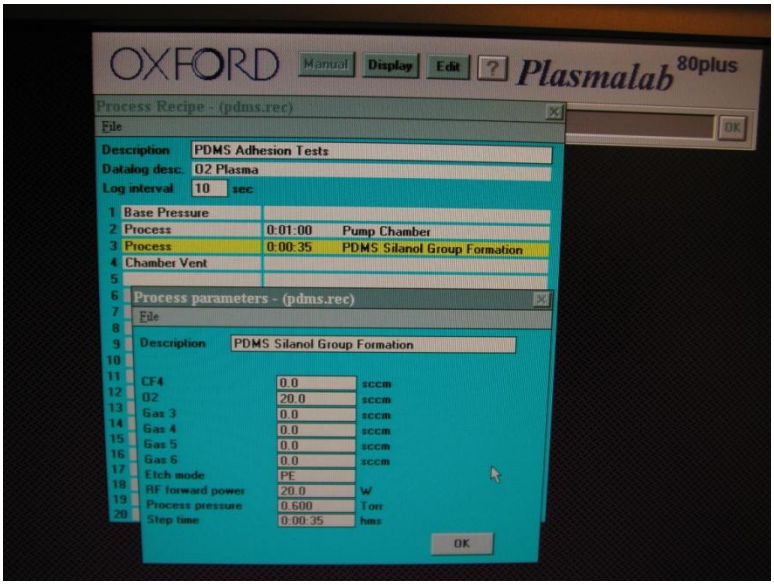

Figure 3.56: Oxygen-Plasma Recipe for PDMS Sealing

Figure 3.57: Plasmalab 80 Plus utilized for Sealing PDMS

Oxygen-plasma treatment provides a seal that is irreversible and essential air tight. This procedure allows a permanent seal for the PDMS micropump and prevents leakage due to activation and testing. See figure 3.57 which illustrates the Oxygen-Plasma equipment utilized to seal the PDMS micropump.

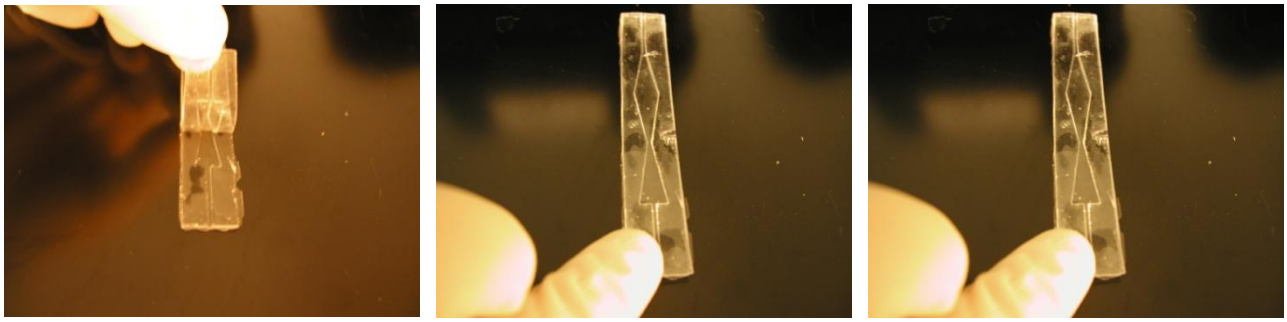

Figure 3.58: Pressing and Sealing PDMS to PDMS after Oxygen Plasma Treatment

Upon completion of the sealing process (Figure 3.58) of the PDMS micropump experimental testing can now be finalized. The PDMS micropump was sealed to two different substrates, PDMS and glass (Figure 3.59). Both pose similar characteristics and appear to function properly with mechanical actuation.

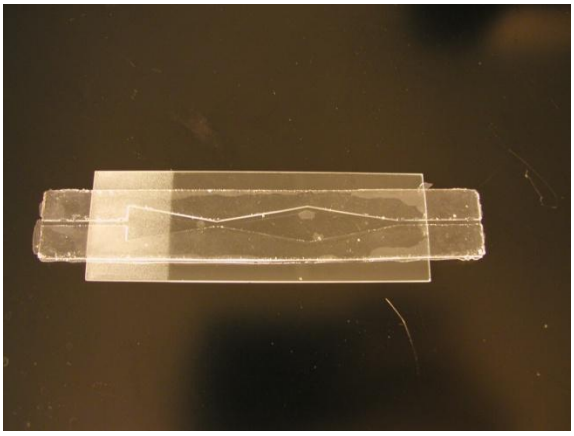

Figure 3.59: PDMS sealed to Glass

3.8: Conclusions

Through careful investigation and study coupled with trial and error several fabrication methods were developed that would allow the development of the PDMS micropump. Each fabrication method was novel and unique in the creation of the micropump design. The first fabrication method required the use of the VMC microelectronics laboratory. This method utilized microelectricalmechanical systems methodology coupled with lithography and sealing processes. The second fabrication method incorporated rapid prototyping technology to produce a mold of the PDMS micropump. Both fabrication methods provided final results that allowed one to experimentally test the micropumps capabilities which will be discussed. These fabrication methods when coupled together allowed the processing and production times of the micropump to be reduced drastically making it ideal for quick and easy manufacturing.

CHAPTER 4 Testing and Characterization

4.1: Introduction to the Types of Testing

After the PDMS micropump was designed and fabricated, it underwent various forms of testing and characterization. The methods of actuation that were investigated involved the use of electrostatic actuation, piezoelectric actuation, magnetic actuation, pneumatic (mechanical reciprocating motor) actuation, and a pressurized vessel actuation method to deliver a fluid under a particular pressure. Each of these methods will be discussed in detail in the following sections.

4.2: Electrostatic Actuation

As previously discussed the fabrication method for the electrostatic pump was quite extensive and novel. The fabrication technique utilized a commonly used polymer, polydimethylsiloxane (PDMS). The pump was constructed from a molded PDMS wafer process, coupled with metal electrodes. After the pump was finished and connections in place it was then sealed to a glass substrate with corresponding metal connections. Sealing of the two structures utilized a unique oxygen plasma treatment between the PDMS and glass wafer structure. A complete electrostatic fabrication wafer is shown in figure 4.1.

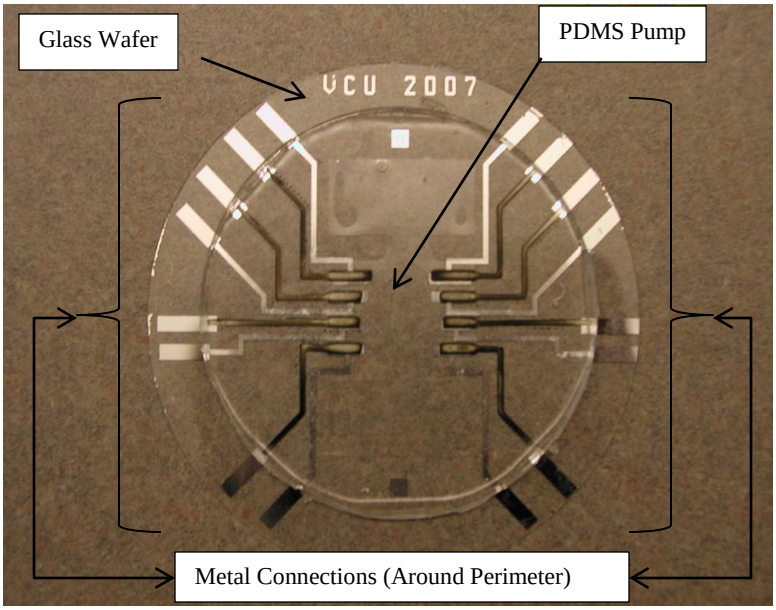

Figure 4.1 – Complete Fabricated Electrostatic PDMS Micropump

In theory the flow regime of the PDMS micropump was to be actuated with six electrostatic pumping chambers as seen above. Each pumping chamber would consist of a thin flexible PDMS wall separating the chambers from the fluid region. As seen in figure 4.1 each pump chamber consisted of two electrodes on both the upper and lower services of the electrostatic pump. The electrodes were created and fabricated to provide independent voltages to each electrode in the sense to create an electrostatic attraction. This attraction would create a change in pressure within the chamber allowing the PDMS sidewalls to expand into the fluid region, thus creating flow. The region of flow was divided into three regions to provide a cascading motion along the walls of the micropump.

When the PDMS micropump was first developed in the microelectronics lab, it was a long process from start to finish. Once the pump was completed, it under went metallization with the use of a shadow mask as previously discussed. As metallization of the electrodes

occurred on the PDMS substrate the appearance of the connections appeared sufficient until testing. It was observed the metal connections would break down over time. Further observations during precise testing indicated that the voltage continuity on the electrical connections would break down preventing current flow. Breaking of the electrical connections was also observed based upon the flexibility of the PDMS. These issues led to minimal to non-visible actuation of the micropump resulting in no positive experimental results.

4.3: Piezoelectric Actuation

Piezoelectric actuation is another method that was investigated. Three types of piezoelectric materials were investigated, PZT, PVDF (Polyvinylidene Fluoride), and MFC (Macro Fiber Composite). Each of these materials has characteristics that can be utilized for the micropump design.

PZT, PVDF, and MFC are piezoelectric materials that can have a voltage applied to them to create a deflection. The experimental setup consists of a function generator and an amplifier as shown in figure 4.2.

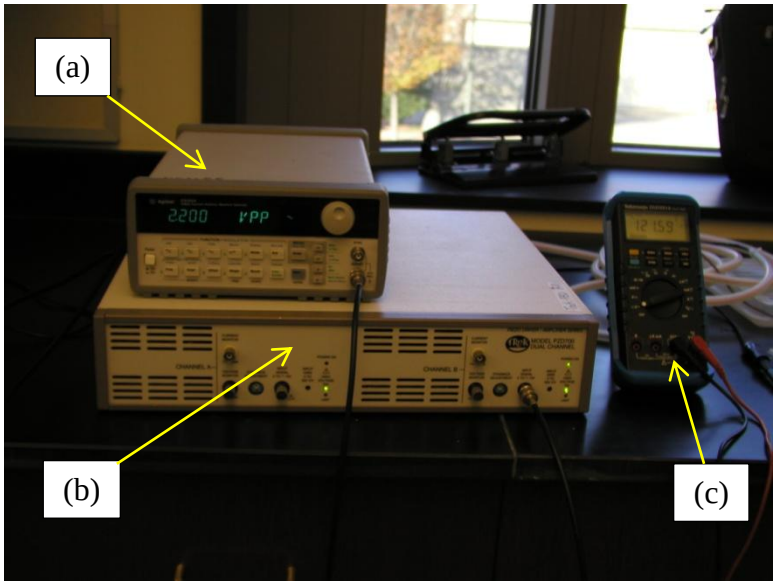

Figure 4.2 – Piezoelectric Testing Setup: (a) Agilent 33120A 15MHz Function/Arbitrary Waveform Generator, (b) TREK Model PZD700 Dual Channel Piezo Driver/Amplifier Series, (c) Digital Multi-Meter (DMM)

This setup allowed for the testing of the PZT, PVDF, and MFC. All three piezoelectric materials showed deflection characteristics. For the PZT and PVDF deflection was determined with the use of an oscilloscope. The oscilloscope provided the amount of deflection for both the PZT and PVDF. These two materials deflected on the nano-scale and would not provide sufficient deflection to induce fluid flow within the PDMS micropump. These materials can be utilized in future studies if the micropump is downscaled to the nano level. An example of the testing is shown in figure 4.3.

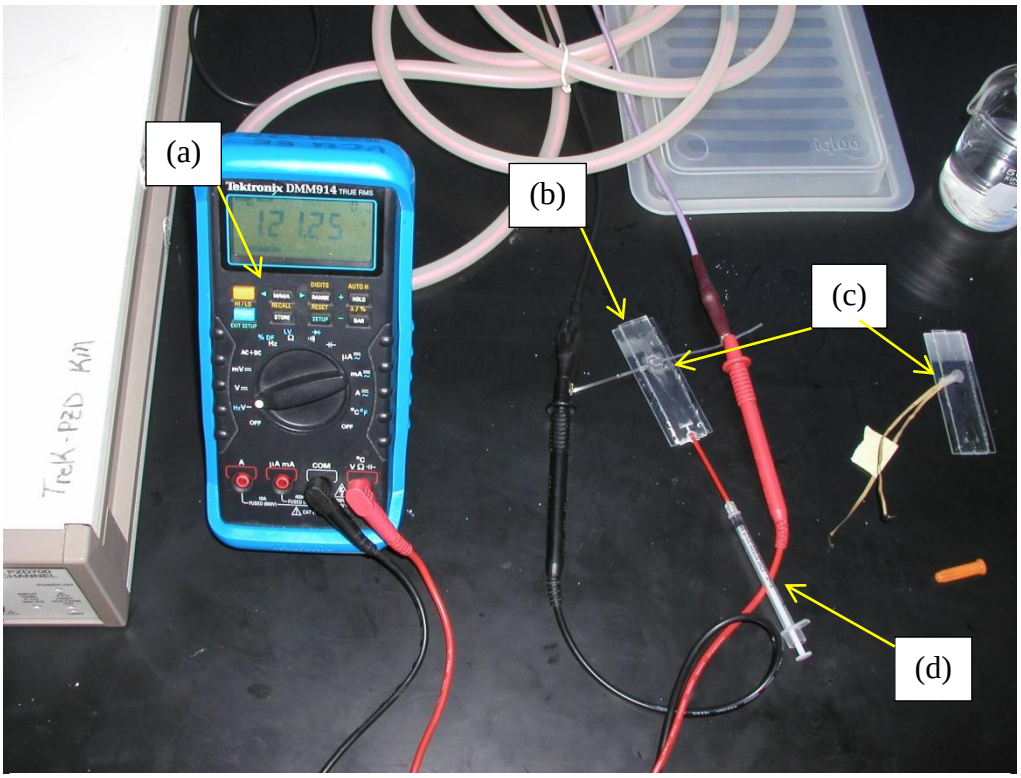

Figure 4.3 – Piezoelectric PZT and PVDF Testing Setup: (a) Digital Multi-Meter Tektronix DMM914, (b) PDMS Fabricate Pump, (c) PZT (left), PVDF (right), (d) Fluid input

MFC (Macro Fiber Composite) was tested and showed greater deflection. This piezoelectric material was placed on top of the PDMS micropump and a voltage was applied with alternating frequencies. The MFC deflected the PDMS minimally and no visual fluid flow was present from inlet to outlet. MFC by itself did depict great deflections at high voltages with different frequencies. This material proves to be a good candidate for micropump actuation, but it must be further investigated to achieve fluid flow results. An image of this material is shown in figure 4.4.

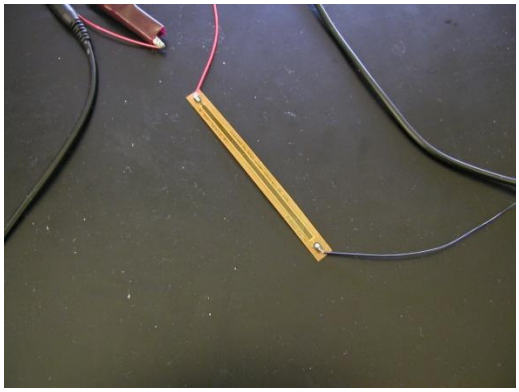

Figure 4.4: MFC Piezoelectric

All three piezoelectric materials did show deflections and movement when voltage was applied across the material. The only drawback to these materials is the high voltage that must be used in order to actuate these materials. These high voltages are acceptable at this time in order to provide actuation methods for the PDMS micropump, but it would be ideal to use lesser amounts of voltage for use in the actuation of the micropump. Out of all three piezoelectric materials the most plausible one to use would be the MFC because it provides a great amount of deflection on the microscale as well as on a scale greater. As for the other two piezoelectric materials, PZT and PVDF, this would be more suitable with a greater surface and/or a smaller nanoscaled micropump. Piezoelectric materials would be an ideal source for actuation in future progress of the micropump.

4.4: Magnetic Actuation

Magnetic actuation was studied and tested for actuation of the micropump. As previously discussed Fe_2B particles was incorporated into the PDMS mixture prior to dispensing on the fabricated molds. This process allowed for the incorporation of magnetic particulates to be in the

mixture to allow for attraction when introduced to a permanent magnetic. The micropumps had magnetic materials incorporated at different percentages in increments of 10 (i.e., 10%, 20%, etc.). It can be seen in figure 4.5 the magnetic micropump is being held in place prior to a permanent magnet being applied.

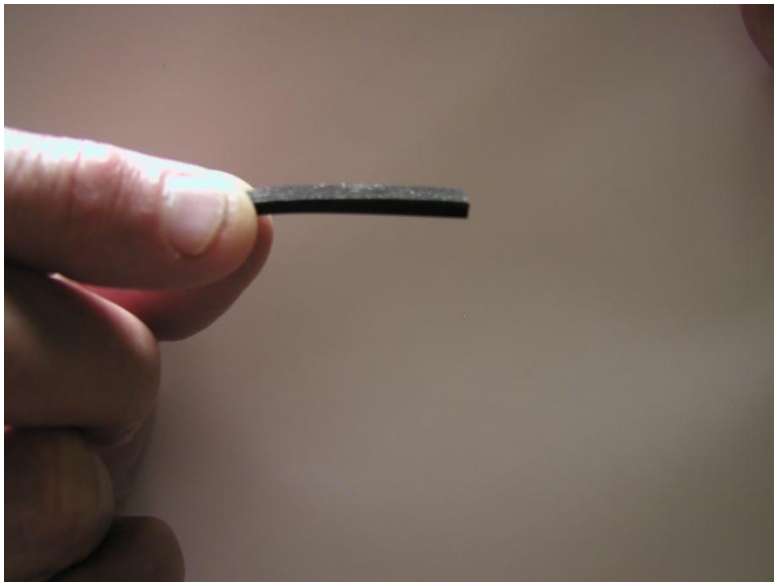

Figure 4.5: Magnetic PDMS Pump prior to Magnet Application (side view)

As a permanent magnet was introduced close to the PDMS micropump infused with the magnetic particulates (Fe_2B), it exhibited signs of attraction towards the magnet. This is illustrated in figures 4.6 and 4.7.

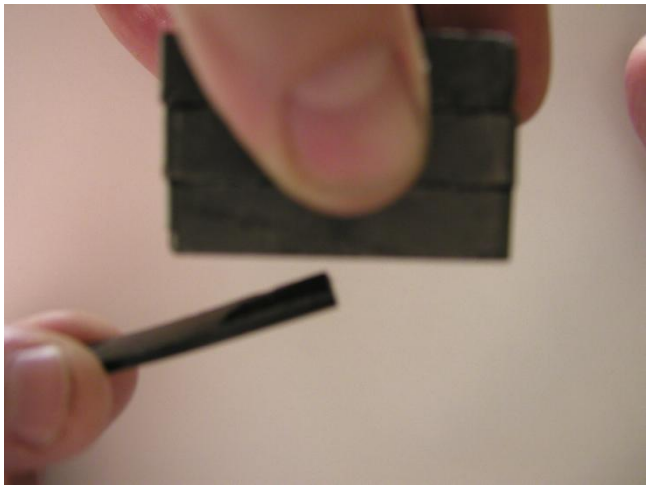

Figure 4.6: Permanent Magnet Attraction

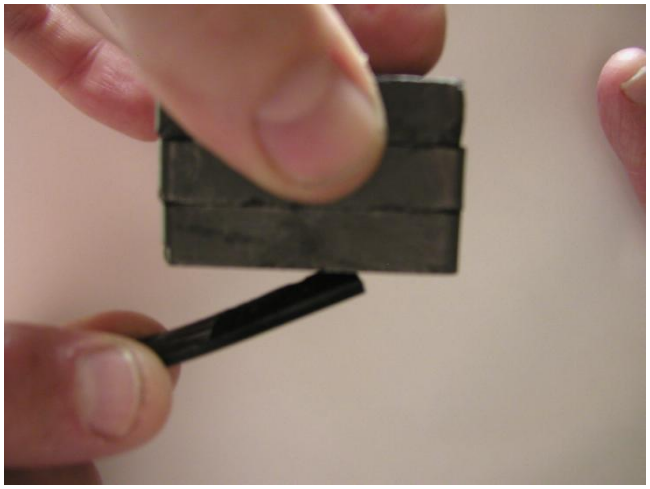

Figure 4.7: Permanent Magnet Attraction Complete

Once the preliminary study of the deflection of the magnetic micropump was studied the pump was then sealed to a substrate to experimental test if it would be functional to move fluid from inlet to outlet. The completed micropump can be seen in figure 4.8. As a permanent magnet was applied to the sealed/mounted micropump no deflection was noticed, thus resulting in no fluid transportation.

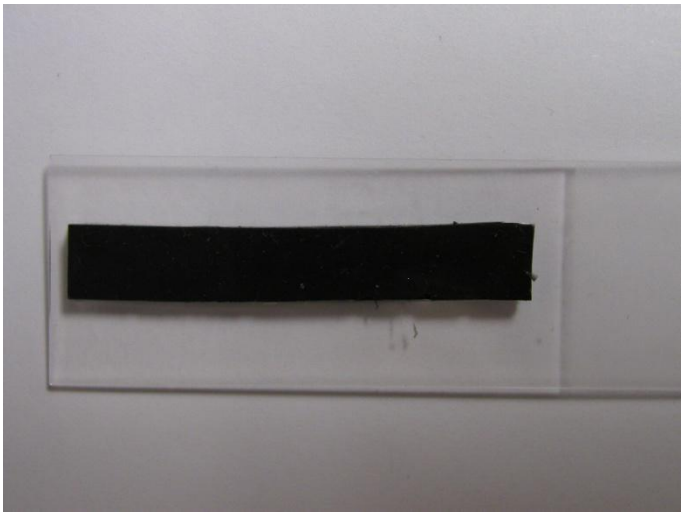

Figure 4.8: Magnetic Micropump Sealed to Substrate

4.5: Mechanical Motor Actuation

For actuation of the PDMS micropump modification of a mechanical reciprocating motor was utilized. The reciprocating motor was placed on top of the micropump device to provide the necessary pressure to actuate the micropump. This setup is shown in Figure 4.9.

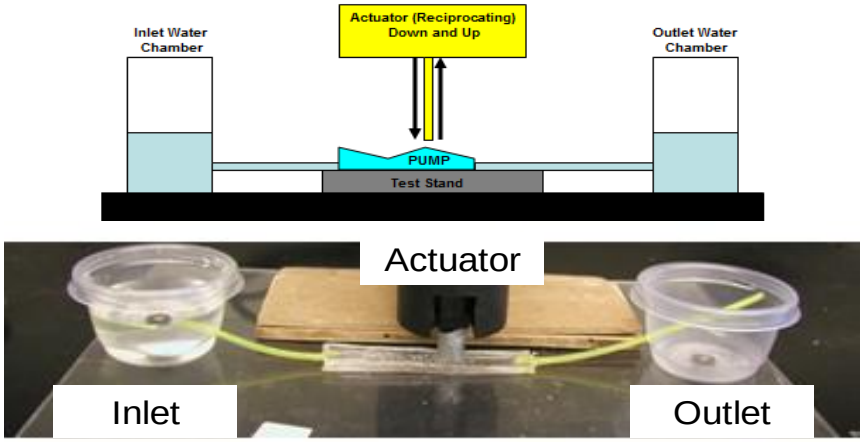

Figure 4.9: Mechanical Actuation Setup

This particular setup has proven very effective and efficient. Fluid is pumped from the outlet to the inlet side of the pump. Five fluids have been tested to determine the frequency at which each fluid will flow at its maximum throughout the micropump. The fluids tested consisted of water (viscosity = 1 cP, density = 1000 kg/m^3), ethanol (viscosity = 1.2 cP, density = 789 kg/m^3), isopropyl alcohol (viscosity = 2.4 cP, density = 786 kg/m^3), water-glycerine (viscosity = 3.5 cP, density = 1060 kg/m^3), and vegetable oil (viscosity = 69 cP, density = 920 kg/m^3). Each fluid was tested numerous times at different speeds based upon the mechanical reciprocating motor. These fluids possessed the following Reynolds Numbers (Table 4.1):

Liquid	**Viscosity (cP)**	**Density (kg/m3)**	**Reynolds Number (Re)**
Water	1.00	1000	583.5
Ethanol	1.2	789	209.2
IPA	2.4	786	72.97
Blood	3.5	1060	57.84
Oil	69	920	0.00424

Table 4.1: Reynolds Numbers for fluids tested

The reciprocating motor was operated at ranges from 250 strokes per minute up to 1250 strokes per minute. Each interval was increased by 250 strokes per minute giving the following intervals: 250, 500, 750, 1000, 1250 strokes per minute. To convert these frequencies utilization of the equation of frequency was utilized.

$$f = \frac{1}{T}$$

Frequency in the equation above is defined as 1 divided by the period, T, which are usually events that repeat per second. To calculate the frequency for strokes per minute, the number of occurrences (strokes) divided by the length of the time interval of the stroke (60 seconds) provided the following frequencies in table 4.2.

SPM	Frequency(Hz)
250	4.16
500	8.33
750	12.5
1000	16.66
1250	20.83

Table 4.2: Frequencies of Mechanical Actuator

Three graphs were created from the five liquids that were tested: Flow rate vs. Stroke per Minute (SPM/Frequency), Viscosity vs. Flow Rate, and Amount of time for beads to flow from the inlet to the outlet of the micropump. Each of these graphs depicts the best frequency at which to operate the micropump to achieve the maximum flow rate. The first graph, second graph, and third graph are shown in figures 4.10, 4.11, and 4.12.

The results of flow rate obtained with varying actuator strokes (frequencies) for different fluids are summarized in figure 4.10. It can be seen from figure 4.10 that flow rate for various fluids follow a similar pattern, with increasing flow rate. The flow rate increases, reaches an optimum and then decreases. Out of the five fluids tested, water with high density has higher flow rate in comparison to the other fluids.

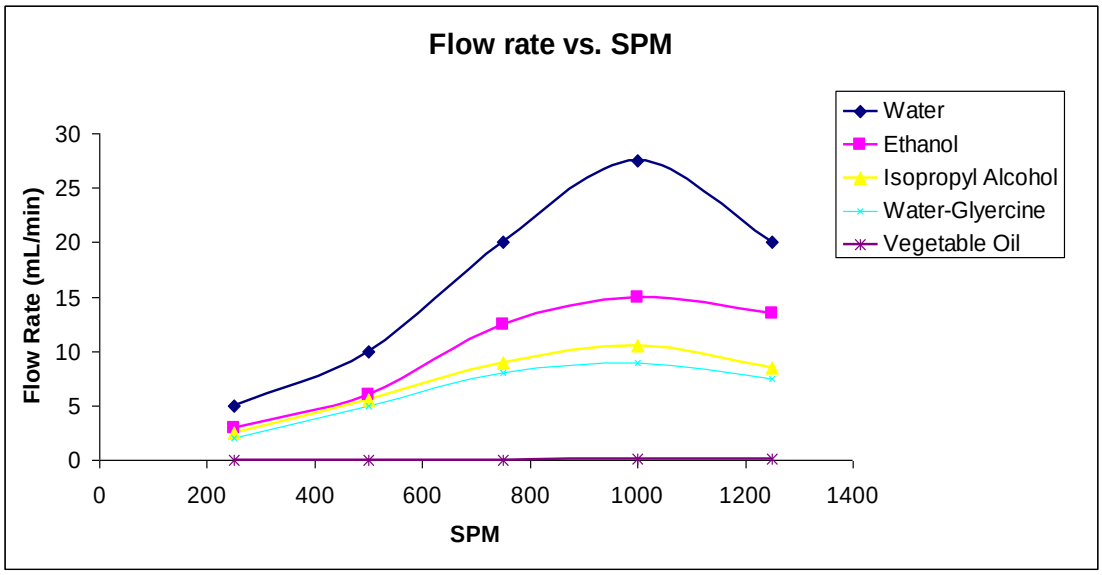

Figure 4.10: Flow rate versus SPM of the micropump performance

From the graph of the flow rate versus SPM (frequency) one may determine the best frequency to operate the micropump to achieve maximum flow rate. Data derived from the experimental testing indicates that the best frequency to operate the micropump is between ten to twenty hertz. Operating between these frequencies the maximum flow of the five fluids were achieved.

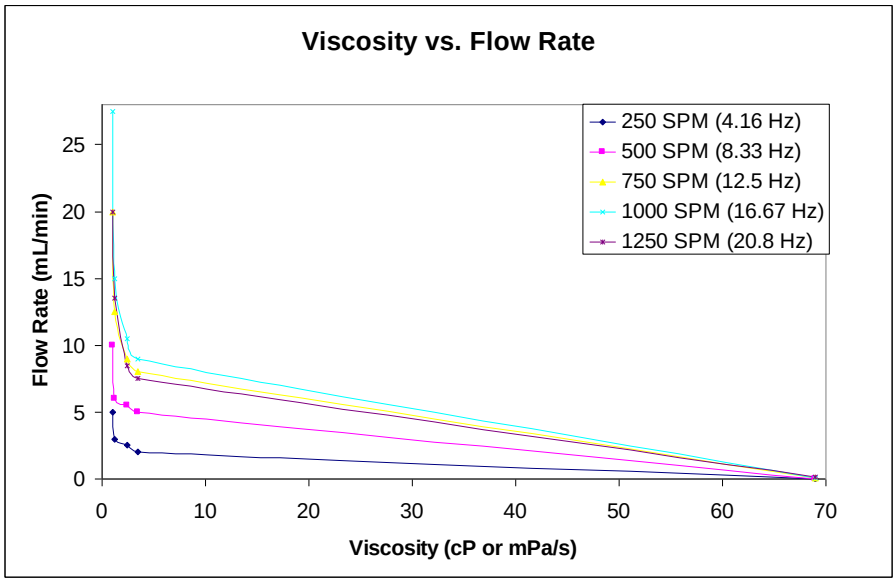

Figure 4.11: Flow rate versus fluid viscosity of the micropump performance

The graph of viscosity vs. flow rate (figure 4.11) shows the flow rate based on the viscosity at each stroke per minute (or frequency). The order of each point is based on the viscosity of the fluid that was tested starting from lowest to highest. Therefore, point one on each graph is water, point two is ethanol, point three is isopropyl alcohol, point four is water-glycerine, and point five is vegetable oil. This graph shows two different types of information. First, it shows at lower viscosities there will be higher flow rates, and at higher viscosities there will be lower flow rates. Looking at the data water (lowest viscosity) flowed quickly while on the other side of the spectrum vegetable oil (highest viscosity) flowed very minimally. Second, looking at the different frequencies one is able to determine again that the best frequency to operate the micropump is between ten and twenty hertz.

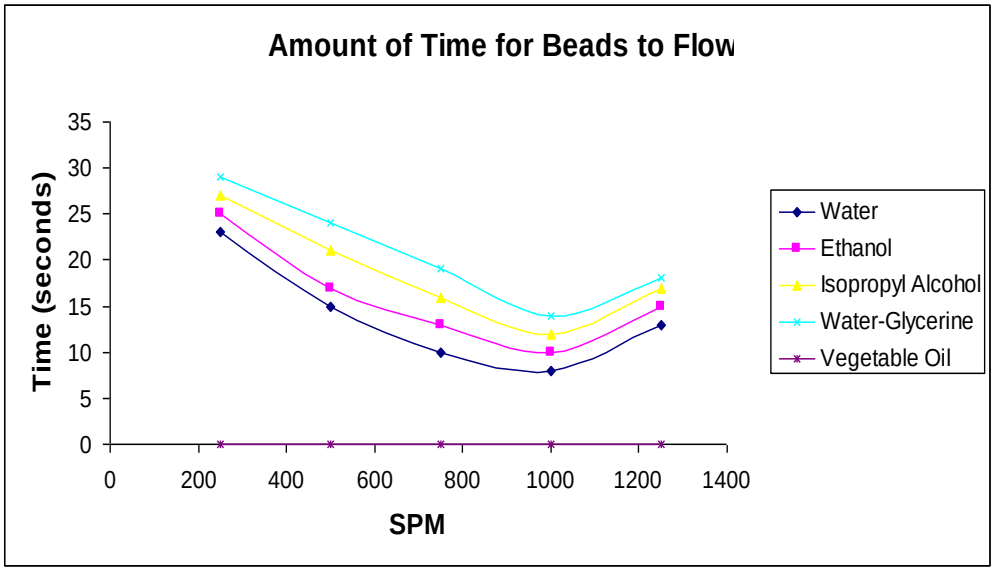

Figure 4.12: The time taken for beads to flow through the micropump with actuation

To determine how the micropump performs during actuation another experiment was conducted using fluid containing particulates. The amount of time for beads to flow from the inlet to the outlet of the micropump was investigated and the results are presented in figure 4.12.

Interestingly, there is also an optimum frequency (strokes) for the beads to travel through the micropump. It can be seen from figure 4.12 that the beads travel fastest at higher frequencies, and upon reaching its lowest point the speed of the beads begins to decrease. The graph depicting the amount of time for beads to flow through the micropump illustrates how much time it will take for beads to flow from the inlet to the outlet of the micropump at a certain frequency. This data again illustrates that the optimum frequency to actuate the micropump is around ten to twenty hertz. At this frequency the beads flowed faster from inlet to outlet as compared to the other frequencies.

Another factor that must be considered is the location of the mechanical actuator. Location of the actuator manipulated the flow rate of the micropump. In figure 4.13 the location of the actuator altered the flow rate. It can be seen from figure 4.13 that the optimum actuator location is at the center of the third chamber of the micropump.

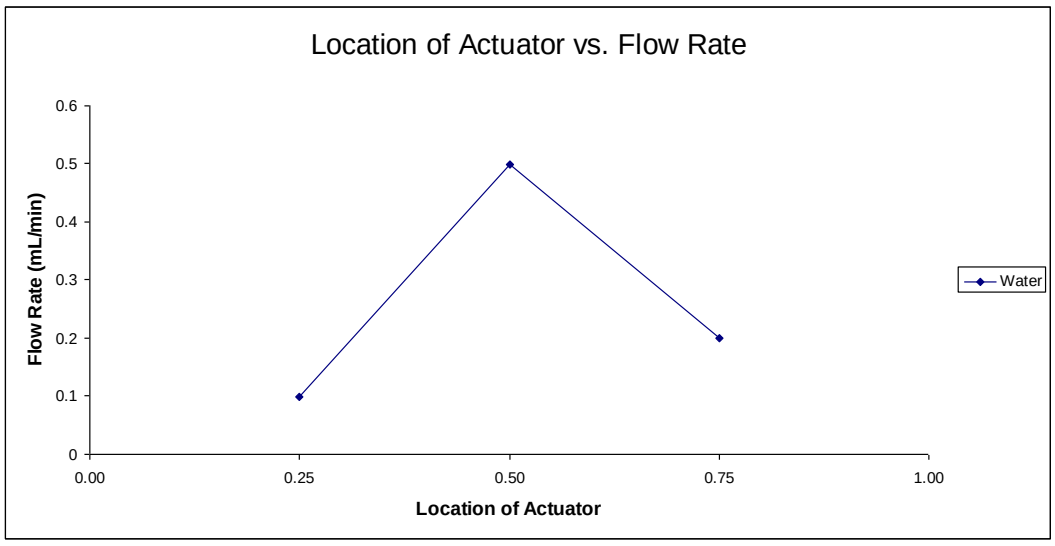

Figure 4.13: Flow rate versus the location of the actuator for optimum performance of the micropump

It must be noted that the flow through the micropump is laminar flow based on the Reynolds number (Table 4.1) for the designed micropump. In most instances the flow for microfluidic devices will be laminar. The flow through a microchannel or micropump can be characterized by the Reynold's number defined as:

$$\mathrm{Re} = \frac{LV_{avg}\rho}{\mu}$$

where L is the most relevant length scale, μ is the viscosity of the fluid, ρ is the fluid density, and V_{avg} is the average velocity of the flow. For many microchannels it is denoted that L is equal to 4A/P, where A is the cross-sectional area of the channel and P is the perimeter of the channel.

From the small dimensions within micropumps and microchannels, the Reynold's number is quite a bit less than one-hundred, and more often less than one. This type of Reynold's number dictates that flow is completely laminar with no turbulence at all. It must be noted that transition to turbulent flow usually occurs around a Reynold's number of two-thousand. Therefore, the micropump possesses laminar flow and with this type of flow molecules or particles can be transported through the micropump with a predictable pathway. It must be noted that even though that laminar flow exists in microchannels it is still possible to have momentum-based phenomenon such as flow separation [106].

These tests were performed on all three micropumps that were fabricated. The micropumps that were tested are shown in figure 4.14, with corresponding dimensions in figure 3.6. Each test followed the same trend and resulted in the same experimental results.

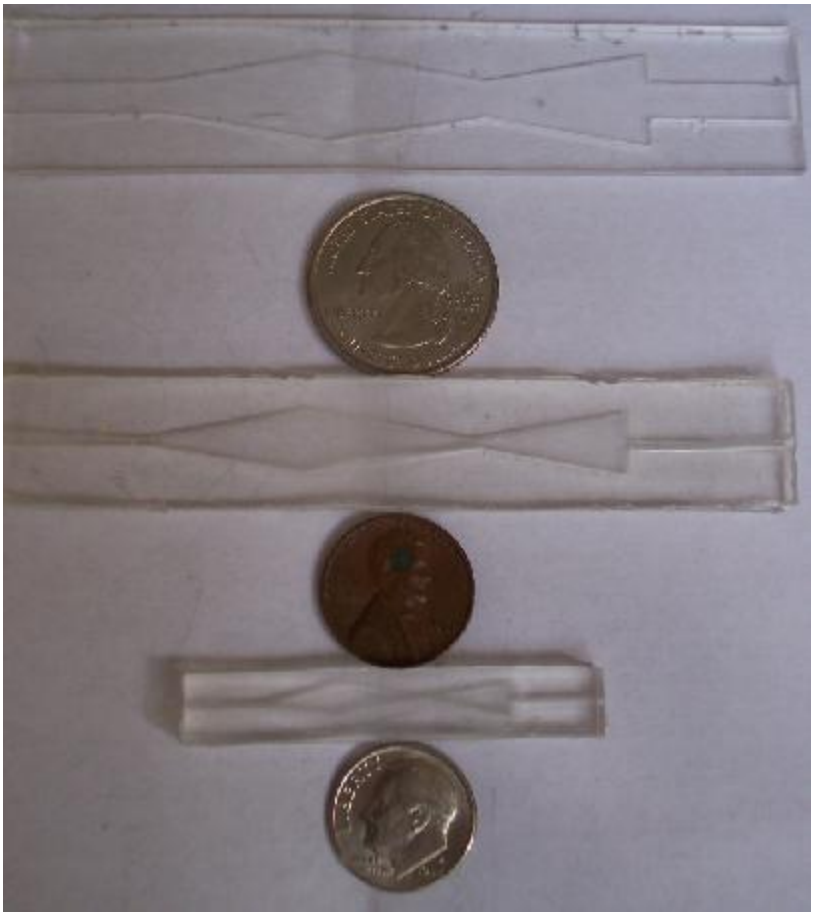

Figure 4.14: Fabricated Micropumps

4.6: Pressurized Inlet Flow Characterization

Another investigative method studied was varying the inlet pressure. The testing apparatus that was developed is shown in figure 4.15. There are two liquid chambers that provided and collected water as it flowed from the inlet and outlet of the micropump.

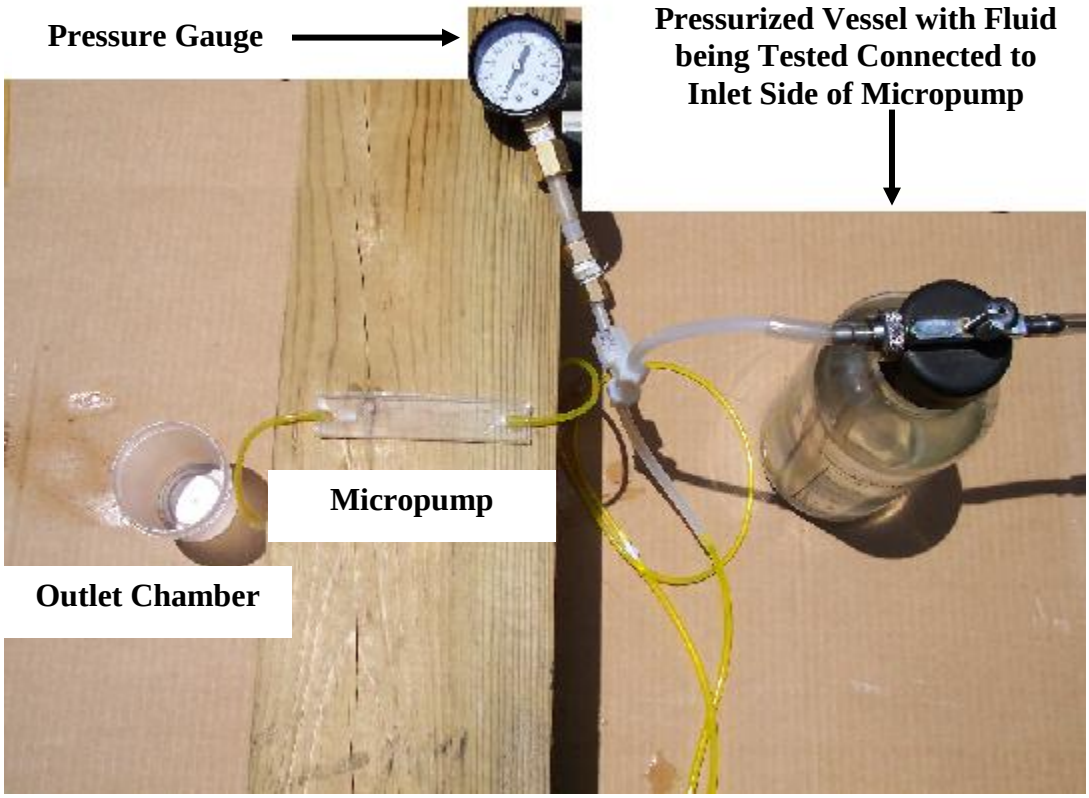

4.15: Pressure Test setup for the micropump flow evaluation

These results for flow rate obtained with varying pressures for different fluids are summarized in figure 4.16 – 4.18. It can be seen in figures 4.16 – 4.18 that flow rate for various fluids follow a similar pattern, with increasing flow rate. The flow rate increases, reaching an

optimum maximum and then remains constant. Out of the five fluids tested, water with the high density had a higher flow rate in comparison to the other fluids.

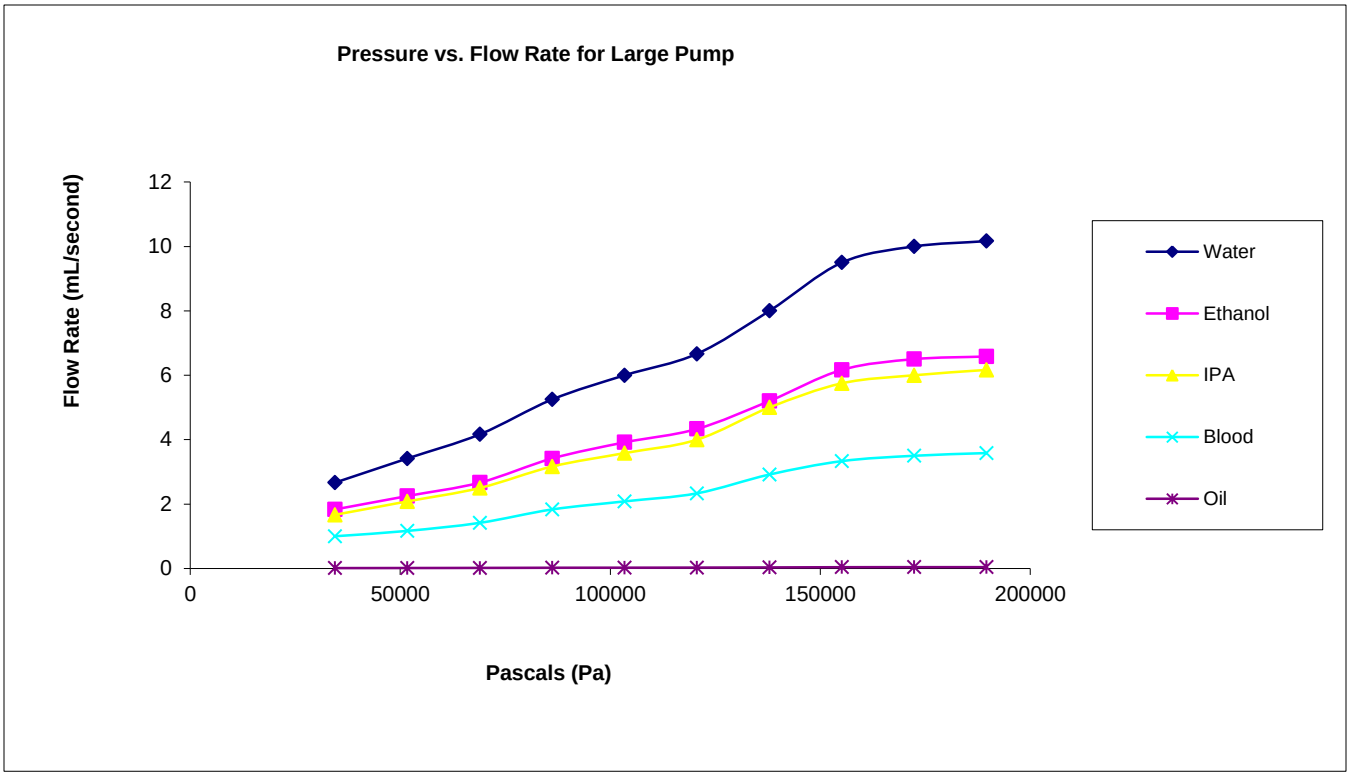

Figure 4.16: Pressure rate versus Flow rate of the micropump for Pressure Performance (Large Pump)

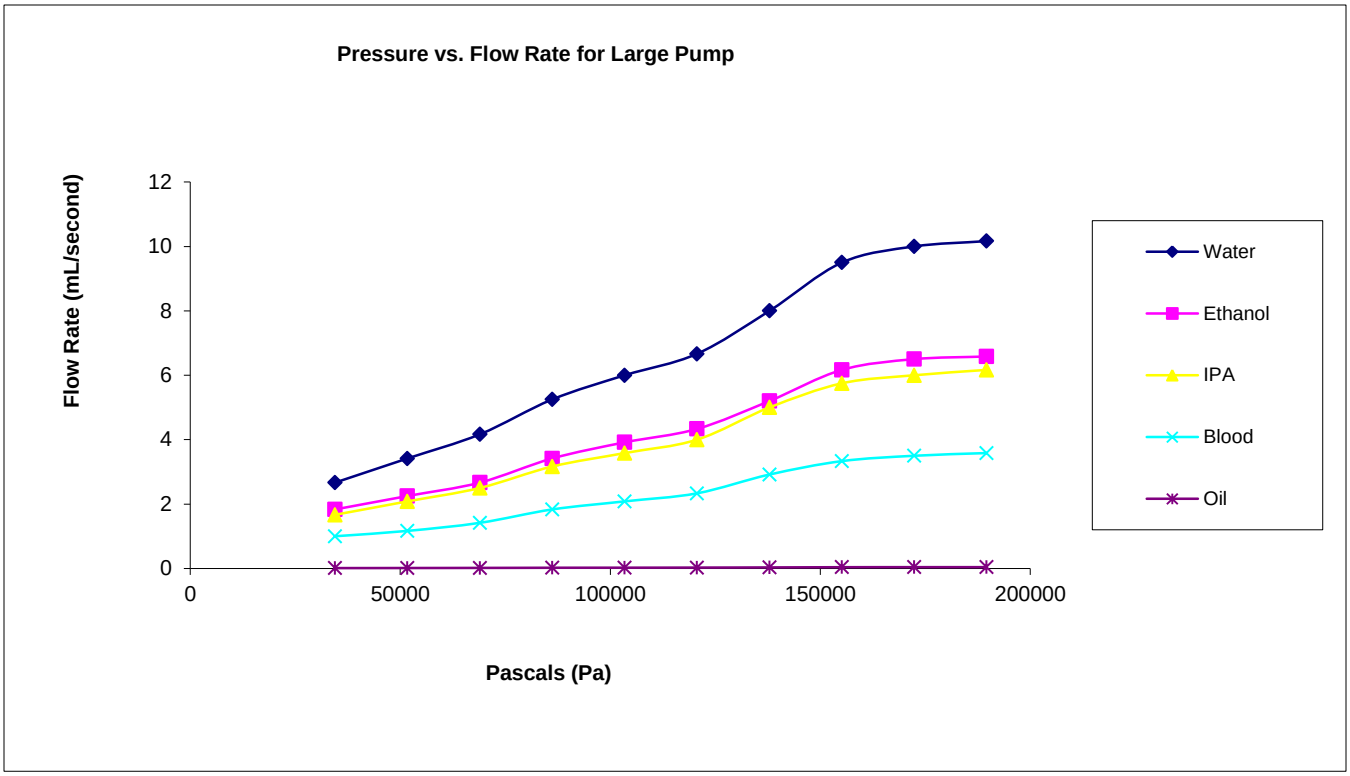

Figure 4.17: Pressure rate versus Flow Rate of the micropump for Pressure Performance (Medium Pump)

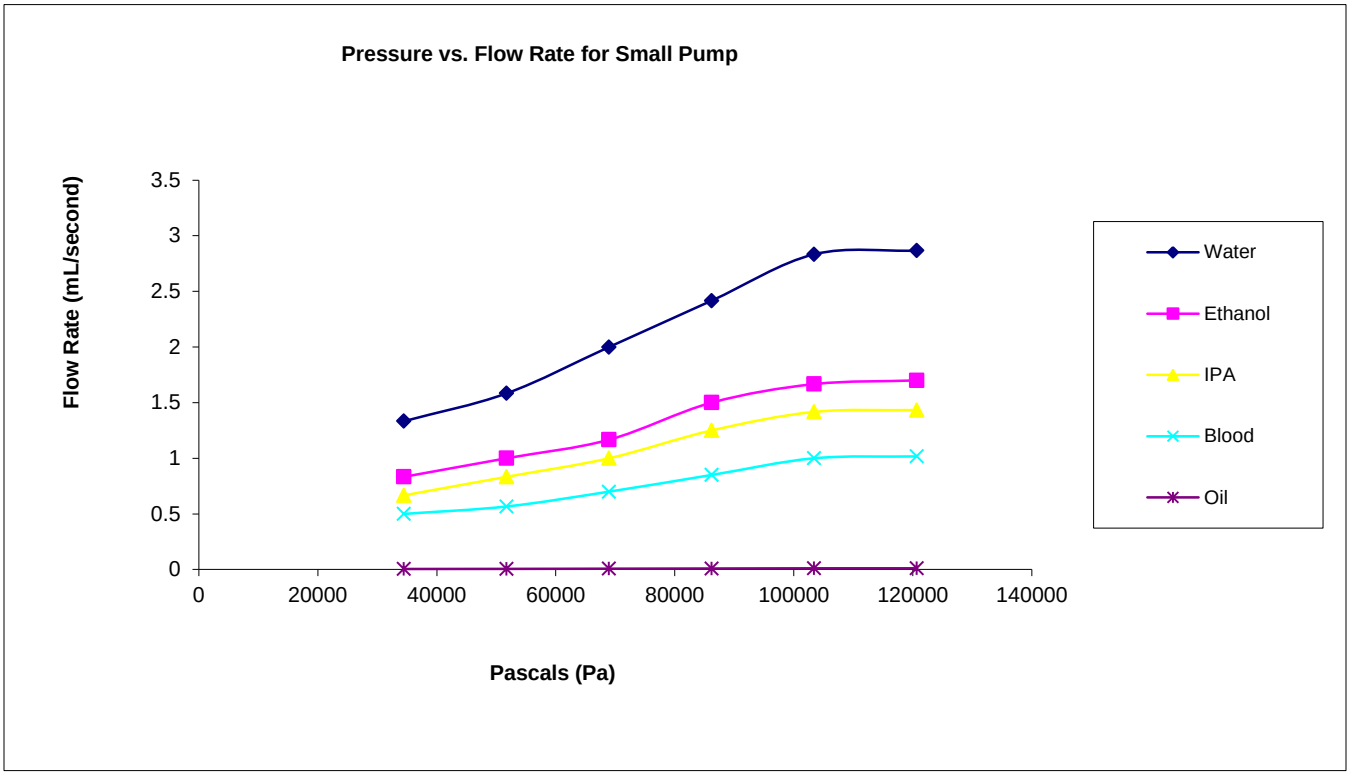

Figure 4.18: Pressure rate versus Flow Rate of the micropump for Pressure Performance (Small Pump)

The results presented illustrate the optimum, maximum pressure the micropump can operate before failure. It can be seen in figures 4.16 – 4.18 the greatest amount of pressure the micropump can undergo before rupture, which ranges from 200 kPa – 34.5 kPa (dependent upon overall size, but follows the same correlation). Prior to obtaining the maximum pressure, the fluids reach an optimum flow rate before leveling off (Note: Pressures may vary dependent upon size of pump, but will experience the same type of results).

4.7: Statistical Results and Discussion

4.7.1 – Theoretical Testing to Compare to Experimental

4.7.1.1 – Micropump Design Concept

The design concept for the micropump consists of a three nozzle/diffuser element that is actuated on top as previously discussed in this paper. The proposed valveless micropump design configuration for transporting drug particles was based on the fabrication process of the polydimethylsiloxane micropump device for fluidic applications by Cartin et. al. [59], with further theoretical studies completed by Su and Pidaparti [58] dealing with top actuation. The specified actuation in the micropump was achieved mainly by a pneumatic actuator. The overall performance of the micropump is determined by specific actuation mechanism and the resulting flow through the micropump. As opposed to existing valveless micropumps, the proposed design provides a new way for transporting liquid drug delivery using three nozzle/diffuser elements with actuating membranes.

4.7.1.2 – Computational Methods

To understand the characteristics of drug delivery through the proposed micropump design three-dimensional flow characterization studies were conducted using combined computational fluid dynamics (CFD) analysis based on Eulerian-Lagrangian methods. The first step to begin this analysis was to create a three-dimensional model of the micropump with the use of a modeling software (figure 4.19).

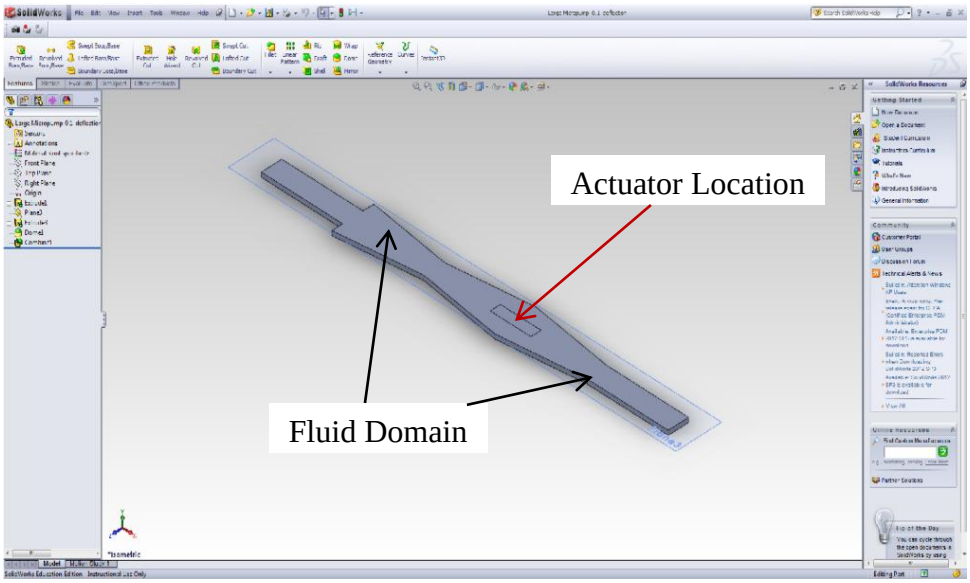

Figure 4.19 – SolidWorks Micropump Rendering

SolidWorks software was used to develop the three-dimensional model of the three nozzle-diffuser micropump. The three-dimensional model then is imported into ICEM mesh software (figure 4.20). This software allows the mesh to be generated and created, which is a standard preprocessor for ANSYS-FLUENT, and finally imported into the FLUENT software. FLUENT is finite element analysis software that utilizes Finite Volume Based methods to mathematical solve non-linear partial differential equations and simplify them into a system of algebraic equations which are solved numerically through various iterations. Values derived from Fluent are stored at the cell center and face values are interpolated from the cell center values for the convective term in the Navier-Stokes equations. Diffusion terms usually undergo discretization using central difference methods and in most instances are second-order accurate.

The three-dimensional, double precision, segregated, unsteady, incompressible solver with dynamics mesh option is chosen which is first order implicit with respect to the time that

makes the model unconditionally stable with time step size. This segregated solver is mainly utilized for flow that is incompressible where the resulting algebraic equations are solved sequentially as opposed to the couple solver which solves the algebraic equations simultaneously due to the inter-dependence of scalars associated with the flow field. The model is also laminar which results in no energy equation being solved. The fluid that was tested was water with the corresponding properties: Density, ρ: 998.2 kg/m^3 and Viscosity, μ: 1x10^{-3} kg/m-s. This analysis will be presented and discussed.

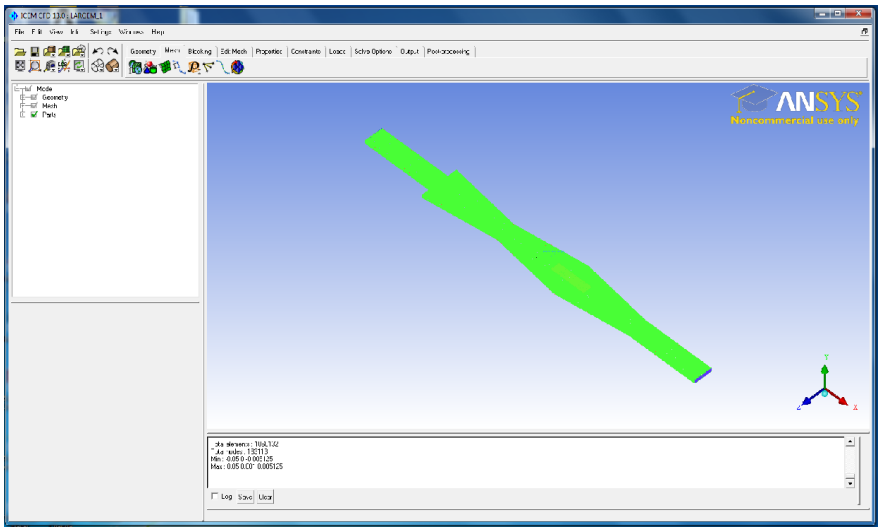

Figure 4.20 – Mesh of Micropump

4.7.1.3 – CFD Analysis

CFD simulations were utilized to analyze the three-dimensional flow within the micropump chamber. The flow in the micropump is assumed to be laminar, isothermal, and incompressible. The transient laminar flow model coupled with moving mesh approach was

employed to simulate the flow field in the micropump with moving boundaries actuated mechanically. The governing equations for the three-dimensional laminar flow are described by the conservation and momentum equations which are expressed as:

$$\frac{\partial \rho}{\partial t} + \nabla \cdot \left(\rho \vec{V} \right) = 0 \qquad equation(1)$$

$$\rho \frac{D\vec{V}}{Dt} = -\nabla P + B + \mu \nabla^2 \vec{V} \qquad equation(2)$$

where $\vec{V}$ is the velocity vector, P is the pressure, ρ is the fluid density, B is the body force, and μ is the dynamic viscosity. Assuming that the fluid density is homogeneous coupled with incompressible flow, the mass conservation, equation (1), becomes the divergence of the flow velocity vector. Conversely, when the flow field varies transiently with the moving membrane, the momentum equation (2) must include the transient velocity vector to acquire the unsteady physics. Since fluid flows within the closed boundaries of the micropump, body forces due to gravity do not influence the motion of the fluid. Therefore, the gravitational effects on the continuous phase are neglected in equation (2). To achieve the flow field characteristics the aforementioned equations were solved numerically on a fluid domain with a moving membrane actuator.

The simulations were completed with the use of computational fluid dynamics software called FLUENT (ANSYS/FLUENT, Inc.). The SIMPLE algorithm was used to solve the pressure-velocity coupling. This procedure is repeated at every time step until a converged solution for instantaneous flow is obtained.

4.7.1.4 – Actuator Motion

A user-defined function written in the C programming language was used to manipulate the movement of the actuator located on top of the micropump. The actuation location was on top of the micropump, which was governed with the following expression(s) in order to create the periodic volume expansion and contraction of the micropump chamber:

```
/************************************************************************/
/* unsteady.c                                                           */
/* UDF for specifying a transient velocity profile boundary condition */
/************************************************************************/

#include "udf.h"

DEFINE_PROFILE(SJ_velocity, thread, position)
{
 face_t f;

 begin_f_loop(f, thread)
  {
   real freq=25.;
   real vol=400.;
   real spd=vol/520.;
   real t = RP_Get_Real("flow-time");
   F_PROFILE(f, thread, position) = spd*sin(freq*(t-0.075)*(2.*3.141592654));
  }
 end_f_loop(f, thread)
}
```

This program was utilized and defined to the actuator of the micropump, which allowed one to manipulate the actuation frequency to determine the flow characteristics of the micropump. The expected operating mode of the micropump was to pump fluid from inlet to outlet, which was studied.

4.7.1.5 – Fluent Theoretical Results of Micropump

Conclusive results obtained for the micropump configuration consisting of a three nozzle/diffuser element were calculated with the use of ANSYS Fluent Analysis (figures 4.21 – 4.28). These results are listed below and will be discussed.

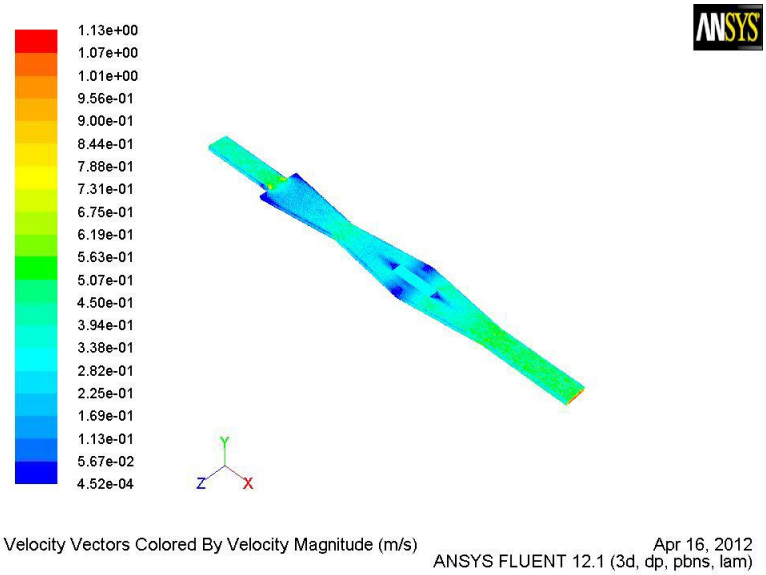

Figure 4.21: Micropump Actuated at 4.167 Hz

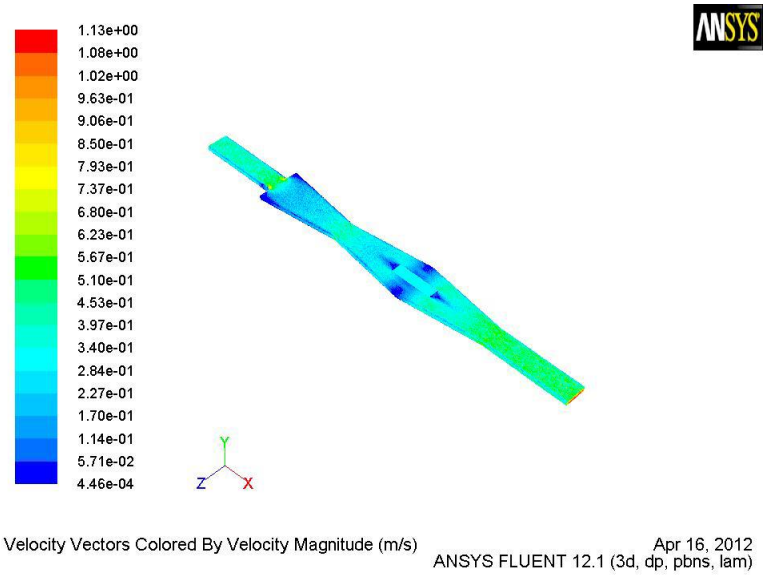

Figure 4.22: Micropump actuated at 8.33 Hertz (Hz)

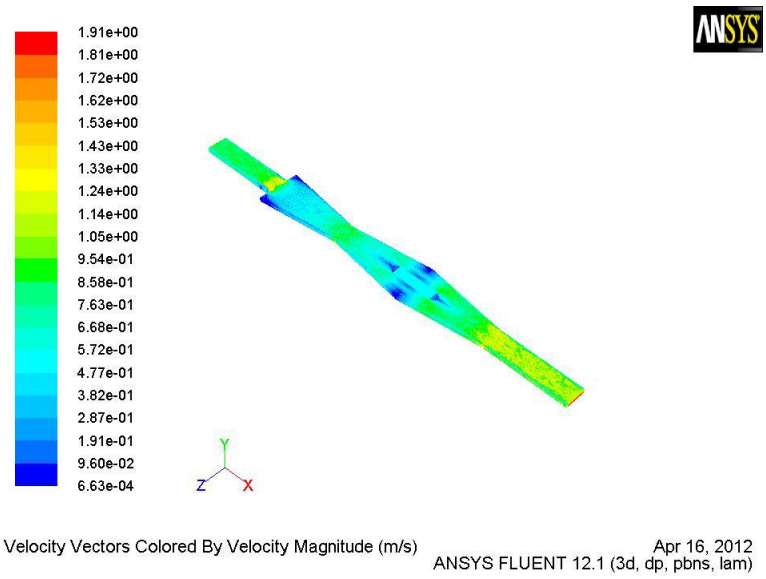

Figure 4.23: Micropump actuated at 12.5 Hertz (Hz)

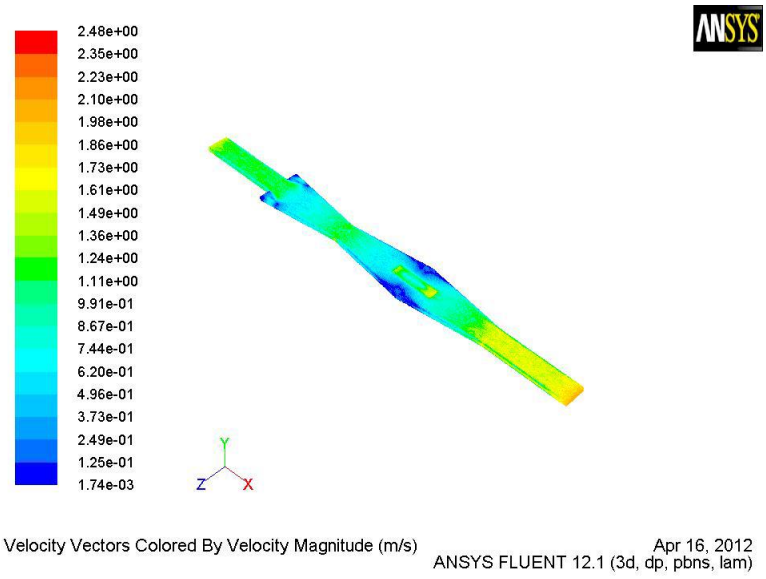

Figure 4.24: Micropump actuated at 16.67 Hertz (Hz)

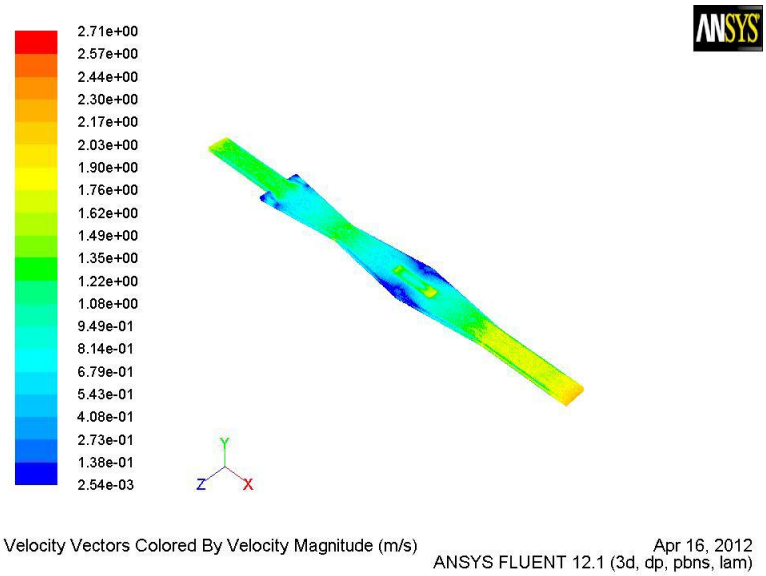

Figure 4.25: Micropump actuated at 20.83 Hertz (Hz)

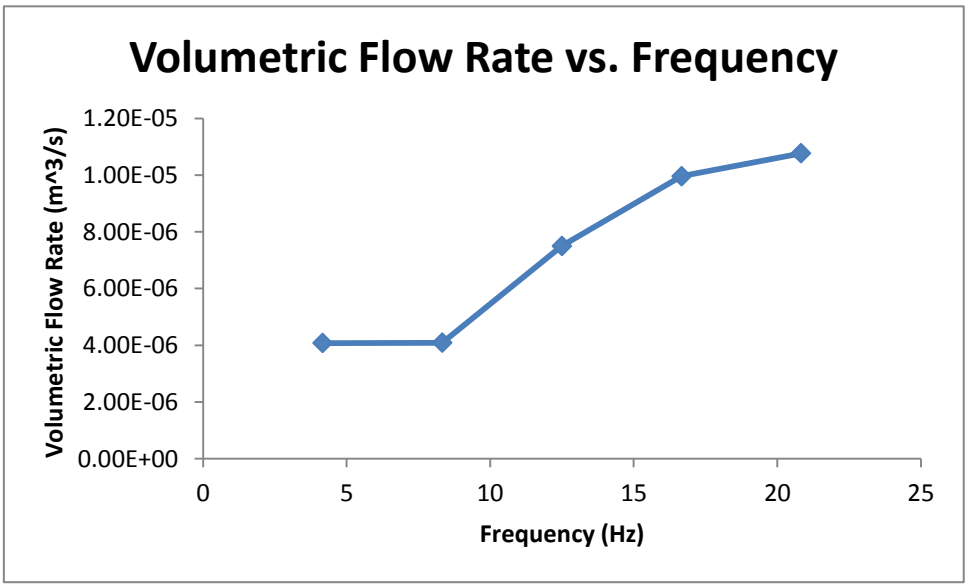

Figure 4.26 – Volumetric Flow Rate vs. Frequency

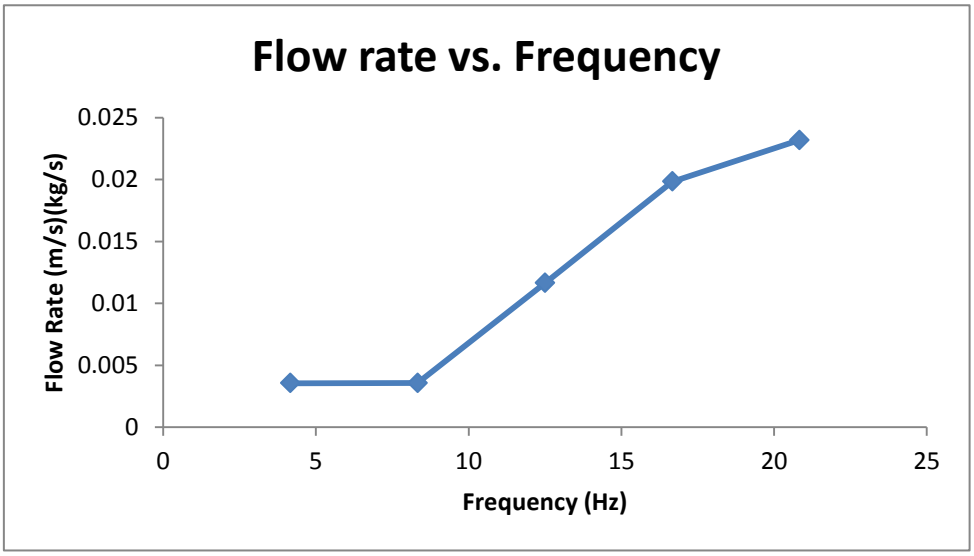

Figure 4.27 – Flow rate vs. Frequency

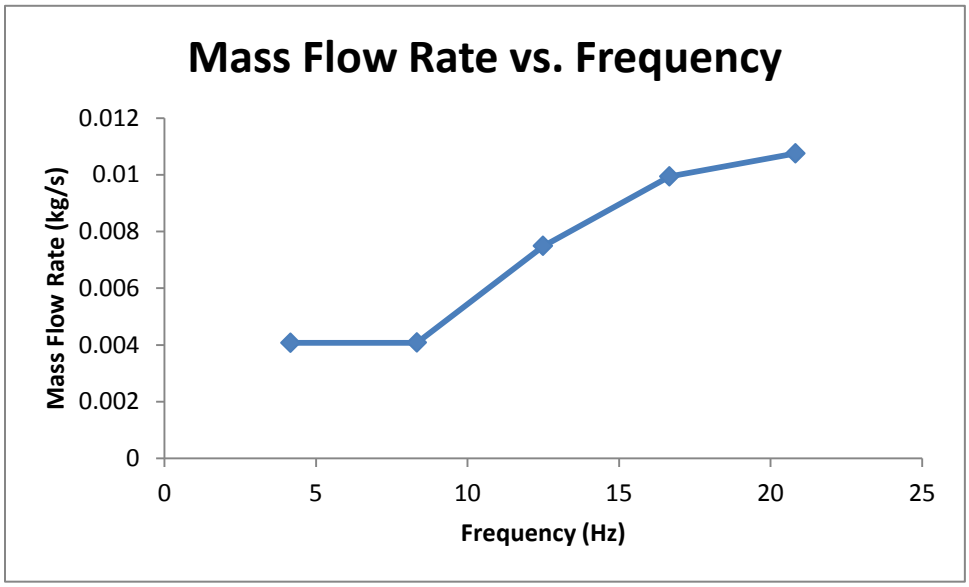

Figure 4.28 – Mass Flow Rate vs. Frequency

From figure 4.26 – 4.28 it can be seen that there is a relationship between the actuation frequency of the actuator located on top of the micropump and the flow rate through the micropump. The results from FLUENT illustrate proportionality between the flow rate and the actuation frequency of the micropump. These graphs depict as actuation frequency increases the flow rate through the micropump increases. The results shown in figure 4.26 – 4.28 illustrate that the novel actuation proposed and tested for the valveless micropump is a suitable candidate for fluid delivery applications.

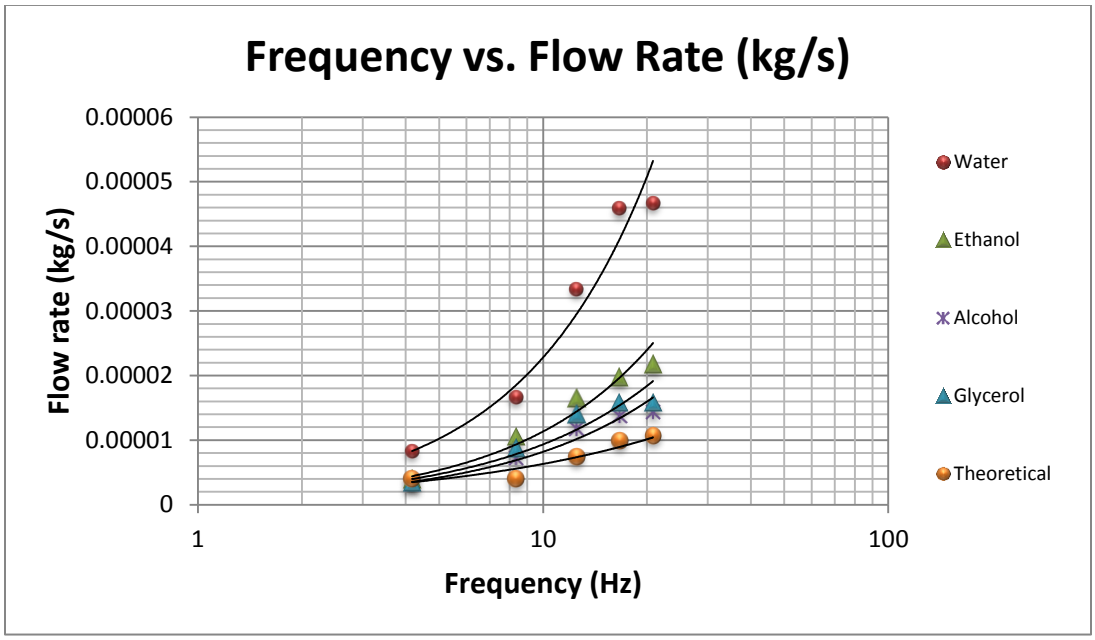

Figure 4.29 – Frequency vs. Flow Rate comparison of Theoretical and Experimental

From figure 4.29 comparison of the theoretical values and experimental values of the smallest pump tested one can see that the flow rates tend to increase with actuation frequency. Also it must be noted the flow rates experimentally tested were slight higher than the theoretical values obtained. It appears from both sets of results that micropump will continue to perform effectively and efficiently as frequency is increased.

In conclusion a systematic study to compare the theoretical and experimental results has been completed. The results obtained demonstrate the feasibility of the valveless micropump to deliver fluids for possible drug delivery applications. For fluid transport it is apparent that the mass flow rate of the liquid pumped by the micropump is proportional to the actuation frequency. Therefore, when frequency continues to increase so will the fluid flow seen theoretical and experimentally.

4.7.2 – Statistical Comparison of Previous Study

The experimental results that were developed with top actuation from the reciprocating motor can be compared to theoretical results that are presented in the paper written by Su and Pidaparti [58]. Their paper takes dimensions, fabrication, and testing procedures presented in Cartin and Pidaparti [59]. Su compared the relationship between the top actuation frequency of the micropump and the net mass flow rate. These results were presented and compared with experimental data collected from the reciprocating motor testing. Figure 4.30 illustrates the statistical data between the theoretical results and experimental results in an exponential curve relationship.

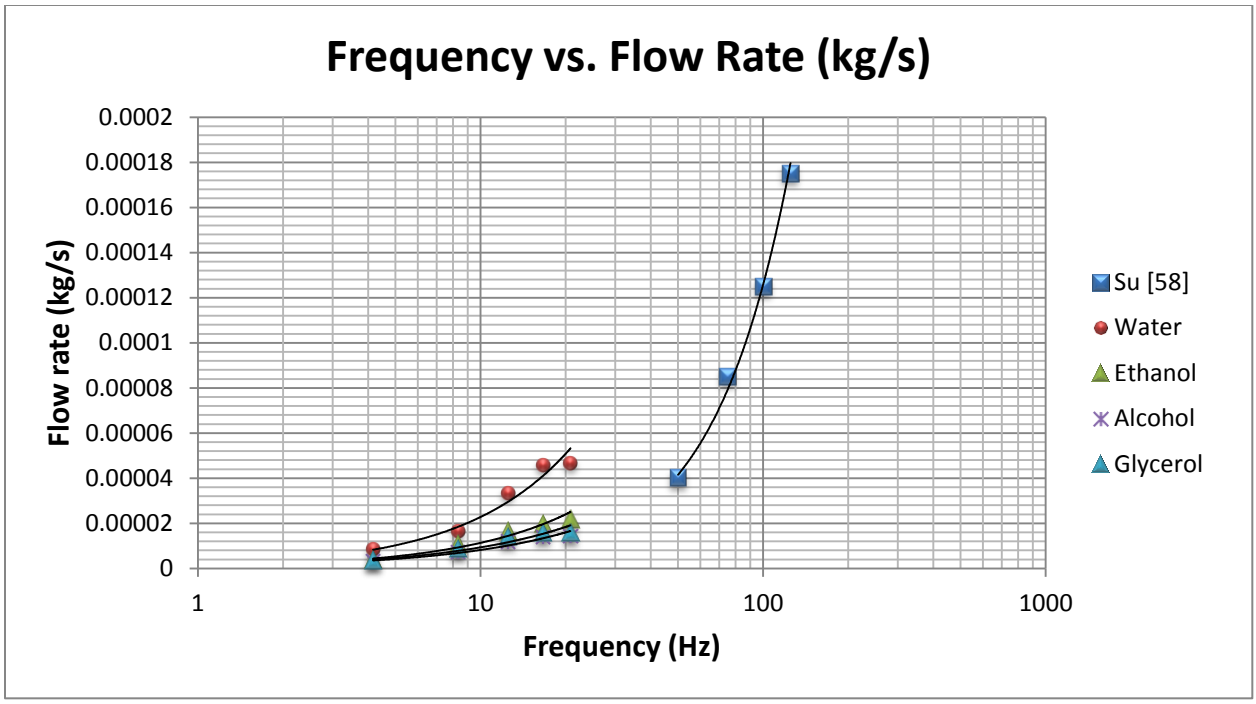

Figure 4.30 – Frequency vs. Flow Rate of Theoretical and Experimental

From the statistical data it can be determined that the experimental results followed closely to the theoretical results. It can be seen from the theoretical data that the flow rate continues to increase with actuating frequency. These results were similar to the experimental results when the micropump was downsized. This aspect of actuation frequency is important for possible drug delivery applications to determine the time for drug delivery based on a specific frequency applied to the micropump.

The present micropump with the three nozzle-diffuser elements appears to be more idealistic for drug delivery applications. As depicted in figure 4.30 the fluid flow through the micropump depends on the actuation characterization. It has been shown that the mass flow rate of liquid pumped through the micropump is proportional to the frequency of the actuator. The current micropump fabricated and tested both theoretically and experimentally requires less energy in comparison to some pressure-driven micropumps. The theoretical and experimental

analysis has presented similar results, thus resulting in a final fabricated product that can be replicated.

4.8: Results and Discussion

Results of flow rates obtained with varying actuator strokes (frequencies) for different fluids are summarized in figure 4.10. Figure 4.10 also shows that flow rate for various fluids follow a similar pattern. As the flow rates of the various tested fluids increased an optimum maximum flow rate was determined within a particular frequency range. Once this range was established and surpassed, flow rates began to drop.

Based on results obtained from the Flow vs. Frequency, Viscosity vs. Flow Rate, and Amount of time for beads to flow from the inlet to the outlet of the micropump one was able to determine the optimum frequency at which to operate the micropump to achieve the maximum flow rate. It can be seen in figure 4.10 that the flow rate versus the frequency is able to determine the best frequency to operate the micropump to maximize the flow rate. The micropump best operated between the ranges of 750 and 1250 SPM resulting in the maximum flow of the five fluids.

The results of flow rate versus fluid viscosity for the five different fluids are shown in figure 4.11, which indicates the flow rate based on the viscosity at each stroke per minute (or frequency). From Fig 4.11 it can be seen that the lower viscosity fluid results in lower flow rate and vice versa. It is also observed that water having low viscosity flowed quicker, in comparison to vegetable oil which has higher viscosity and flowed less.

To determine how the micropump performs pumping with fluid containing particles, another experiment was conducted. The amount of time for beads to flow from the inlet to the outlet of the micropump was investigated and the results were presented in figure 4.6. Interestingly, there is also an optimum frequency (strokes) for the beads to travel through the micropump. It can be seen from figure 4.12 that the beads travel fastest at frequencies between 750 SPM – 1250 SPM.

The effect of actuator location was studied to determine the optimum location along the micropump to place the mechanical actuator. The results of flow rate based on actuator location are shown in figure 4.13. It can be seen in figure 4.13 that the optimum actuator location is at the center of the micropump. It is also noted that the flow through the micropump to be laminar flow based on the Reynolds number for the designed micropump illustrated in table 4.1.

The effect of applying a pressure to drive the fluid through the pump from inlet to outlet was studied to determine the maximum rate of flow and pressure the micropump could withstand. Based on figure 4.16 – 4.18 one can see that the size of the micropump determines the amount of maximum flow and pressure the pump can undergo. As the pump is downsized the micropump experiences the same flow characteristics, but at lower pressures. Prior to reaching the maximum pressure, the fluids reach an optimum flow rate before leveling off. It must also be noted that the pressure may vary dependent upon the size of the pump, but will experience similarities in final results.

4.9: Conclusions

In this study, the performance of a micropump consisting of three nozzle/diffuser elements designed and fabricated from PDMS material and actuated on top by a reciprocal motor and pressurization was evaluated. The performance characteristics of flow rate obtained from testing demonstrated the efficiency of the micropump. The results obtained illustrate the relationship between actuation frequency and fluid flow through the micropump. Final results indicate the flow rate increases with actuation frequency, reaches an optimum and then decreases after that. Based on the performance studies conducted, the designed micropump performs reasonably well.

CHAPTER 5 Conclusions and Recommendations

5.1: Conclusions

The theoretical research utilizing ANSYS software proved that the three-wall micropump (nozzle/diffuser/nozzle) would outperform other micropumps consisting of only one-wall (nozzle) or two-wall configurations (nozzle/diffuser). Each test conducted and analyzed with the use of ANSYS confirmed that the experimental micropump developed both in the VMC microfabrication lab and the SolidWords/Rapid-Prototyping labs performed similar to the projected theoretical experiments. It must also be noted that top actuation and piezoelectric actuation was theoretically studied and proven to be effective in solid and fluid interaction, allowing one to determine the optimum frequency to actuate the micropump.

Overall research for fabricating the micropump was successful on two levels. The first level utilized the microfabrication techniques that focused on a method for coating SU-8 photoresist to develop the pump. Secondly, the use of SolidWorks and Rapid prototyping allowed for development of the micropump in half the time. Investigation of these two fabrication techniques allowed one to select the best fabrication process to reduce production time and cost to potential consumers.

Several positive outcomes can be concluded from the overall research. First, PDMS molding and PDMS sealing methods are used to reduce the process time for production, thus reducing the cost for mass production possibilities. Second, the fabrication methods are easy to manipulate and control in order to change dimensions based on overall design considerations.

Third, the transportation of the fluids throughout the micropump is laminar with optimum flow rates which allow for a higher accuracy of fluid flow.

5.1.1 – Design Concept

The design concept was originally developed as a four wall micropump, but from analysis was changed to a three wall micropump. The pump would be actuated on the top and sides of the micropump. Pump actuation on the top was hypothesized to be done with a pressure applied to the top surface of the micropump. Designs were simulated and tested with ANSYS and proved to be theoretically possible.

5.1.2 – Fabrication Methods

Two fabrication methods were investigated: VMC cleanroom fabrication and Rapid-prototyping. The VMC cleanroom fabrication proved to be quite difficult and time consuming. A great amount of time was placed in development of the design and processing the fabrication procedure through cleanroom procedures. The procedures and protocols in the cleanroom proved to be possible, but with difficulties. Difficulties revolved around learning how to use equipment, equipment down time, and processing failures. Other issues that occurred were determining the best photoresist to use for fabrication, the overall lithography process, exact development times of the PDMS mold, and removal procedures. All of the cleanroom fabrication methods were utilized to produce several pump designs already discussed in this paper. These processes did require much time and several months of preparation. As with any

fabrication and process development there will be many failures. Many of the fabrication methods led to failures in the end, but yielded ideas on how to improve the micropump fabrication methods resulting in a more desirable and reliable device. Even though many drawbacks and failures did exist, these failures allowed revisions to be implemented in the process resulting in a final product.

Rapid-prototyping methods proved to lessen the amount of time to create the micropump, but still resulted in a time consuming procedure. A SolidWorks file had to be designed and uploaded into the SLA rapid-prototyper. The prototyping procedure could take anywhere from two hours to six hours depending on the resolution and tolerances required for the micropump. After the prototype is accomplished PDMS was poured and cured for approximately a couple of days. Even though this procedure required less lab facilities, time for part production still took the same amount of time.

5.1.3 – PDMS Mixing, Curing, and Degassing

PDMS was a two part mixing process that took a considerable amount of time to determine the best mixing and curing process. At the beginning of the PDMS mixing process several defects occurred such as air-bubbles, micropump weakness, cracking, and micropump sagging. Due to these issues the introduction of a vacuum chamber and microparticles was incorporated. The vacuum chamber was utilized to remove air bubbles from the mixture and the microparticles were integrated to provide more strength to the PDMS polymer. These changes helped reduce defects and molding problems, but in some instances during the baking procedure defects at times still occurred such as bubbling due to excess heat. It should be noted that the

mixing process must be done precisely with an electronic mass scale to make sure the ratio is 10:1. The use of an electronic scale allowed for one to precisely add the microparticles in percentages of 10, 20, etc. Depending on how one desires the PDMS to be, rigid or flexible, the mix ratio and microparticles can be altered to produce results that are desirable to one's experiment. Curing the PDMS resulted in bubbling or overbaking of the PDMS. After several test runs with curing the PDMS, the best results were obtained by baking it a lower temperatures then allowing it to cure an additional twenty-four to forty-eight hours at room temperature. This method produced the best results after numerous times of experimentation with curing the PDMS micropumps. It was also observed that simply allowing the PDMS to cure at room temperature for several days (approximately three) produced extraordinary results. Dependent upon time constraints and desired results the best theory is to produce quality over quantity. Therefore, allowing the PDMS to sit several days would yield better micropumps free of defects. Thus, several micropump molds were developed to allow for several to be made simultaneously.

5.1.4 – PDMS Sealing

Sealing of PDMS to a substrate took a substantial amount of time to determine and yield a sealed pump. This type of sealing has not been tested or investigated that much prior to the fabrication of the PDMS Micropump. To determine the sealing recipe, several steps were taken using the oxygen-plasma machine to develop the best procedure necessary to seal the PDMS to a substrate. The process pressure that final gave adequate sealing results was approximately 600 mTorr. At this pressure sealing of the PDMS was capable and satisfactory.

Other issues that revolved around the sealing process were the cleaning of the PDMS and substrate in order to provide a clean surface for proper adhesion. The cleaning procedure was investigated and two procedures were developed in order to provide proper adhesion. These two methods were a Piranha etch and a Methanol/Acetone/Isopropyl Alcohol/DI Water dipping. Each of these methods was tested numerous times to determine the amount of time and how long the PDMS and the substrate had to undergo cleaning to acquire good adhesion characteristics. It must be noted that the above methods for cleaning may cause negative characteristic changes to the PDMS. PDMS when introduced to chemicals, such as Methanol and Acetone results in undesirable outcomes. The negative side effects that occur when PDMS is introduced to these chemicals are expansion/swelling, tackiness (stickiness), deformations, and overall destruction of the device. This was observed a few times prior to finally determining some of these methods were not the best. In the end the best method was to clean the PDMS was with slight IPA and DI water rinse.

5.1.5 – Electrostatic Actuation

The fabrication method for the electrostatic pump was quite extensive and novel. The fabrication technique utilized a commonly used polymer, polydimethylsiloxane (PDMS). The pump was constructed from a molded PDMS wafer process, coupled with metal electrodes. After the pump was finished and connections in place it was then sealed to a glass substrate with corresponding metal connections. Sealing of the two structures utilized a unique oxygen plasma treatment between the PDMS and glass wafer structure. A complete electrostatic fabrication wafer was shown in figure 4.1.

The PDMS micropump was developed in the microelectronics lab and required a large amount of time from start to finish. Once the pump was completed, it under went metallization with the use of a shadow mask as previously discussed. As metallization of the electrodes occurred on the PDMS substrate the appearance of the connections appeared sufficient until testing. It was observed the metal connections would break down over time. Further observations during precise testing indicated that the voltage continuity on the electrical connections would break down preventing current flow. Breaking of the electrical connections was also observed based upon the flexibility of the PDMS. These issues led to minimal to non-visible actuation of the micropump resulting in no positive experimental results.

5.1.6 – Piezoelectric Actuation

Actuation with the use of piezoelectric has been investigated. A total of three piezoelectric materials have been focused upon, PZT, PVDF, and MFC. The first two, PZT and PVDF, piezoelectric materials provided no considerable movement of fluid through the micropump that was tested. The piezoelectric materials were tested with an oscilloscope to determine if they were functioning properly. Each was functional and had deflections that were in the nano-scale. These piezoelectric materials could be utilized in future work if the micropump is downsized to smaller scales and dimensions. If nanoscale micropumps are sought in the future, then these materials may provide useful characteristics.

MFC the last piezoelectric tested provided some movement of the micropump top wall, but with virtually no fluid movement. This piezoelectric material needs to be investigated further to determine if it will eventually provide fluid flow through the micropump. This is a

relatively new material and appears to be a very flexible, moveable piezoelectric that would complement the PDMS material.

5.1.7 – Magnetic Actuation

Magnetic actuation of the micropump was considered during fabrication and testing. Incorporation of Fe_2B magnetic particles was accomplished and completed for the PDMS micropump as previously discussed. After the magnetic PDMS micropump was sealed to PDMS and/or glass the application of a permanent magnetic did not provide a deflection or fluid transportation through the micropump. Possible reasons for no deflection can be a host of issues dealing with magnetics, which could lead to a new research topic.

Some of the problems with magnetic actuation for this research for actuating the micropump can be due to the particles used and the magnet or magnetic force applied. As previously discussed the incorporation of magnetic particles in the PDMS mixture was performed. The issue most likely involving the incorporation was applying a magnetic field during the curing process. Applying a magnetic field would allow the magnetic particles to align themselves within the PDMS mixture. This was attempted with a permanent magnet, but did not lead to consistent results.

Recall that the magnetic force is related to magnetic permeability (μ), H-field (magnetic field), the gradient, and the magnetization (M). Determining the field gradient is not a short term process. Characterization of the magnetic field just to determine a plausible actuation method for this PDMS micropump structure would be not only time consuming, but would lead to a new research method for micropump actuation. If this actuation method is studied and executed in

the future the incorporation of an electromagnet would be ideal. An electromagnet consists of an electric current that can be utilized for making temporary magnets. Electromagnets work on the magnetic effect associated with current flow. It has been studied that a soft iron core (rod) can be situated within a solenoid (wound wire), resulting in a strong magnetic field due to the iron core being magnetized by induction. Combination of the iron core and solenoid is considered an electromagnet.

Electromagnets act as a magnet only when current is flowing through the solenoid. Once the current is turned off, the solenoid becomes demagnetized. The core of the electromagnet must be soft iron (in most instances) because soft iron tends to lose all of its magnetization characteristics once the coil is turned off. This design consisting of iron cores and solenoids can allow electromagnets to consist of various shapes and sizes for different applications. The main factors affecting the strength of an electromagnet is directly proportional to the number of turns in the coil (solenoid), directly proportional to the current flow, and inversely proportional to the length of air gap between the poles. In conclusion, an electromagnet would be more ideal than a permanent magnetic due to the fact that it can produce very strong magnetic fields and its strength can be manipulated by varying the number of turns in the coil or by simply changing the current flow through the coil.

5.1.8 – Mechanical Actuation

This method of actuating the micropump resulted in much time in figuring out how to provide top actuation. A reciprocating mechanical motor was acquired in order to provide the top actuation method for the micropump. This method allowed the micropump to be tested.

Testing allowed one to determine the best frequency to acquire the maximum flow rate. From the three graphs that were developed one is able to determine several characteristics.

Three conclusions can be formed from the data acquired through mechanical testing. The first conclusion from the graph of flow rate versus frequency is that as frequency increases the flow rate for a fluid will increase up to a point where the optimum flow rate and frequency occurs. After the optimum flow rate and frequency is achieved, one can see that as frequency continues to increase flow rate beings to drop back down. This date allows one to determine that optimum frequency to operate the micropump to achieve the maximum flow rate.

From the graph of viscosity versus flow rate, one can come to the second conclusion that proves the basic theory of viscosity. As viscosity decreases the flow rate increases and as viscosity increases the flow rate decreases. This is seen through the testing of the five fluids that were investigated within the micropump.

The last graph depicting the amount of time for beads to flow from inlet to outlet provides one with conclusion three. From this graph it can be shown that as frequency increases the amount of time for beads to flow from the inlet to the outlet of the pump will decrease. This means that as frequency increases the time for the beads to travel the overall micropump will be quicker. Eventually an optimum frequency will give the fastest time that is required for particle travel. Once this optimum frequency is passed and continues to increase the time for particle travel will increase as well. This means that once we surpass the optimum value the time for particle travel will go from a fast regime to a slower regime.

5.1.9 – Pressure Actuation

The results presented illustrate the optimum, maximum pressure the micropump can operate before failure. As previously discussed in the previous chapter the greatest amount of pressure the micropump can undergo before rupture, which ranges from 200 kPa – 34.5 kPa (dependent upon overall size, but follows the same correlation). Prior to obtaining the maximum pressure, the fluids reach an optimum flow rate before leveling off (Note: Pressures may vary dependent upon size of pump, but will experience the same type of results). The results obtained from this experimental test resulted in flaws in the sealing and PDMS curing. It was observed that the sealing of the PDMS may be irreversible, but not permanent when environment and pressure is altered. As it was observed the pressure increase resulted in rupture of the seal or PDMS where defects were not visible, such as microcracks or bubbling associated with curing. Theses defects allow one to understand material flaws and possibly material selection. It may be wise to investigate other polymer materials and/or process that may withstand higher pressures, stresses, and strains over time.

5.1.10 – Overall Conclusions

Development and design of the micropump consumed much time. Fabrication methods for the micropump were difficult and very time consuming. The material utilized for this project, PDMS, is a material that has not been utilized much in processing procedures. Much time was taken to determine the best methods to fabricate the micropump in the fastest amount of time. Each method of fabrication proved to be time consuming and consisted of many days.

After both methods were fine-tuned and tested numerous times, each still resulted in approximately a one week to two week turn around time. The time to make the pump could also be delayed farther depending on equipment downtime and failure.

Sealing and testing the micropump required more time in order to obtain the optimum method and results. Testing and characterization was able to be completed with top actuation. Sidewall actuation was unable to be achieved at this time due to the desired thickness not being acquired. Improper thickness resulted in sidewalls that would not move or flex properly to provide fluid interaction. Actuation of the sidewalls will be further investigated in the future with a better, more devised actuation method. Even though there were many issues and drawbacks during the design, fabrication, and testing of the micropump, it has been proven that it can be accomplished as seen in figures 4.1 and 4.2.

5.2: Summarization of Objectives

The main objective was to determine fabrication methods that would allow the development of the theoretical three-wall micropump studied in ANSYS. Each fabrication method was novel and unique in the creation of the micropump design. The first fabrication method required the use of the VMC microelectronics laboratory. This method utilized microelectricalmechanical systems methodology coupled with lithography and sealing processes. The second fabrication method incorporated rapid prototyping technology to produce a mold of the PDMS micropump. Both fabrication methods provided optimum final results that allowed one to experimentally test the micropumps capabilities. These fabrication methods when

coupled together allowed the processing and production times of the micropump to be reduced drastically making it ideal for quick and easy manufacturing.

Finally the last objective was to experimentally test the micropump to determine the best actuation methods for fluid flow. Several experimental pumps were created, such as electrostatic, piezoelectric, magnetic, mechanical, and pressurized. From all of these testing methods the two that produced the best results were mechanical actuation and pressurized actuation. Mechanical actuation of the micropump was investigated and corresponded with theoretical results computed with ANSYS. From experimentally data it was proven that the optimum frequencies to operate the device ranged from ten to twenty hertz, with best flow rates falling at an operating frequency of fourteen to sixteen hertz. Theoretically it was proven that the flow rate through the micropump was proportional to the actuation frequency. Comparison of both theoretical and experimental results proved that the frequencies to actuate the micropump were similar.

5.3: Research Contributions

The main goal of this project was to investigate the feasibility of a valveless micropump and study its performance experimentally that would pump fluids of different viscosities efficiently and effectively. Based on previous micropump design simulations the pump was redesigned and fabricated to investigate further the performance characteristics.

Two fabrication methods were studied and created to bring the three nozzle/diffuser micropump into a functioning prototype. The cleanroom process incorporated techniques that allowed the design to be fabricated through a step by step process to achieve a finished product.

This procedure allowed the development of an irreversible sealing technique that had not been developed prior to this research. This technique was done with low voltage and pressure to provide a permanent seal for the PDMS fabricated pump. Coupling the cleanroom processes with rapid-prototyping the overall fabrication and development of the micropump was accomplished. This type of design and fabrication process can be extended for the development and testing of new design models for many applications.

Through experimental testing it was determined that the micropump would require a displacement to the walls of the pump to achieve desired flow characteristics through the entire pump, such as laminar flow, minimal backflow, and continual increase of flow. Several techniques were investigated such as electrostatics, piezoelectric, magnetic, mechanical, and pressure actuation to produce wall motion. From electrostatic actuation a method was created to actually metalize the PDMS material for a short time with proper connections to supply current. This technique was virtually a novel concept that was developed to actuate the pump. It was discovered that after the metal was placed on the PDMS it would deteriorate over time due to characteristics of the material itself. For piezoelectric actuation it was studied for actuation methods concerning the micropump. It was observed that piezoelectric materials would not achieve the desired displacement required to manipulate fluid flow through the micropump chamber. Next magnetic actuation did provide movement of the PDMS membrane, but lacked consistent results for attraction/deflection. It was determined and concluded that the incorporation of magnetic medium with the PDMS mixture must undergo a constant electromagnetic field in order to align the particulates within the PDMS material. This concept would involve fabricating and constructing an electromagnetic setup to create enough magnetism to cure and actuate the micropump. This in turn would be bulky and not very efficient in terms

of moving fluid through the micropump. The main actuation method that provided ample results was mechanical. With this method a pneumatic motor was utilized to acquire displacement on the top of the micropump. As previously stated and reported this method provided the desired results that were expected as compared to the theoretical. It was observed on the bigger micropump designs that backflow was present, but as the micropump went smaller and smaller the backflow characteristic gradually decreased. It was observed that as frequency increased flow increased through the pump as well. This was shown both theoretically from previous studies and experimentally through the research presented.

5.4: Recommendations and Future Work

This study has proven the micropump must be developed with at least three-walls to achieve maximum flow rate with minimal backflow characteristics. A future prospect would focus on developing the micropump into an advanced three-dimensional device that can be actuated around the whole perimeter. Also, incorporation of a filtering device would be a future design that would allow for sorting within drug delivery or biological devices. Installation or fabrication of a flap in the interior of the micropump chamber would eliminate any possible backflow.

As previously stated future research possibilities include an attempt to expand the horizon of the PDMS micropump from a simple three-dimensional to a more complex three-dimensional conical design. To date this new concept has been theorized with the use of SolidWorks and ANSYS. The design created in SolidWorks is shown below with accompanied dimensions.

Note: this is a conceptual theory that is currently being investigated for future graduate students (figure 5.1).

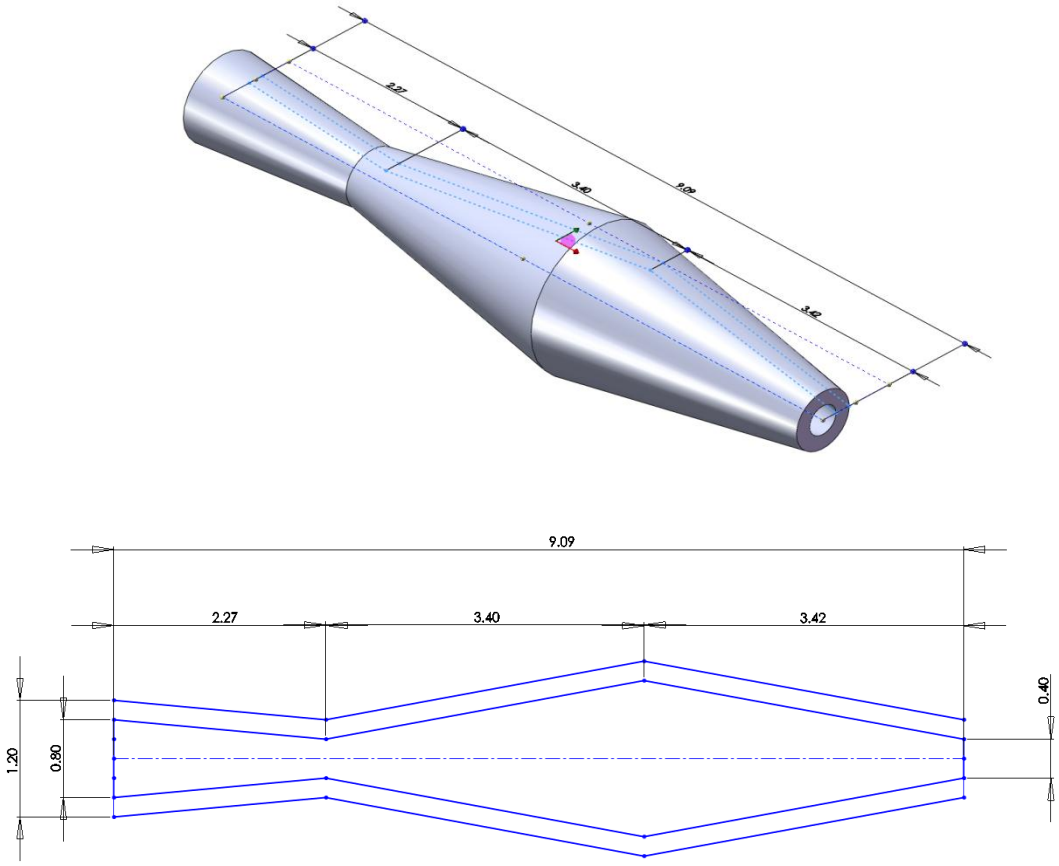

Figure 5.1: Design Concept of 3-Dimensional Micropump

The aforementioned micropump is made up of PDMS material. The following properties were utilized to begin analysis on this conceptual design.

- Material – PDMS
- Young's Modulus - 750 kPa
- Poisson's Ratio - 0.49

For structural testing with ANSYS the following properties were utilized:

- Load - 3 kPa (applied to one side at a time, and then all three at once)
- Non-linear deformation
- Symmetry
- Mesh:
- Nodes: 59381
- Elements: 11904

Images (figures 5.2 – 5.10) of the structural test is shown below and followed by the load testing done with the use of ANSYS.

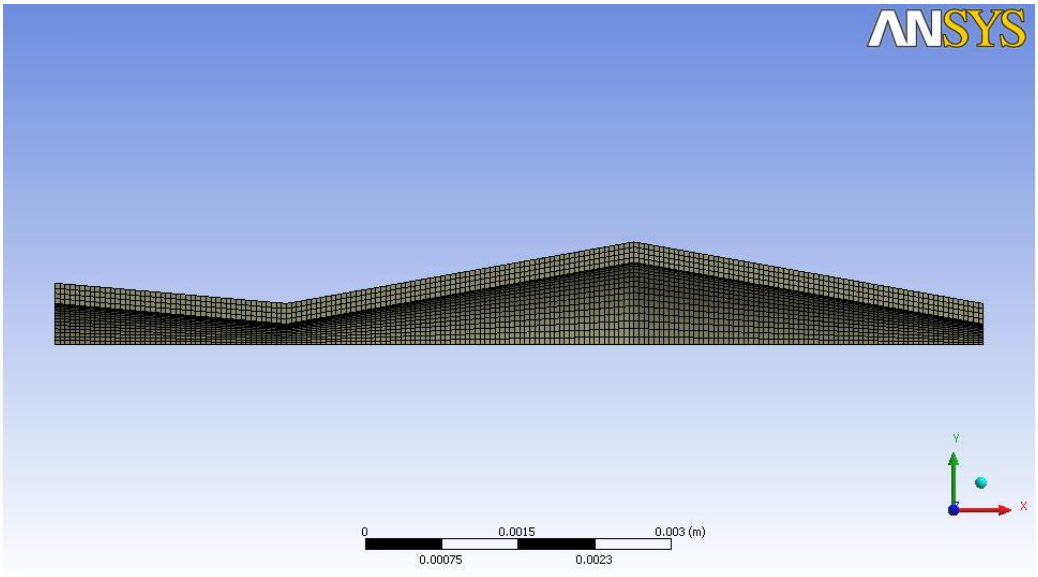

Figure 5.2: Meshed Symmetric 3D-Micropump

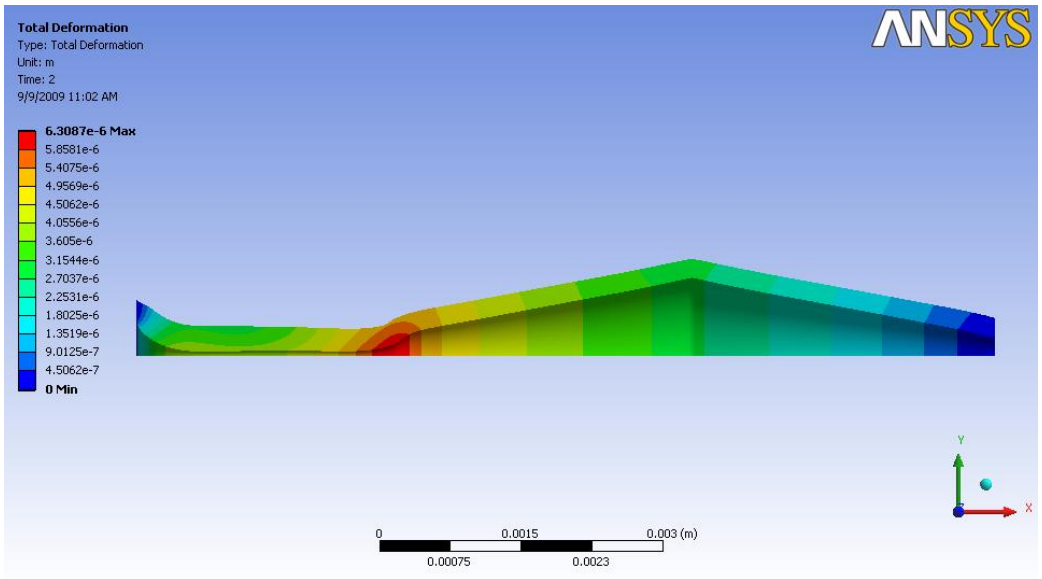

Figure 5.3: Total Deformation with applied Load at First Wall (Left most)

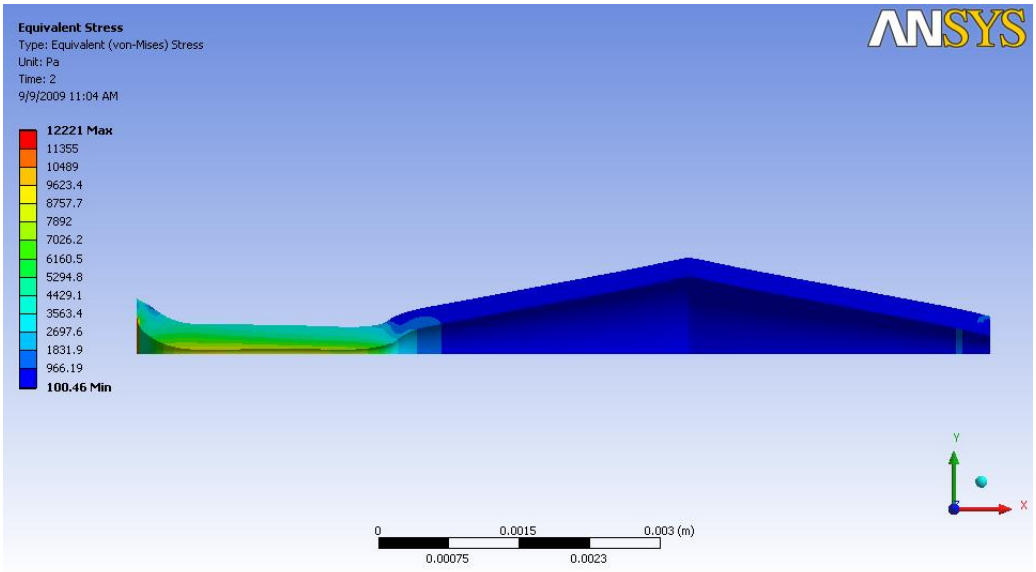

Figure 5.4: Total Stress experienced under applied Load at First Wall (Left Most)

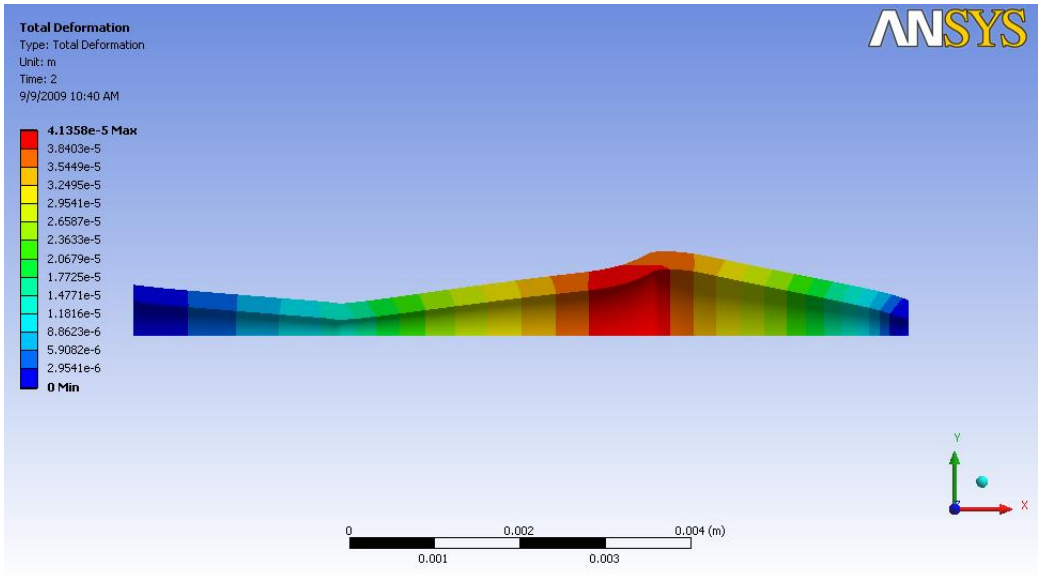

Figure 5.5: Total Deformation with applied Load at Second Wall (Middle)

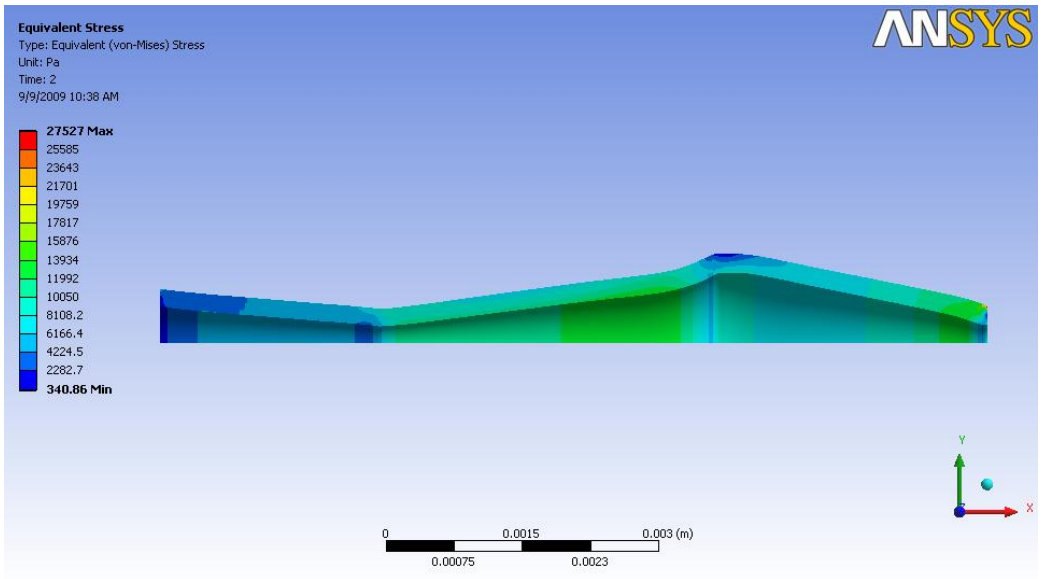

Figure 5.6: Total Stress experienced under applied Load at Second Wall (Middle)

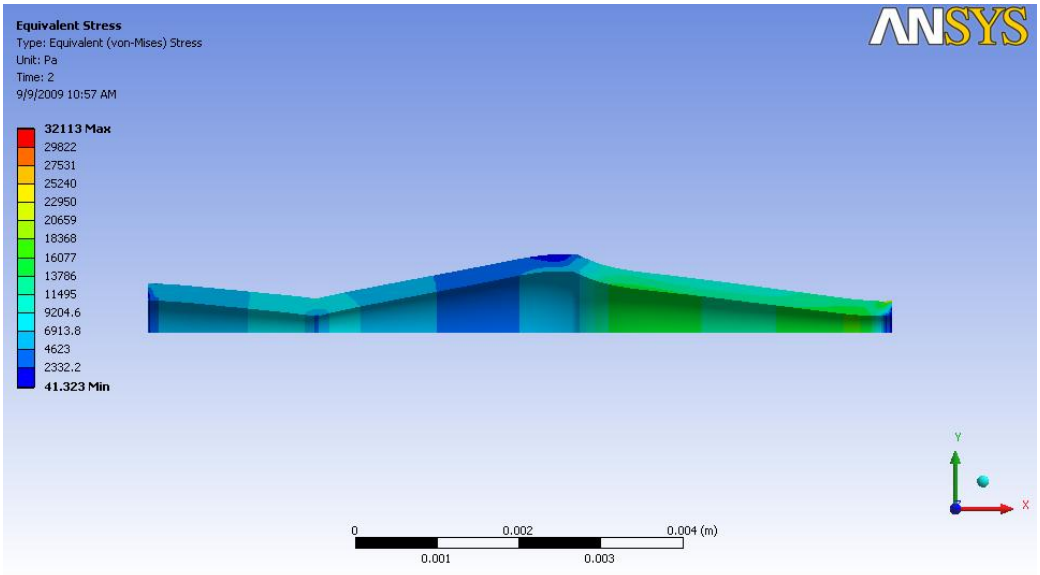

Figure 5.7: Total Deformation with applied Load at Third Wall (Right Most)

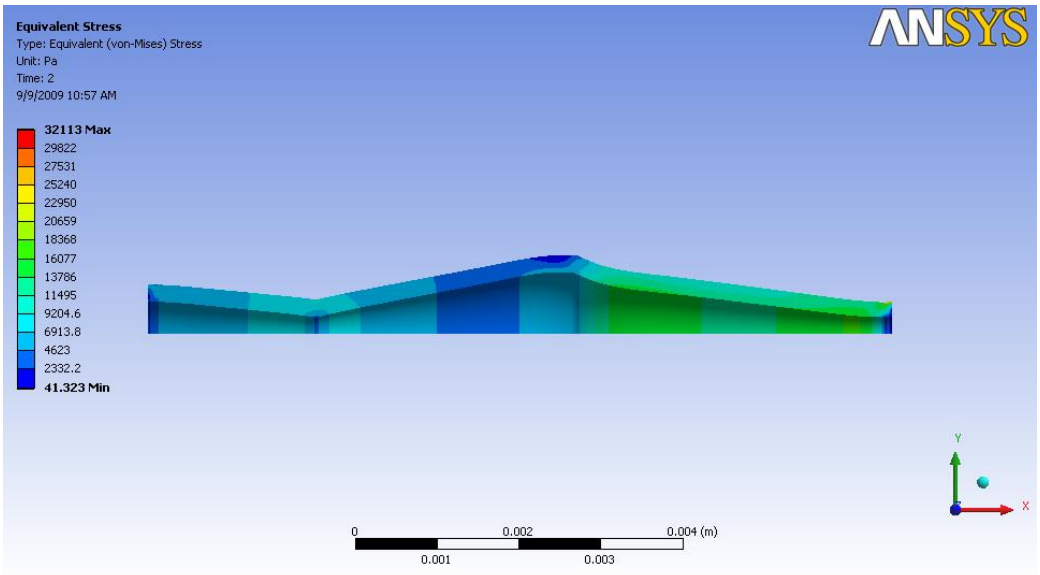

Figure 5.8: Total Stress experienced under applied Load Third Wall (Right Most)

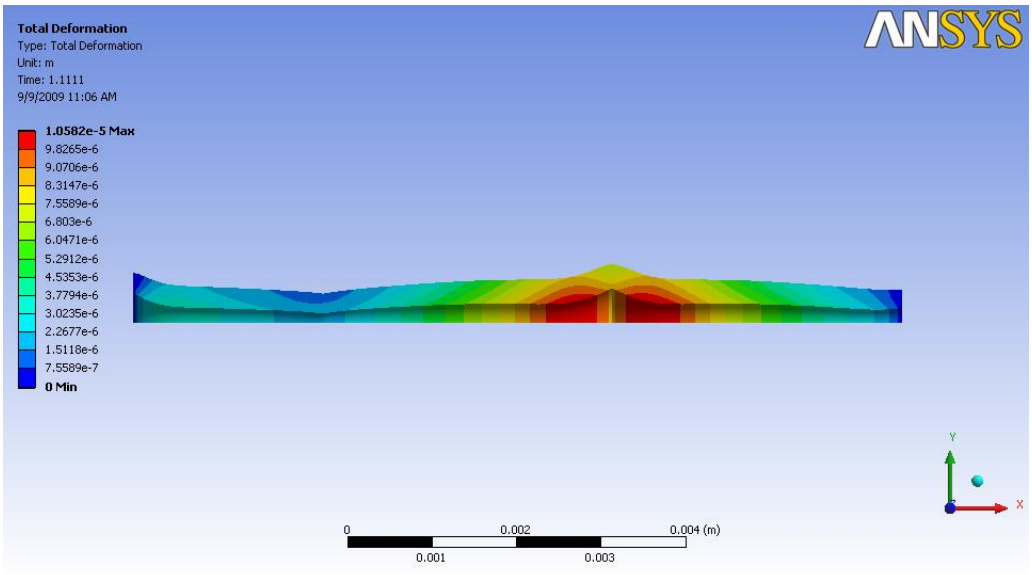

Figure 5.9: Total Deformation with applied Load on all walls

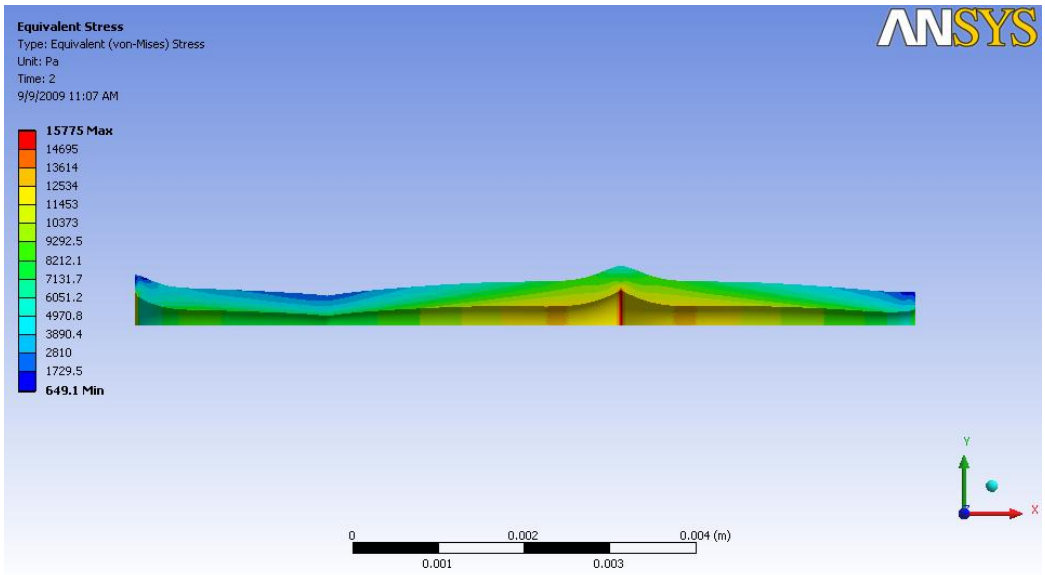

Figure 5.10: Total Stress with applied Load on all walls

Next a fluid flow test was utilized with the following parameters and conditions within ANSYS, they are as follows:

- Fluid: Water
- Viscosity: 0.001
- Density: 1000 kg/m^3
- Mesh:
- Nodes: 6789
- Elements: 6624
- Boundaries:
- Inlet: 1mm/s
- Outlet: 0 Pa (atmospheric)
- Wall Velocity: 0 m/s

These studies are illustrated in figures 5.11 – 5.13, below and on the following page(s).

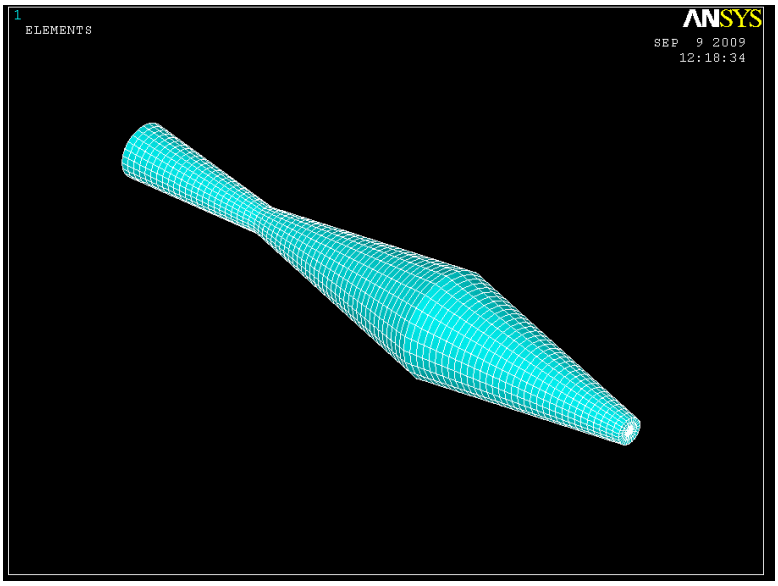

Figure 5.11: Three-Dimensional Mesh of Micropump

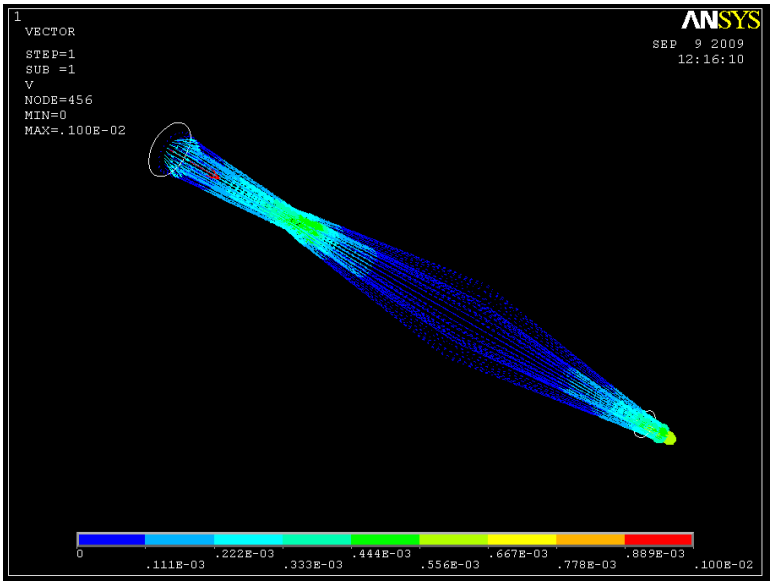

Figure 5.12: Fluid Flow Results of 3D pump

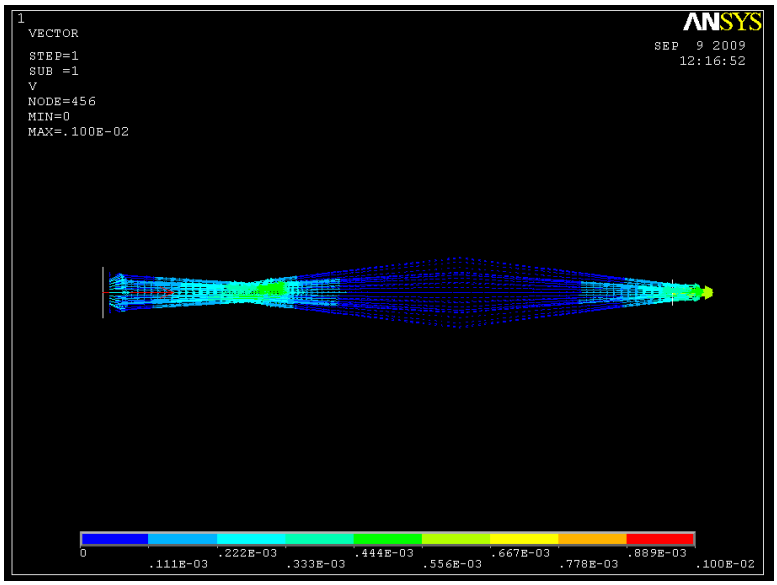

Figure 5.13: Fluid Flow Results of 3D Pump (side view)

These analysis were completed using ANSYS and depict a successful, theoretical micropump that would efficiently work in a three-dimensional version. This has led to the development of a three-dimensional experimental design, shown in the following images (figures 5.14 and 5.15):

Figure 5.14: Three-dimensional micropump Fabricated

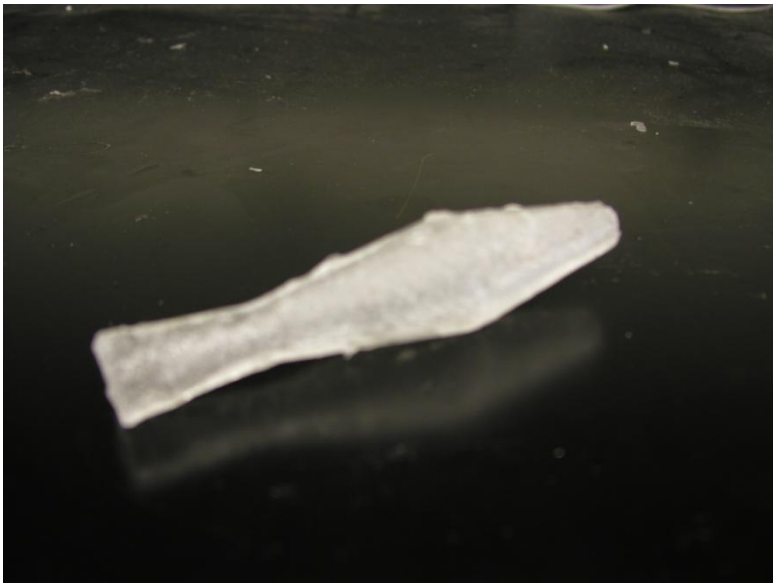

Figure 5.15: Three-dimensional micropump Fabricated

The three-dimensional micropump is currently undergoing testing and experimentation. If it is successful, it can then be downsized and tested in order to provide a more economical, microscale device that can be utilized in DNA analysis, chemical analysis, and drug delivery applications.

REFERENCES

[1] Narasimhan, J., Papautsky, I., *J. Micromech. Microeng.,* 2002, 14, pp. 96 – 103

[2] Yussuf, A., Sbarski, I., Hayes, J., Solomon, M., *Sealing and Bonding Techniques for Polymer-Based Microfluidic Devices,* 2001, pp. 269-275.

[3] Whitesides, G. M., (2006, July) The origins and the future of microfluidics. *Nature.* [Online]. 442, pp. 368-373. Available: http://ww.nature.com/nature/journal/v442/n7101/full/nature05058.html

[4] Shaikh, K. A., Ryu, K. S., Goluch, E. D., Nam, J. M., Liu, J., Lu, Y., Mirkin, C. A., Liu, C., *A Methodology for Rapid Prototyping Microfluidic Devices with Sophisticated Functionality.* 2005, pp. 1063-1065.

[5] Ng, J. M. K., Gitlin, I., Stroock, A. D., Whitesides, G. M., *Electrophoreis* 2002, 23, pp. 3461-3473

[6] Vlachopoulou, M. E., Tserepi, A., Vourdas, N., Gogolides, E., Misiakos, K., *Journal of Physics: Conference Series* 10, 2005, pp. 293-296.

[7] Lu, H., Koo, L. Y., Wang, Lauffenburger, D. A., Griffith, L. G., Jensen, K. F., *Anal. Chem.* 2004, 76, pp. 5257-5264

[8] Anderson, J. R., Chiu, D. T., Jackman, R. J., Cherniavskaya, O., McDonald, J. C., Wu, H., Whitesides, S. H., Whitesides, G. M., *Anal. Chem.* 2000, 72, pp. 3158-3164.

[9] McDonald, J. C., Whitesides, G. M., *Acc. Chem. Res.* Res. 2002, 35, pp. 491-499.

[10] Chaudary, M. K., Whitesides, G. M., *Langmuir* 1991, 7, pp. 1013-1025

[11] Morra, M., Occhiello, E., Marola, R., Garbassi, F., Humphrey, P., Johnson, D., *J. Colloid Interface Sci.* 1990, 137, pp. 11-24.

[12] Papra, A., Bernar, A., Juncker, D., Larsen, N. B., Michel, B., Delamarche, E., *Langmuir* 2002, 19, pp. 1518-1527

[13] McDonald, J. C., Duffy, D. C., Anderson, J. R., Chiu, D. T., Wu, H., Whitesides, G. M., *Electrophoresis* 2000, 21, pp. 27-40.

[14] Owen, M. J., Smith, P. J., *J. Adhesion Sci. Technol.* 1994, 9, pp. 1063-1075.

[15] Unger, M. A., Chou, H., Thorsen, T., Schere, a., Quake, S. R., *Science* 2000, 288, pp. 113-116.

[16] Chiu, D. T., Jeon, N. L., Huang, S., Kane, R., Wargo, C. J., Choi, I. S., Ingber, D. E., Whitesides, G. M., *Proc. Natl. Acad. Sci. USA* 2000, 97, pp. 2408-2413.

[17] McDonald, J.C., Chabinyc, M. L., Metallo, S., Anderson, J. R., Stroock, A. D., Whitesides, G. M., *Anal. Chem.* 2002, 74, pp. 1537-1545.

[18] Tsai, J. H., Lin, L., *J. Micromech. Microeng.* 2001, 11. pp. 577-581.

[19] Kopp, M. U., Crabtree, H. J., Manz, A., *Curr. Opin. Chem. Biol.* 1997, 1, pp. 410-419.

[20] Meng, E., Wu, S., Tai, Y. C., *Fresenius' J. Anal. Chem.* 2001, 371, pp. 270-275.

[21] Kenis, P. J. A., Ismagilov, R. F., Takayama, S., Whitesides, G. M., Li, S., White, H. S., *Acc. Chem. Res.* 2000, 33, pp. 841-847.

[22] A.C. Cohen, Feeding adaptations of some predaceous hemiptera, Ann. Entomol. Soc. Am. 83 (6) (1990) 1215–1223.

[23] A.C. Cohen, Extra-oral digestion in predaceous terrestrial arthropoda, Annu. Rev. Entomol. 40 (1995) 85–103.

[24] L.J. Thomas, S.P. Bessman, Prototype for an implantable micropump powered by piezoelectric disk benders, Trans. Am. Soc. Artif. Organs 21 (1975) 516–520.

[25] W.J. Spencer, W.T. Corbett, L.R. Dominguez, B.D. Shafer, An electronically controlled piezoelectric insulin pump and valves, IEEE Trans. Sonics Ultrason. SU-25 (1978) 153–156.

[26] J.G. Smits, Piezoelectric micropump with three valves working peristaltically, Sens. Actuators A 21–23 (1990) 203–206.

[27] H.T.G. van Lintel, F.C.M. van de Pol, S. Bouwstra, A piezoelectric micropump based on micromachining of silicon, Sens. Actuators 15 (1988) 153–167.

[28] F.C.M. van de Pol, H.T.G. van Lintel, M. Elvenspoek, J.H.J. Fluitman, A thermopneumatic micropump based on micro-engineering techniques, Sens. Actuators A 21–23 (1990) 198–202.

[29] A. Wego, L. Pagel, A self-filling micropump based on PCB technology, Sens. Actuators A 88 (2001) 220–226.

[30] M.C. Acero, J.A. Plaza, J. Esteve, M. Carmona, S. Marco, J. Samitier, Design of a modular micropump based on anodic bonding, J. Micromech. Microeng. 7 (1997) 179–182.

[31] B. Büstgens, W. Bacher, W. Bier, R. Ehnes, D. Maas, R. Ruprecht, W.K. Schomburg, L. Keydel, Micromembrane pump manufactured by molding, in: Proceedings of the Actuator ‘94, Bremen, Germany, 15–17 June 1994, pp. 86–90.

[32] R. Linnemann, P. Woias, C.-D. Senfft, J.A. Ditterich, A self-priming and bubble-tolerant silicon micropump for liquids and gases, in: Proceedings of the MEMS ‘98, Heidelberg, Germany, 25–29 January 1998, pp. 532–537.

[33] P. Woias, R. Linnemann, M. Richter, A. Leistner, B. Hillerich, in: D.J. Harrison, A. van den Berg (Eds.), Micro Total Analysis Systems ‘98, Kluwer Academic Publishers, Dordrecht, 1998, pp. 383–386.

[34] J. Döpper, M. Clemens, W. Ehrfeld, K.-P. Kämper, H. Lehr, Development of low-cost injection moulded micropumps, in: Proceedings of the Actuator ‘96, Bremen, Germany, 26–28 June 1996, pp. 37–40.

[35] S. Böhm, M. Dierselhuis, W. Olthuis, P. Bergveld, in: D.J. Harrison, A. van den Berg (Eds.), Micro Total Analysis Systems ‘98, Kluwer Academic Publishers, Dordrecht, 1998, pp. 391–394.

[36] M.C. Carrozza, N. Croce, B. Magnani, P. Dario, A piezoelectricallydriven stereolithography-fabricated micropump, J. Micromech. Microeng. 5 (1995) 177–179.

[37] P. Dario, N. Croce, M.C. Carrozza, G. Varallo, A fluid handling system for a chemical microanalyzer, Technical Digest of the MME ’95, Sixth Workshop on Micromachining, Micromechanics and Microsystems, Copenhagen, Denmark, 3–5 September 1995, pp. 140–143.

[38] S. Böhm, W. Olthuis, P. Bergveld, A plastic micropump constructed with conventional techniques and materials, Sens. Actuators 77 (1999) 223–228.

[39] J. Judy, T. Tamagawa, D.L. Polla, Surface-machined micromechanical membrane pump, in: Proceedings of the MEMS ‘91, Nara, Japan, 30 January–2 February 1991, pp. 182–186.

[40] R. Zengerle, S. Kluge, M. Richter, A. Richte, A bidirectional silicon micropump, in: Proceedings of the MEMS ‘95, Amsterdam, The Netherlands, 29 January–2 February 1995, pp. 19–24.

[41] T. Bourouina, A. Bosseboeuf, J.-P. Grandchamp, Design and simulation of an electrostatic micropump for drug-delivery applications, J. Micromech. Microeng. 7 (1997) 186–188.

[42] E. Makino, T. Mitsuya, T. Shibata, Fabrication of TiNi shape memory micropump, Sens. Actuators A 88 (2001) 256–262.

[43] S. Kluge, G. Neumayer, U. Schaber, M. Wackerle, M. Maichl, P. Post, M. Weinmann, R. Wanner, Pneumatic silicon microvalves with piezoelectric actuation, in: Proceedings of the Transducers ‘01/Eurosensors XV, Munich, Germany, 10–14 June 2001, pp. 924–927.

[44] M. Richter, J. Kruckow, J. Weidhaas, M. Wackerle, A. Drost, U. Schaber, M. Schwan, K. Kühl, Batch fabrication of silicon micropumps, in: Proceedings of the Transducers ‘01/Eurosensors XV, Munich, Germany, 10–14 June 2001, pp. 936–939.

[45] M. Koch, N. Harris, A.G.R. Evans, N.M. White, A. Brunnschweiler, A novel micromachined pump based on thick-film piezoelectric actuation, in: Proceedings of the Transducers ‘97, vol. 1, Chicago, USA, 16–19 June 1997, pp. 353–356.

[46] M. Koch, A.G.R. Evans, A. Brunnschweiler, The dynamic micropump driven with a screen printed PZT actuator, J. Micromech. Microeng. 8 (1998) 119–122.

[47] C.J. Morris, F.K. Forster, Optimization of a circular piezoelectric bimorph for a micropump driver, J. Micromech. Microeng. 10 (2000) 459–465.

[48] E. Stemme, G. Stemme, A valveless diffuser/nozzle-based fluid pump, Sens. Actuators A 39 (1993) 159–167. *P. Woias / Sensors and Actuators B 105 (2005) 28–38* 37

[49] A. Olsson, Valve-less diffuser pumps for liquids, Ph.D. Thesis, Stockholm, 1996.

[50] A. Olsson, P. Enoksson, G. Stemme, E. Stemme, A valve-less planar pump in silicon, in: Proceedings of the Transducers ‘95/Eurosensors IX, Stockholm, Sweden, 25–29 June 1995, pp. 291–294.

[51] F.K. Foster, R.L. Bardell, M.A. Afromowitz, N.R. Sharma, A. Blanchard, Design, fabrication and testing of fixed-valve micro-pumps, in: Proceedings of the ASME Fluids Engineering Division, IMECE 95, vol. 234, 1995, pp. 39–44.

[52] N. Tesla, Valvular conduit, US patent 1 329 559 (1920).

[53] T. Gerlach, M. Schuenemann, H. Wurmus, A new micropump principle of the reciprocating type using pyramidic micro flowchannels as passive valves, J. Micromech. Microeng. 5 (1995) 199–201.

[54] A. Olsson, G. Stemme, E. Stemme, A numerical design study of the valveless diffuser pump using a lumped-mass model, J. Micromech. Microeng. 9 (1999) 34–44.

[55] M. Heschel, M. Muellenborn, S. Bouwstra, Fabrication and characterization of truly 3-D diffuser/nozzle microstructures in silicon, IEEE J. Microelectromech. Syst. 6 (March (1)) (1997) 41–47.

[56] M. Stehr, S. Messner, H. Sandmaier, R. Zengerle, The VAMP—a new device for handling liquids or gases, Sens. Actuators A 57 (1996) 153–157.

[57] M. Stehr, H. Gruhler, H. Straatmann, S. Messner, H. Sandmaier, R. Zengerle, The selfpriming VAMP, in: Proceedings of the Transducers '97, vol. 1, Chicago, USA, 16–19 June 1997, pp. 351–352.

[58] Guoguang Su and Ramana M. Pidaparti, "Drug Particle Delivery Investigation through a Valveless Micropump," *Journal of Microelectromechanical Systems,* vol. 19, no. 6, pp. 1390 – 1399, December 2010

[59] C. Cartin, R. M. Pidaparti, and G. M. Atkinson, "Design and fabrication of a PDMS micropump with moving membranes," in *Proc. Univ., Gov., Ind. Micro-Nano Symp.,* Louisville, KY, Jul. 13–16, 2008, pp. 249–253.

[60] H. Andersson, W. van der Wijngaart, P. Nilsson, P. Enoksson, and G. Stemme, "A valve-less diffuser micropump for microfluidic analytical systems," *Sens. Actuators B, Chem.,* vol. 72, no. 3, pp. 259–265, Feb. 2001.

[61] R. Zengerle, M. Leitner, S. Kluge, A. Richter, Carbon dioxide priming of micro liquid systems, in: Proceedings of the MEMS '95, Amsterdam, The Netherlands, 29 January–2 February 1995, pp. 340–343.

[62] P. Gravesen, J. Branebjerg, O.S. Jensen, Microfluidics—a review, J. Micromech. Microeng. 3 (1993) 168–182.

[63] M. Richter, R. Linnemann, P. Woias, Robust design of gas and liquid micropumps, Sens. Actuators A 68 (1998) 480–486.

[64] D. Maillefer, H. van Lintel, G. Rey-Mermet, R. Hirschi, A high-performance silicon micropump for an implantable drug delivery system, in: Proceedings of the MEMS '99, Orlando, USA, 17–21 January 1999, pp. 541–546.

[65] D. Maillefer, S. Gamper, B. Frehner, P. Balmer, H. van Lintel, P. Renaud, A high-performance silicon micropump for disposable drug delivery systems, in: Proceedings of the MEMS '01, Interlaken, Switzerland, 21–25 January 2001, pp. 413–417.

[66] K.-P. Kämper, J. Döpper, W. Ehrfeld, S. Oberbeck, A self-filling low-cost membrane micropump, in: Proceedings of the MEMS '98, Heidelberg, Germany, 25–29 January 1998, pp. 322–327.

[67] A. Olsson, O. Larsson, J. Holm, L. Lundbladh, O. Oehman, G. Stemme, Valve-less diffuser micropumps fabricated using thermoplastic replication, Sens. Actuators A 64 (1998) 63–68.

[68] S.F. Bart, M. Mehregany, L.S. Tavrow, J.H. Lang, Microfabricated electrohydrodynamic pumps, Transducers ‘89, Book of Abstracts, Montreux, Switzerland, 25–30 June 1989, p. 113.

[69] A. Richter, H. Sandmaier, An electrohydrodynamic micropump, in: Proceedings of the MEMS ‘90, Napa Valley, USA, 11–14 February 1990, pp. 99–104.

[70] A. Richter, A. Plettner, K.A. Hoffmann, H. Sandmaier, Electrohydrodynamic pumping and flow measurement, in: Proceedings of the MEMS ‘91, Nara, Japan, 30 January–2 February 1991, pp. 271–276.

[71] S.E. McBride, R.M. Moroney, W. Chiang, in: D.J. Harrison, A. van den Berg (Eds.), Micro Total Analysis Systems ‘98, Kluwer Academic Publishers, Dordrecht, 1998, pp. 45–48.

[72] A. Manz, E. Verpoorte, D.E. Raymond, C.S. Effenhauser, N. Burggraf, H.M. Widmer, in: A. van den Berg, P. Bergveld (Eds.), Micro Total Analysis Systems, Mesa-Monograph, vol. 1, Kluwer Academic Publishers, Dordrecht, 1995, pp. 5–27.

[73] A. Manz, The secret behind electrophoresis microstructure design, in: Proceedings of the 2nd International Symposium on Miniaturized Total Analysis Systems, Basel, Switzerland, 19–22 November 1996, pp. 28–30.

[74] D.J. Harrison, C. Wang, P. Thibeault, F. Ouchen, S.B. Bang, in: A. van den Berg, et al. (Eds.), Micro Total Analysis Systems 2000, Kluwer Academic Publishers, Dordrecht, 2000, pp. 195–204.

[75] P.H. Paul, D.W. Arnold, D.J. Rakestraw, in: D.J. Harrison, A. van den Berg (Eds.), Micro Total Analysis Systems ‘98, Kluwer Academic Publishers, Dordrecht, 1998, pp. 49–52.

[76] R.M. Moroney, R.M. White, R.T. Howe, Ultrasonically induced microtransport, in: Proceedings of the MEMS ‘91, Nara, Japan, 30 January–2 February 1991, pp. 277–282.

[77] S. Miyazaki, T. Kawai, M. Araragi, A piezo-electric pump driven by a flexural progressive wave, in: Proceedings of the MEMS ‘91, Nara, Japan, 30 January–2 February 1991, pp. 283–288.

[78] J.C. Rife, M.I. Bell, J.S. Horwitz, M.N. Kabler, R.C.Y. Auyeung, W.J. Kim, Miniature valveless ultrasonic pumps and mixers, Sens. Actuators 86 (2000) 135–140.

[79] N.T. Nuyen, R.M. White, Design and optimization of an ultrasonic flexural plate wave micropump using numerical simulation, Sens. Actuators 77 (1999) 229–236.

[80] J. Jang, S.S. Lee, Theoretical and experimental study of MHD (magnetohydrodynamic) micropump, Sens. Actuators 80 (2000) 84–89.

[81] A.V. Lemoff, A.P. Lee, An AC electrohydrodynamic micropump, Sens. Actuators B 63 (2000) 178–185.

[82] D. O'Keefe, C.O. Herlihy, Y. Gross, J.G. Kelly, Patient-controlled analgesia using a miniature electrochemically driven infusion pump, Br. J. Anaesth. 73 (1994) 843–846.

[83] S. Böhm, The comprehensive integration of microdialysis membranes and silicon sensors, Ph.D. Thesis, University of Twente, The Netherlands, 2000.

[84] S. Böhm, B. Timmer, W. Olthuis, P. Bergveld, in: A. van den Berg, et al. (Eds.), Micro Total Analysis Systems 2000, Kluwer Academic Publishers, Dordrecht, 2000, pp. 347–350.

[85] G.J. Kellogg, T.E. Arnold, B.L. Carvalho, D.C. Duffy, N.F. Sheppard Jr., in: A. van den Berg, et al. (Eds.), Micro Total Analysis Systems 2000, Kluwer Academic Publishers, Dordrecht, 2000, pp. 239-242.

[86] N. Thomas, A. Ocklind, I. Blikstad, S. Griffiths, M. Kenrick, H. Derand, G. Ekstrand, C. Ellström, A. Larsson, P. Andersson, in: A. van den Berg, et al. (Eds.), Micro Total Analysis Systems 2000, Kluwer Academic Publishers, Dordrecht, 2000, pp. 249–252.

[87] Kilani, M., Demming, S., Feldmann, M., Buttgenbach, S., Al-Salaymeh, and Al Halhouli, A. 2008, "Performance characterization of a miniature spiral-channel viscous pump," Science Direct, Sensors and Actuators A 142, pp. 256 – 262.

[88] Blanchard, D., Ligrani, P., and Gale, B. 2006, "Miniature Single-Disk Viscous Pump (Single-DVP), Performance Characterization," ASME, Vol. 128 pp. 602 – 610.

[89] Blanchard, D., Ligrani, P., and Gale, B. 2005, "Single-disk and double-disk viscous micropumps," Science Direct, Sensors and Actuators A 122 pp. 149 – 158.

[90] A. Manz, N. Graber, H.M. Widmer, Miniaturized total chemical analysis systems: a novel concept for chemical sensing, Sens. Actuators B 1 (1990) 244–248.

[91] W. Gumbrecht, W. Schelter, B. Montag, Online blood electrolyte monitoring with a ChemFET microcell system, Sens. Actuators B 1 (1990) 477–480.

[92] P. Woias, Ionensensitive Feldeffekttransistoren als Meßwandler in chemischen Analysensystemen auf Fließinjektionsbasis, Ph.D. Thesis, TU Munich, 1995.

[93] P. Woias, S. Koch, E. Müller, D. Barrow, J. Cefai, G. Curtis, H. Hughes, An ISFET-FIA system for high precision pH recording, Sens. Actuators B 15–16 (1993) 68–74.

[94] B. van der Schoot, S. Jeanneret, A. van den Berg, N.F. de Rooij, A silicon integrated miniature chemical analysis system, Sens. Actuators B 6 (1992) 57–60.

[95] M. Richter, A. Prak, J. Naundorf, M. Eberl, H. Leeuwis, P. Woias, A. Steckenborn, A chemical microanalysis system as a microfluid system demonstrator, in: Proceedings of the Transducers 97, vol. 1, Chicago, USA, 16–19 June 1997, pp. 303–306.

[96] S. Drost, W. Wörmann, P. Woias, B. Ross, O. Köster, W. Konz, B. Edler, W. Schuhmann, L. Meixner, R. Ferretti, Microanalytical system for environmental control, in: Proceedings of the Transducers 97, vol. 2, Chicago, USA, 16–19 June 1997, pp. 931–934.

[97] E. Verpoorte, A. Manz, H.M. Widmer, B. van der Schoot, N.F. de Rooij, A three-dimensional micro flow system for a multi-step chemical analysis, Technical Digest, Transducers '93, Yokohama, 7–10 June 1993, pp. 939–942.

[98] A. van den Berg (Ed.), Micro Total Analysis Systems '94, Proceedings of the _TAS '94 Workshop, 22–24 November 1994, Enschede, Netherlands, Kluwer Academic Publishers, 1994.

[99] H.M. Widmer (Ed.), _TAS '96, Proceedings of the 2nd International Symposium on Miniaturized Total Analysis Systems, Basel, Switzerland, 19–22 November 1996.

[100] D.J. Harrison, A. van den Berg (Eds.), Micro Total Analysis Systems '98, Proceedings of the _TAS '98 Workshop, 13–16 October 1998, Banff, Canada, Kluwer Academic Publishers, 1998.

[101] A. van den Berg, W. Olthuis (Eds.), Micro Total Analysis Systems 2000, Proceedings of the _TAS 2000 Symposium, 14–18 May 2000, Enschede, Netherlands, Kluwer Academic Publishers, 2000.

[102] P. Bergveld, Thirty years of ISFETOLOGY - What happened in the past 30 years and what may happen in the next 30 years, Sens. Actuators B 88 (2003) 1–20.

[103] Azaroff, L.V. and J. J. Brophy, *Electronic Processes in Materials*, McGraw-Hill Book Company, New York, 1963, Chapter 13. Reprinted by CBLS Publishers, Marietta, OH, 1990.

[104] "The Physics of Magnetism." http://www.ucpress.edu/content/chapters/11183.ch01.pdf, Web 24 Feb. 2012.

[105] "The Magnetic Field." http://media.wiley.com/product_data/excerpt/9X/07803602/078036029X.pdf, Web 24 Feb. 2012

[106] "Basic Microfluidic Concepts." (September 7, 2001): Online. http://faculty.washington.edu/yagerp/microfluidicstutorial/basicconcepts/basicconcepts.htm . Nov. 21, 2009.

VITA

Charles Patrick Cartin was born on June 27th, 1982, in Hopewell, Virginia and is an American Citizen. He graduated from Hopewell High School, Hopewell, Virginia in 2000. He received his Associates in Arts from Richard Bland College, Petersburg, VA in 2002. He obtained his Bachelor of Science in Mechanical Engineering from Virginia Commonwealth University, Richmond, Virginia in 2006 and his Master of Science in Mechanical Engineering from Virginia Commonwealth University, Richmond, Virginia in 2007. Since 2007 he has been working as a faculty member at various colleges and universities around the Richmond metro area, while continuing on track to complete his PhD requirements.

EDUCATION:

Ph.D., Mechanical Engineering, Virginia Commonwealth University, 2012
Dissertation: Fabrication and Simulation of a PDMS Micropump with moving membranes

M.S., Mechanical Engineering, Virginia Commonwealth University, 2007
Concentrations: Design Optimization and Solid Mechanics

B.S., Mechanical Engineering, Virginia Commonwealth University, 2006

A.A., Richard Bland College, 2002

EXPERIENCE:

Collateral Mechanical Engineering Instructor, 2010 – Present
Virginia Commonwealth University, Richmond, VA

Adjunct Engineering Faculty, 2011 – Present
J. Sargeant Reynolds Community College, Richmond, VA

Electronic Course Designer, 2011 – Present
J. Sargeant Reynolds Community College, Richmond, VA

Adjunct Mathematics and Physics Faculty, 2007 – 2010
John Tyler Community College JTCC, Chester, VA

Research Assistant, 2006 – Present
Virginia Commonwealth University, Richmond, VA

Teaching Assistant, 2008
Virginia Commonwealth University, Richmond, VA
Course: Mechatronics

Engineer Technician, 2006 – Present
G & C Engineering, Hopewell, VA

Technician, 1997 - 2006
VAMED Technical Center, Hopewell, VA

RESEARCH SKILLS:

Extensive knowledge of microfabrication, manufacturing, polymer, and cleanroom procedures.

PRESENTATIONS:

"Fabrication and Simulation of PDMS Valveless Micropump." GSA 12th Annual Research Symposium and Exhibit, April 21, 2009, Virginia Commonwealth University, Richmond, VA

"Design and Fabrication of PDMS Micropump with Moving Membranes." IEEE Poster Conference, April 30, 2007, Virginia Commonwealth University, Richmond, VA

PUBLICATIONS:

Cartin, C.P. and Pidaparti, R. M., "Design, Fabrication, and Testing of a Nozzle/Diffuser PDMS Micropump with Top Actuation," Micro and Nanosystems Journal 2011.

C. P. Cartin, K. Koombua, R. M. Pidaparti, and G. M. Atkinson, "Fabrication and Simulation of PDMS Valveless Micropump," ICMEMS 2009 - International Conference on MEMS, Chennai, India (2009)

Cartin, C. P., K. Koombua, Pidaparti, R. M., Atkinson, G. M., "Fabrication and Simulation of a PDMS Valveless Micropump," Proceedings of the 2009 International Conference on MEMS, IIT Madras, Jan 3-5, 2009.

K. Koombua, Cartin, C. P., Pidaparti, R. M., and Atkinson, G. M., "Evaluation of the Fabricated PDMS Micropump with Multiple Actuators using Computations," Sensors and Actuators Journal 2008.

C. Cartin, R.M. Pidaparti, and G.M. Atkinson, "Design and fabrication of a PDMS micropump with moving membranes," in *Proc. Univ., Gov., Ind. Micro-Nano Symp.,* Louisville, KY, Jul. 13 – 16, 2008, pp. 249 – 253.

Cartin, C. P., Pidaparti, R. M., Atkinson, G. M., "Design and Fabrication of a PDMS Micropump with Moving Membranes," University/Government/Industry Micro/Nano Symposium (UGIM), 17th Biennial Volume, Issue 13 – 16 July 2008, pp. 249 – 253.

GRANTS AND FELLOWSHIPS:

National Science Foundation (NSF), ECCS – 0725496

AWARDS AND HONORS:

Second Place, IEEE Poster Contest, Richmond Section, IEEE Chapter, April 30, 2008

SKILLS AND QUALIFICATIONS:

SolidWorks, ANSYS, AutoCad, AutoCad Inventor, Mathcad, Matlab, OrCad Pspice, Microsoft Office Suite (Excel, Word, Powerpoint), IC Station.

Windows 95-XP/7, Unix

Basic, C, C++, Turbo Pascal

MEMS (microelectromechanical systems) technology and cleanroom fabrication

PROFESSIONAL SOCIETIES

American Society of Mechanical Engineers, Student Member
IEEE, Student Member

PERSONAL DETAILS

US Citizen and Married

REFERENCES:

Available upon request